Int. J. Anal. Appl. (2026), 24:157

International Journal of Analysis and Applications

Compactness Theory in Complex Neutrosophic Soft Spaces and Its Application to Visual Cosine Similarity Analysis

Jamil J. Hamja[1], Raed Hatamleh[2], Diana Amin Mohammad Mahmoud[3], Giorgio Nordo[4], Haitham Qawaqneh[5], Aqeedat Hussain[6], Regimar A. Rasid[7], Aliazer H. Jinang[8], Arif Mehmood[9,*], Cris L. Armada[10,11]

[1]*Department of Mathematics, College of Mathematical Sciences, Mindanao State University Tawi-Tawi College of Technology and Oceanography, Philippines*

[2]*Department of Mathematics, Faculty of Science, Jadara University, P.O. Box 733, Irbid 21110, Jordan*

[3]*Amman Arab University, College of Arts and Sciences, Department of Mathematics, P.O. Box 2234, Amman 11953, Jordan*

[4]*MIFT Department of Mathematics and Computer Science, Physical Sciences and Earth Sciences - University of Messina, 98166 Sant'Agata, Messina, Italy*

[5]*Al-Zaytoonah University of Jordan, Amman 11733, Jordan*

[6]*Department of Mathematics, Institute of Numerical Sciences, Gomal University, Dera Ismail Khan 29050, KPK, Pakistan*

[7]*Department of Statistics, College of Mathematical Sciences, MSU - Tawi-Tawi College of Technology and Oceanography, 7500 Philippines*

[8]*MSU-TCTO Sintangkai Junior High School, Secondary Education Department, Mindanao State University Tawi-Tawi College of Technology and Oceanography, Philippines*

[9]*Department of Mathematics, Institute of Numerical Sciences, Gomal University, Dera Ismail Khan 29050, KPK, Pakistan*

[10]*Vietnam National University Ho Chi Minh City, Linh Trung Ward, Thu Duc City, Ho Chi Minh City, Vietnam*

[11]*Department of Applied Mathematics, Faculty of Applied Science, Ho Chi Minh City University of Technology (HCMUT), 268 Ly Thuong Kiet, Ward 14, District 10, Ho Chi Minh City, Vietnam*

[*]*Corresponding author:* mehdaniyal@gmail.com

Received: Dec. 17, 2025.

2020 *Mathematics Subject Classification.* 68M10.

Key words and phrases. complex neutrosophic soft topology; compactness; local compactness; Hausdorff and normal spaces; cosine similarity; hybrid visual-metric framework; PCA and t-SNE visualization.

https://doi.org/10.28924/2291-8639-24-2026-157
ISSN: 2291-8639

Abstract. In the framework of complex neutrosophic soft topology, the paper investigates locally compact spaces and complex neutrosophic soft compact spaces. Complex neutrosophic soft open covers, finite sub-covers, closed set intersections, centered families, and several comparable requirements are used to define the idea of compactness. Compact subsets of Hausdorff space were shown to be closed, and compact Hausdorff spaces were shown to be normal. The relationships between compactness axioms, closed ness axioms, Hausdorff ness axioms, normalcy axioms, and separation axioms (T_1, T_2, T_3) are investigated. The concept of complicated neutrosophic soft local compactness, which is a weakening of compactness expressed in terms of neighborhoods with compact closures, is then defined. Refined neighborhood confinement is established, and it is shown that both open and closed subspaces of locally compact Hausdorff spaces exhibit local compactness. These results provide a solid foundation for modeling the localized uncertainty and are generalized to the complex neutrosophic soft environment from the classical compactness theory. Using both quantitative and advanced visualization methods, this research offers a thorough and graphical analysis of the cosine similarity trends between the different dimensional cues and class templates. The strongest relationship is always found between Signal S_2 and Template T_1. Each of the cosine similarity scores is evaluated separately to display the predominant, moderate, and weak signal-template cross section. Through a number of complementary visual techniques such as normalized heatmaps, 2D and 3D bar graphs, surface plots, spline interpolations, PCA projection, and t-SNE embedding, the similarity matrix is rendered as an informative geometric structure in the form of peaks, ridges, and valleys. These visualizations offer an insightful understanding of the level of agreement, robustness and sensitivity by exhibiting stable similarity points, transitions and fragile points. Moreover, stable and sensitive matches where the confidence for classification is the highest and where we need to be careful are detected through the sensitivity and derivative analysis of the landscape. In general, the hybrid visual-metric approach provides a formal yet intuitive way to understand the correlation between signal and template that explains why the cosine similarity is a successful method of pattern recognition, clustering, and interpretation of multidimensional data.

1. Introduction

Uncertain and imprecise information has been a fundamental issue in mathematics and decision making. This started with the fundamental concept of fuzzy sets (FSs) [1], which generalised the notion of crisp sets to the case of membership with degree. This was followed by Atanassov's intuitionistic fuzzy sets (IFSs) [2] that added the degree of non-membership along with the degree of membership, thereby increasing the level of uncertainty. The study of fuzzy paradigms then branched out in many directions, such as the structure of fuzzy graphs and hypergraphs [4], and the analysis of fuzzy complex numbers [3]. The notion of complex fuzzy sets (CFSs), whose membership function is complex-valued, came as a breakthrough by Ramot et al. [5]. Meanwhile, the characteristics of CFSs were explored in terms of operations and delta-equalities [8] and IFSs were applied to multi-criteria decision-making [6] and pattern recognition [7]. Intuitionistic fuzzy graphs were created by extending the ideas of IFSs to graph theory [9]. Alkouri and Salleh devised complex intuitionistic fuzzy sets (CIFSs) [10] and complex Atanassov's intuitionistic fuzzy relations [11] to represent larger uncertainties. Special structures including intuitionistic fuzzy planar graphs [12], directed hypergraphs [13], and double domination of intuitionistic fuzzy graphs [14] have been studied further. Neutrosophic sets (NSs), which Smarandache presented as an extension of IFSs with truth, indeterminacy, and falsity, have advanced quickly in the meanwhile [44]. As a result, various similarity metrics for NSs [15]-[17], interval neutrosophic sets [18], neutrosophic soft

sets (NSSs) [19, 20], neutrosophic refined sets [21], and their use in medical diagnosis [22] have been developed. Additionally, complex hesitant fuzzy sets (CHFSs) [24, 25] and bipolar neutrosophic sets [23] have been shown. New similarity metrics and hybrid versions have proliferated recently. For instance, new measures have been given for interval-valued intuitionistic fuzzy sets (IVIFSs) [28], rigorous intuitionistic fuzzy measures utilizing Jensen-Shannon divergence [29], intuitionistic fuzzy sets [27], and neutrosophic fuzzy soft sets [26]. New techniques for comparing intuitionistic fuzzy values [31] and image processing with intuitionistic fuzzy sets of root type [30] are examples of new applications.

1.1. **Literature Review.** Strong intuitionistic fuzzy graphs [32], operations on CIFSs [33], Pythagorean fuzzy sets [34], and graph-theoretic ideas [35]-[37] are examples of theoretical developments. Neutrosophic hesitant fuzzy sets [38], CHFSs [40], distance measures using single-valued neutrosophic sets [39], and possibility neutrosophic soft expert sets [41] have all been used with vector similarity measures. Similarity and entropy measurements are also defined for emerging structures such as circular intuitionistic fuzzy sets (CIFSs) [42]. Furthermore, uncertainty modeling has been incorporated into other areas of mathematics. Floquet engineering, for example, has been used to topological superconductors [43], and early developments in soft set theory [45] have produced topological spaces [48], relations [47], and neutrosophic soft sets [46]. These concepts have been extended in the most recent work to complex neutrosophic soft sets and their topological spaces [49], irreversible k-threshold conversion numbers of neutrosophic graphs [51], complex tangent trigonometric methods for rung fuzzy sets [52], topological spaces based on symbolic n-plithogenic intervals [53], and numerical solutions of neutrosophic singular boundary value problems [50]. Lastly, a number of recent contributions have included fixed-point theory in various metric spaces [54]-[59] as well as real-world applications in domains like deep learning-based COVID-19 detection [60] and IoT-enabled learning environments [61]. When combined, these pieces demonstrate the continuous advancement and many uses of uncertainty theories in decision-making, artificial intelligence, and pure mathematics. A generalized framework for type-nnn extensions of fuzzy, neutrosophic, and plithogenic offsets as well as novel definitions and connections between these extensions have been proposed by Abualhomos et al. [62]. Their research enhances the ability of traditional theories of uncertainty to model multiple uncertain information by providing a structured approach to extend them to the next level. These extensions are useful in the cases of complex decision-making, where the conventional fuzzy models may not be adequate. Ahmad et al. [63] numerically studied the neutrosophic derivative problems using Newton's Central Difference Formula (CDF) and Backward Difference Formula (BDF). They proposed extensions of traditional numerical techniques in a neutrosophic environment to solve problems involving derivatives of uncertain data. This study links the theory of uncertainty with numerical analysis. Likewise, Edduweh et al. [64] proposed several types of first-order first-degree WFC-ODEs and analysed weak fuzzy complex differential equations. These findings offer fresh insights into the structure and behaviour of fuzzy complex dynamical systems, which are

valuable in signal processing, physics and engineering in the presence of uncertainty in amplitude and phase. Abualhomos et al. [65] provided a powerful method for solving weak fuzzy complex Diophantine equations in two variables, furthering the algebraic aspects of fuzzy mathematics. This study brings up new possibilities for discrete uncertain systems and highlights the value of fuzzy-complex techniques in number theory and computer algebra. Additionally, computational techniques for the fuzzy heat equation with complex Dirichlet boundary conditions were provided by Zureigat et al. [66]. The promise of fuzzy numerical techniques in PDEs is demonstrated in this work, especially in thermal systems impacted by unknown parameters and boundary conditions. Non-Hermitian second-order topological phases and bipolar skin effect in photonic kagome crystals were described by X. Yang et al. [67].

1.2. **Motivation.** Uncertainty, indeterminacy, and incomplete truth are characteristics of many real-world systems, particularly decision-making, pattern recognition, signal analysis, and others. Traditionally, the best metrics for classical topology and similarity are based on rigid binary assumptions or crispness, which do not account for such complex behavior. The cosine similarity is an effective geometrical scale for inferring the directional relationship of multi-dimensional data, and complex neutrosophic soft topology is a more mathematically rich framework with truth, indeterminacy, and falsity present simultaneously. However, the need for a consistent theoretical and analytical framework that can be both mathematically rigorous and visually explainable arises from the lack of well-developed compactness and local compactness structures within the complex neutrosophic soft spaces, as well as the interpretability of similarity measures in high dimensional environments.

1.3. **Research Gap.** Although compactness is a well-known term in fuzzy and classical topology, there is currently little systematic research on it in complicated neutrosophic soft topological spaces. The majority of the material that is currently available focuses on separation axioms and finite set-theoretic operations; compactness and local compactness, as well as how they interact with Hausdorff and normalcy qualities, are not thoroughly examined. Concurrently, cosine similarity is widely used in signal processing and pattern identification; however, most investigations depend solely on numerical thresholds with no information on structural stability, sensitivity, or geometry across templates. Particularly when considering an uncertain-sensitive neutrosophic framework, it is clear that there is a lack of connection between the advancement of better topological compactness theories and the use of multidimensional similarity visualization and sensitivity analysis.

1.4. **Novelty and Contributions.** By explicitly describing the theory of complex neutrosophic soft compact and locally compact spaces and providing a number of alternative formulations utilizing open covers, finite sub-covers, closed set intersections, and centered families, this article fills in one of the highlighted gaps. In the complicated neutrosophic soft setting, it rigorously investigates the relationship between compactness, closedness, Hausdorffness, normalcy, and greater separation axioms (T_1, T_2, T_3). Additionally, the study develops inheritance features of open and closed

subspaces and offers and investigates complex neutrosophic soft local compactness, a weaker but structurally crucial concept. In order to reveal the stability, sensitivity, and geometric structure of signal-template correlation, it also proposes a hybrid visual-metric model of cosine similarity analysis that combines Heatmaps, bar graphs, surface plots, spline interpolation, PCA, and t-SNE. In order to improve the uncertainty-resistant classification, weak associations with robust alignments are eliminated by combining surface analyses based on sensitivity and derivatives. Together, these contributions provide a strong and comprehensible foundation for the modeling of localized uncertainty of multidimensional systems by extending traditional compactness theory and similarity analysis into the rich neutrosophic soft space.

2. Preliminaries

We offer some basic terminology and background information in this part that will be helpful as our investigation develops further.

Definition 2.1. *[44] The expression for a neutrosophic set A defined on a discourse universe $\mathbb{X}$ is*

$$A = \{\langle x, T_A(x), I_A(x), F_A(x)\rangle : x \in \mathbb{X}\}$$

where, $T, I, F : \mathbb{X} \longrightarrow]0,1[$ *and* $0 \leq T_A(x) + I_A(x) + F_A(x) \leq 3$.

Definition 2.2. *[45] Let $P(\mathbb{X})$ be the power set of $\mathbb{X}$, $\mathbb{X}$ be a universal set, and $\mathcal{E}$ be a collection of parameters. When $\mathcal{F}$ is a mapping $\mathcal{F} : \acute{\mathcal{E}} \longrightarrow P(\mathbb{X})$, then $(\mathcal{F}, \acute{\mathcal{E}})$ is referred to as a soft set over $\mathbb{X}$. Put differently, a parameterized family of subsets of $\mathbb{X}$ is referred to as a soft set. The set of e-elements of the soft set $(\mathcal{F}, \acute{\mathcal{E}})$, or the set of e-approximate elements of the soft set, is represented by $\mathcal{F}(e)$ for each parameter $e \in \acute{\mathcal{E}}$, i.e.,*

$$(\mathcal{F}, \acute{\mathcal{E}}) = \{(e, \mathcal{F}(e)) : e \in \acute{\mathcal{E}}, \mathcal{F} : \acute{\mathcal{E}} \longrightarrow P(\mathbb{X})\}$$

Maji [46] was the first to propose the idea of the neutrosophic soft set, which Deli and Broumi [47] later developed as described below.

Definition 2.3. *Let $\acute{\mathcal{E}}$ be a set of parameters and $\mathbb{X}$ be a universal set. The collection of all neutrosophic sets on $\mathbb{X}$ is represented by $P(\mathbb{X})$. An approximate function of the neutrosophic soft set $(\tilde{\mathcal{F}}, \acute{\mathcal{E}})$ is $\tilde{\mathcal{F}}$, where $\tilde{\mathcal{F}}$ is defined by a set valued function $\tilde{\mathcal{F}} : \acute{\mathcal{E}} \longrightarrow P(\mathbb{X})$. It can be expressed as a parameterized family of neutrosophic sets on $P(\mathbb{X})$.*

$$(\tilde{\mathcal{F}}, \acute{\mathcal{E}}) = \{(e, \langle x, T_{\tilde{\mathcal{F}}(e)}(x), I_{\tilde{\mathcal{F}}(e)}(x), F_{\tilde{\mathcal{F}}(e)}(x)\rangle : x \in \mathbb{X}) : e \in \acute{\mathcal{E}}\}$$

where $T_{\tilde{\mathcal{F}}(e)}(x), T_{\tilde{\mathcal{F}}(e)}(x), F_{\tilde{\mathcal{F}}(e)}(x) \in [0,1]$ *are the truth membership, indeterminacy membership, and falsity membership of $\tilde{\mathcal{F}}(e)$. The inequality* $0 \leq T_{\tilde{\mathcal{F}}(e)}(x) + I_{\tilde{\mathcal{F}}(e)}(x) + F_{\tilde{\mathcal{F}}(e)}(x) + F_{\tilde{\mathcal{F}}(e)}(x) \leq 3$ *is evident since the supremum of each* $T, I, and F$ *is* 1.

Definition 2.4. *[48] Consider the neutrosophic soft set $(\tilde{\mathcal{F}}, \acute{\mathcal{E}})$ on $\mathbb{X}$. $(\tilde{\mathcal{F}}, \acute{\mathcal{E}})^c$ represents the complement of $(\tilde{\mathcal{F}}, \acute{\mathcal{E}})$, which is defined by:*

$$(\tilde{\mathcal{F}}, \acute{\mathcal{E}})^c = \{(e, \langle x, F_{\tilde{\mathcal{F}}(e)}(x), 1 - I_{\tilde{\mathcal{F}}(e)}(x), T_{\tilde{\mathcal{F}}(e)}(x)\rangle : x \in \mathbb{X}) : e \in \acute{\mathcal{E}}\}$$

$((\tilde{\mathcal{F}},\acute{\mathcal{E}})^c)^c = (\tilde{\mathcal{F}},\acute{\mathcal{E}})$ *is clearly true.*

Definition 2.5. *[46] Assume that* $(\tilde{\mathcal{F}},\acute{\mathcal{E}})$ *and* $(\tilde{\mathcal{G}},\acute{\mathcal{E}})$ *are neutrosophic soft sets on* $\mathbb{X}$. $(\tilde{\mathcal{F}},\acute{\mathcal{E}})$ *is the neutrosophic soft subset of* $(\tilde{\mathcal{G}},\acute{\mathcal{E}})$ *if* $T_{\tilde{\mathcal{F}}(e)}(x) \leq T_{\tilde{\mathcal{G}}(e)}(x), I_{\tilde{\mathcal{F}}(e)}(x) \leq I_{\tilde{\mathcal{G}}(e)}(x), F_{\tilde{\mathcal{F}}(e)}(x) \geq F_{\tilde{\mathcal{G}}(e)}(x)$, *for every* $x \in \mathbb{X}$, *for every* $e \in \acute{\mathcal{E}}$. $(\tilde{\mathcal{F}},\acute{\mathcal{E}}) \subseteq (\tilde{\mathcal{G}},\acute{\mathcal{E}})$ *is the notation for it.* $(\tilde{\mathcal{F}},\acute{\mathcal{E}})$ *is neutosophic soft set equal to* $(\tilde{\mathcal{G}},\acute{\mathcal{E}})$ *if* $(\tilde{\mathcal{F}},\acute{\mathcal{E}})$ *is a neutrosophic soft subset of* $(\tilde{\mathcal{G}},\acute{\mathcal{E}})$ *and* $(\tilde{\mathcal{G}},\acute{\mathcal{E}})$ *is a soft neutrosophic subset of* $(\tilde{\mathcal{F}},\acute{\mathcal{E}})$. $(\tilde{\mathcal{F}},\acute{\mathcal{E}}) = (\tilde{\mathcal{G}},\acute{\mathcal{E}})$ *is the notation for it.*

Definition 2.6. *[49]Consider the CNS sets* $(\tilde{\mathcal{F}}_1,\acute{\mathcal{E}})$ *and* $(\tilde{\mathcal{F}}_2,\acute{\mathcal{E}})$ *on* $\mathbb{X}$ *then their union is represented as* $(\tilde{\mathcal{F}}_1,\acute{\mathcal{E}}) \Cup (\tilde{\mathcal{F}}_2,\acute{\mathcal{E}}) = (\tilde{\mathcal{F}}_3,\acute{\mathcal{E}})$ *is signified by:*

$$(\tilde{\mathcal{F}}_3,\acute{\mathcal{E}}) = \left\{\left(e, \langle x, T_{\tilde{\mathcal{F}}_3(e)}(x), I_{\tilde{\mathcal{F}}_3(e)}(x), F_{\tilde{\mathcal{F}}_3(e)}(x)\rangle : x \in \mathbb{X}\right) : e \in \acute{\mathcal{E}}\right\},$$

where

$$\begin{aligned} T_{\tilde{\mathcal{F}}_3(e)}(x) &= \max\{T_{\tilde{\mathcal{F}}_1(e)}(x), T_{\tilde{\mathcal{F}}_2(e)}(x)\} \\ I_{\tilde{\mathcal{F}}_3(e)}(x) &= \max\{I_{\tilde{\mathcal{F}}_1(e)}(x), I_{\tilde{\mathcal{F}}_2(e)}(x)\} \\ F_{\tilde{\mathcal{F}}_3(e)}(x) &= \min\{F_{\tilde{\mathcal{F}}_1(e)}(x), F_{\tilde{\mathcal{F}}_2(e)}(x)\} \end{aligned}$$

Definition 2.7. *[49]Consider the CNS sets* $(\tilde{\mathcal{F}}_1,\acute{\mathcal{E}})$ *and* $(\tilde{\mathcal{F}}_2,\acute{\mathcal{E}})$ *on* $\mathbb{X}$. *The expression for their intersection is* $(\tilde{\mathcal{F}}_1,\acute{\mathcal{E}}) \Cap (\tilde{\mathcal{F}}_2,\acute{\mathcal{E}}) = (\tilde{\mathcal{F}}_3,\acute{\mathcal{E}})$. *defined as:*

$$(\tilde{\mathcal{F}}_3,\acute{\mathcal{E}}) = \left\{\left(e, \langle x, T_{\tilde{\mathcal{F}}_3(e)}(x), I_{\tilde{\mathcal{F}}_3(e)}(x), F_{\tilde{\mathcal{F}}_3(e)}(x)\rangle : x \in \mathbb{X}\right) : e \in \acute{\mathcal{E}}\right\},$$

Where

$$\begin{aligned} T_{\tilde{\mathcal{F}}_3(e)}(x) &= \min\{T_{\tilde{\mathcal{F}}_1(e)}(x), T_{\tilde{\mathcal{F}}_2(e)}(x)\} \\ I_{\tilde{\mathcal{F}}_3(e)}(x) &= \min\{I_{\tilde{\mathcal{F}}_1(e)}(x), I_{\tilde{\mathcal{F}}_2(e)}(x)\} \\ F_{\tilde{\mathcal{F}}_3(e)}(x) &= \max\{F_{\tilde{\mathcal{F}}_1(e)}(x), F_{\tilde{\mathcal{F}}_2(e)}(x)\} \end{aligned}$$

Definition 2.8. *[49] Consider the CNS sets* $(\tilde{\mathcal{F}}_1,\acute{\mathcal{E}})$ *and* $(\tilde{\mathcal{F}}_2,\acute{\mathcal{E}})$ *on* $\mathbb{X}$. *Then,* $(\tilde{\mathcal{F}}_1,\acute{\mathcal{E}})$ *difference* $(\tilde{\mathcal{F}}_2,\acute{\mathcal{E}})$ *operation on these sets is represented by* $(\tilde{\mathcal{F}}_1,\acute{\mathcal{E}}) \setminus (\tilde{\mathcal{F}}_2,\acute{\mathcal{E}}) = (\tilde{\mathcal{F}}_3,\acute{\mathcal{E}})$, *and is given as* $(\tilde{\mathcal{F}}_1,\acute{\mathcal{E}}) \Cap (\tilde{\mathcal{F}}_2,\acute{\mathcal{E}})^c = (\tilde{\mathcal{F}}_3,\acute{\mathcal{E}})$

$$(\tilde{\mathcal{F}}_3,\acute{\mathcal{E}}) = \left\{\left(e, \langle x, T_{\tilde{\mathcal{F}}_3(e)}(x), I_{\tilde{\mathcal{F}}_3(e)}(x), F_{\tilde{\mathcal{F}}_3(e)}(x)\rangle : x \in \mathbb{X}\right) : e \in \acute{\mathcal{E}}\right\},$$

where

$$\begin{aligned} T_{\tilde{\mathcal{F}}_3(e)}(x) &= \min\{T_{\tilde{\mathcal{F}}_1(e)}(x), F_{\tilde{\mathcal{F}}_2(e)}(x)\} \\ I_{\tilde{\mathcal{F}}_3(e)}(x) &= \min\{I_{\tilde{\mathcal{F}}_1(e)}(x), 1 - I_{\tilde{\mathcal{F}}_2(e)}(x)\} \\ F_{\tilde{\mathcal{F}}_3(e)}(x) &= \max\{F_{\tilde{\mathcal{F}}_1(e)}(x), T_{\tilde{\mathcal{F}}_2(e)}(x)\} \end{aligned}$$

Definition 2.9. *[49] Suppose that* $\{(\tilde{\mathcal{F}}_i,\acute{\mathcal{E}}) : i \in I\}$ *be a collection of CNS sets defined on* $\mathbb{X}$. *So,*

$$\bigcup_{i\in I}(\tilde{\mathcal{F}}_i,\acute{\mathcal{E}}) = \left\{\left(e, \langle x, \sup_{i\in I} T_{\tilde{\mathcal{F}}_{i(e)}}(x), \sup_{i\in I} I_{\tilde{\mathcal{F}}_{i(e)}}(x), \inf_{i\in I} F_{\tilde{\mathcal{F}}_{i(e)}}(x)\rangle : x \in \mathbb{X}\right) : e \in \acute{\mathcal{E}}\right\}.$$

$$\bigcap_{i\in I}(\tilde{\mathcal{F}}_i,\acute{\mathcal{E}}) = \left\{\left(e, \langle x, \inf_{i\in I} T_{\tilde{\mathcal{F}}_{i(e)}}(x), \inf_{i\in I} I_{\tilde{\mathcal{F}}_{i(e)}}(x), \sup_{i\in I} F_{\tilde{\mathcal{F}}_{i(e)}}(x)\rangle : x \in \mathbb{X}\right) : e \in \acute{\mathcal{E}}\right\}.$$

Definition 2.10. *[49] Consider the CNS sets $(\tilde{\mathcal{F}}_1, \acute{\mathcal{E}})$ and $(\tilde{\mathcal{F}}_2, \acute{\mathcal{E}})$ on $\mathbb{X}$. The AND operation between them is then expressed as: $(\tilde{\mathcal{F}}_1, \acute{\mathcal{E}}) \wedge (\tilde{\mathcal{F}}_2, \acute{\mathcal{E}}) = (\tilde{\mathcal{F}}_3, \acute{\mathcal{E}} \times \acute{\mathcal{E}})$*

$$(\tilde{\mathcal{F}}, \acute{\mathcal{E}} \times \acute{\mathcal{E}}) = \left\{ \left((e_1, e_2), \langle x, T_{\tilde{\mathcal{F}}_3(e_1,e_2)}(x), I_{\tilde{\mathcal{F}}_3(e_1,e_2)}(x), F_{\tilde{\mathcal{F}}_3(e_1,e_2)}(x) \rangle : x \in \mathbb{X} \right) : (e_1, e_2) \in \acute{\mathcal{E}} \times \acute{\mathcal{E}} \right\}.$$

where

$$\begin{aligned} T_{\tilde{\mathcal{F}}_3(e_1,e_2)}(x) &= \min \left\{ T_{\tilde{\mathcal{F}}_1(e_1,e_2)}(x), T_{\tilde{\mathcal{F}}_2(e_1,e_2)}(x) \right\}, \\ I_{\tilde{\mathcal{F}}_3(e_1,e_2)}(x) &= \min \left\{ I_{\tilde{\mathcal{F}}_1(e_1,e_2)}(x), I_{\tilde{\mathcal{F}}_2(e_1,e_2)}(x) \right\}, \\ F_{\tilde{\mathcal{F}}_3(e_1,e_2)}(x) &= \max \left\{ F_{\tilde{\mathcal{F}}_1(e_1,e_2)}(x), F_{\tilde{\mathcal{F}}_2(e_1,e_2)}(x) \right\}. \end{aligned}$$

Definition 2.11. *[49] Consider the CNS sets $(\tilde{\mathcal{F}}_1, \acute{\mathcal{E}})$ and $(\tilde{\mathcal{F}}_2, \acute{\mathcal{E}})$ on $\mathbb{X}$. The OR operation that is then applied to these sets is indicated by $(\tilde{\mathcal{F}}_1, \acute{\mathcal{E}}) \vee (\tilde{\mathcal{F}}_2, \acute{\mathcal{E}}) = (\tilde{\mathcal{F}}_3, \acute{\mathcal{E}} \times \acute{\mathcal{E}})$ and is given by:*

$$(\tilde{\mathcal{F}}, \acute{\mathcal{E}} \times \acute{\mathcal{E}}) = \left\{ \left((e_1, e_2), \langle x, T_{\tilde{\mathcal{F}}_3(e_1,e_2)}(x), I_{\tilde{\mathcal{F}}_3(e_1,e_2)}(x), F_{\tilde{\mathcal{F}}_3(e_1,e_2)}(x) \rangle : x \in \mathbb{X} \right) : (e_1, e_2) \in \acute{\mathcal{E}} \times \acute{\mathcal{E}} \right\}.$$

where

$$\begin{aligned} T_{\tilde{\mathcal{F}}_3(e_1,e_2)}(x) &= \max \left\{ T_{\tilde{\mathcal{F}}_1(e_1,e_2)}(x), T_{\tilde{\mathcal{F}}_2(e_1,e_2)}(x) \right\}, \\ I_{\tilde{\mathcal{F}}_3(e_1,e_2)}(x) &= \max \left\{ I_{\tilde{\mathcal{F}}_1(e_1,e_2)}(x), I_{\tilde{\mathcal{F}}_2(e_1,e_2)}(x) \right\}, \\ F_{\tilde{\mathcal{F}}_3(e_1,e_2)}(x) &= \min \left\{ F_{\tilde{\mathcal{F}}_1(e_1,e_2)}(x), F_{\tilde{\mathcal{F}}_2(e_1,e_2)}(x) \right\}. \end{aligned}$$

Definition 2.12. *[49] A null CNS set is defined as a CNS set $(\tilde{\mathcal{F}}, \acute{\mathcal{E}})$ on $\mathbb{X}$ if*

$$T_{\tilde{\mathcal{F}}(e)}(x) = 0, \quad I_{\tilde{\mathcal{F}}(e)}(x) = 0, \quad F_{\tilde{\mathcal{F}}(e)}(x) = 1, \quad \forall\, e \in \acute{\mathcal{E}}, \forall\, x \in \mathbb{X}.$$

$0_{(\mathbb{X}, \acute{\mathcal{E}})}$ is the symbol for it.

Definition 2.13. *[49] $(\tilde{\mathcal{F}}, \acute{\mathcal{E}})$ on $\mathbb{X}$ is referred to as a CNS set absolute CNS set if*

$$T_{\tilde{\mathcal{F}}(e)}(x) = 1, \quad I_{\tilde{\mathcal{F}}(e)}(x) = 1, \quad F_{\tilde{\mathcal{F}}(e)}(x) = 0, \quad \forall\, e \in \acute{\mathcal{E}}, \forall\, x \in \mathbb{X},$$

Evidently,

$$0^c_{(\mathbb{X}, \acute{\mathcal{E}})} = 1_{(\mathbb{X}, \acute{\mathcal{E}})}, \quad 1^c_{(\mathbb{X}, \acute{\mathcal{E}})} = 0_{(\mathbb{X}, \acute{\mathcal{E}})}.$$

Definition 2.14. *[49] The family of all CNS sets defined on $\mathbb{X}$ and $\tau \subset CNSS(\mathbb{X}, \acute{\mathcal{E}})$ is represented by the CNS set $(\mathbb{X}, \acute{\mathcal{E}})$. The CNS topology on $\mathbb{X}$ is therefore defined as τ if*

(1) $0_{(\mathbb{X}, \acute{\mathcal{E}})}$ and $1_{(\mathbb{X}, \acute{\mathcal{E}})} \in \tau$,

(2) If any number of CNS sets are taken from τ, their union also lies in τ,

(3) If a finite number of CNS sets are taken from τ, then their intersection also lies in τ.

Then, a CNST space (CNSTS) over $\mathbb{X}$ is defined as $(\mathbb{X}, \tau, \acute{\mathcal{E}})$. A CNS open set is defined for each element of τ.

Definition 2.15. *[49] The CNST space $(\mathbb{X}, \tau, \acute{\mathcal{E}})$ and the CNS set $(\tilde{\mathcal{F}}, \acute{\mathcal{E}})$ over $\mathbb{X}$ are considered. If and only if its counterpart is a CNS open set, then $(\tilde{\mathcal{F}}, \acute{\mathcal{E}})$ is a CNS closed set.*

Definition 2.16. *[49] The family of all CNS sets in the universe $\mathbb{X}$ is represented by the CNS set $(\mathbb{X}, \acute{\mathcal{E}})$.*

(1) If $\tau = \{0_{(\mathbb{X},\acute{\mathcal{E}})}, 1_{(\mathbb{X},\acute{\mathcal{E}})}\}$, then τ is referred to as a CNS indiscrete topology, and $(\mathbb{X}, \tau, \acute{\mathcal{E}})$ is defined as a CNS indiscrete topological space over $\mathbb{X}$.

(2) If $\tau = CNSS(\mathbb{X}, \acute{\mathcal{E}})$, then τ is called a CNS discrete topology and $(\mathbb{X}, \tau, \acute{\mathcal{E}})$ is referred to as a CNS discrete topological space over $\mathbb{X}$.

Definition 2.17. *[49] Let $(\mathbb{X}, \tau, \acute{\mathcal{E}})$ be a CNST space over $\mathbb{X}$ and $(\tilde{\mathcal{F}}, \acute{\mathcal{E}}) \in CNSS(\mathbb{X}, \acute{\mathcal{E}})$ be a CNS set. Then, the CNS interior of $(\tilde{\mathcal{F}}, \acute{\mathcal{E}})$, represented by $(\tilde{\mathcal{F}}, \acute{\mathcal{E}})^\circ$ is referred to as the neutrosophic soft union of all CNS open subsets of $(\tilde{\mathcal{F}}, \acute{\mathcal{E}})$.*
Clearly $(\tilde{\mathcal{F}}, \acute{\mathcal{E}})^\circ$ is the greatest CNS open subset contained within $(\tilde{\mathcal{F}}, \acute{\mathcal{E}})$.

Definition 2.18. *[49] Suppose that $(\mathbb{X}, \tau, \acute{\mathcal{E}})$ be a CNST space over $\mathbb{X}$ and $(\tilde{\mathcal{F}}, \acute{\mathcal{E}}) \in CNSS(\mathbb{X}, \acute{\mathcal{E}})$ be a CNSS. Then, the CNS closure of $(\tilde{\mathcal{F}}, \acute{\mathcal{E}})$, denoted by $\overline{(\tilde{\mathcal{F}}, \acute{\mathcal{E}})}$ is given by the CNS intersection of all the CNS closed supersets of $(\tilde{\mathcal{F}}, \acute{\mathcal{E}})$.*
Clearly $\overline{(\tilde{\mathcal{F}}, \acute{\mathcal{E}})}$ is the minimal CNS closed set that contains $(\tilde{\mathcal{F}}, \acute{\mathcal{E}})$.

3. Complex Neutrosophic Soft Compact Spaces

Definition 3.1. *The complex neutrosophic soft set $x^{\grave{e}}_{\langle s'_1, s'_2, s'_3\rangle}$ is called a complex neutrosophic soft point for every point $\mathbf{x} \in \mathbf{X}$, $0 \preceq s'_1, s'_2, s'_3 \preceq 1, \grave{e} \in \mathcal{E}$, and is given by:*

$$x^{\grave{e}}_{\langle s'_1, s'_2, s'_3\rangle}(\grave{e}')(y) = \begin{cases} \langle s'_1, s'_2, s'_3\rangle, & \text{if } \grave{e}' = \grave{e} \text{ and } y = x, \\ (0,0,1), & \text{if } \grave{e}' \neq \grave{e} \text{ or } y \neq x. \end{cases}$$

Definition 3.2. *Let $(\mathbf{X}, \tau^{CNSS}, \mathcal{E})$ be a complex neutrosophic soft topological space over $\mathbf{X}$. And $(\tilde{F}, \mathcal{E}) \in CNSS(\mathbf{X}, \mathcal{E})$. Then $(\tilde{F}, \mathcal{E})$ is called CNS neighbourhood of a CNS point $x^{\grave{e}}_{(s'_1, s'_2, s'_3)} \in (\tilde{F}, \mathcal{E})$, if there exists a CNS open set $(\tilde{G}, \mathcal{E})$ such that $x^{\grave{e}}_{(s'_1, s'_2, s'_3)} \in (\tilde{G}, \mathcal{E}) \subset (\tilde{F}, \mathcal{E})$.*

Definition 3.3. *Let $(\mathbf{X}, \tau^{CNSS}, \mathcal{E})$ be a complex neutrosophic soft topological space over $\mathbf{X}$ and $(x^{\grave{e}}_{(s'_1, s'_2, s'_3)})$ and $(y^{\grave{e}'}_{(s'_1, s'_2, s'_3)})$ are distinct complex neutrosophic soft points. If there exist complex neutrosophic soft open sets $(\tilde{F}, \mathcal{E})$ and $(\tilde{G}, \mathcal{E})$, such that $(x^{\grave{e}}_{(s'_1, s'_2, s'_3)}) \in (\tilde{F}, \mathcal{E})$ and*

$$(x^{\grave{e}}_{(s'_1, s'_2, s'_3)}) \in (\tilde{F}, \mathcal{E}) \cap (\tilde{G}, \mathcal{E}) = 0_{(\mathbf{X}, \mathcal{E})}.$$

or $(y^{\grave{e}'}_{(s'_1, s'_2, s'_{3,})}) \in (\tilde{G}, \mathcal{E})$ and

$$(y^{\grave{e}'}_{(s'_1, s'_2, s'_{3,})}) \cap (\tilde{F}, \mathcal{E}) = 0_{(\mathbf{X}, \mathcal{E})}.$$

Then $(\mathbf{X}, \tau^{CNSS}, \mathcal{E})$ is called complex neutrosophic soft T_1 space.

Definition 3.4. *Let $(\mathbf{X}, \tau, \mathcal{E})$ be a complex neutrosophic soft topological space over $\mathbf{X}$ and $(x^{\grave{e}}_{(s'_1, s'_2, s'_3)})$ and $(y^{\grave{e}'}_{(s'_1, s'_2, s'_3)})$ are distinct complex neutrosophic soft points. If there exist complex neutrosophic soft open sets $(\tilde{F}, \mathcal{E})$ and $(\tilde{G}, \mathcal{E})$, such that $(x^{\grave{e}}_{(s'_1, s'_2, s'_3)}) \in (\tilde{F}, \mathcal{E})$, $(y^{\grave{e}'}_{(s'_1, s'_2, s'_3)}) \in (\tilde{G}, \mathcal{E})$ and*

$$(\tilde{F}, \mathcal{E}) \cap (\tilde{G}, \mathcal{E}) = 0_{(\mathbf{X}, \mathcal{E})}.$$

Then $(\mathbf{X}, \tau, \mathcal{E})$ is called complex neutrosophic soft T_2 space (neutrosophic soft Hausdroff space).

Definition 3.5. *A complex neutrosophic soft topological space $(\mathbf{X}, \tau^{CNSS}, \mathcal{E})$ over $\mathbf{X}$ is called a complex neutrosophic soft normal space if for every pair of disjoint complex neutrosophic soft closed sets $(\tilde{F}_1, \mathcal{E})$, $(\tilde{F}_2, \mathcal{E})$, there exists disjoint complex neutrosophic soft open sets $(\tilde{G}_1, \mathcal{E})$, $(\tilde{G}_2, \mathcal{E})$ such that $(\tilde{F}_1, \mathcal{E}) \subset (\tilde{G}_2, \mathcal{E})$ and $(\tilde{F}_2, \mathcal{E}) \subset (\tilde{G}_2, \mathcal{E})$. Then, $(\mathbf{X}, \tau^{CNSS}, \mathcal{E})$ is said to be complex neutrosophic soft $T_4 -$ space if it is a complex neutrosophic soft normal and complex neutrosophic soft $T_1 -$ space.*

Definition 3.6. *Let $(\mathbf{X}, \tau^{CNSS}, \mathcal{E})$ be a complex neutrosophic soft topological space over $\mathbf{X}$ and $(\tilde{F}, \mathcal{E})$ be an arbitrary complex neutrosophic soft set. Then*

$$\tau = \{(\tilde{F}, \mathcal{E}) \cap (\tilde{H}, \mathcal{E}) : (\tilde{H}, \mathcal{E}) \in \tau\}$$

is said to be complex neutrosophic soft topology on $(\tilde{F}, \mathcal{E})$ and $(\mathbf{X}, \tau^{CNSS}, \mathcal{E})$ is called a quadri-partitioned neutrosophic soft topological subspace of $(\mathbf{X}, \tau^{CNSS}, \mathcal{E})$.

Definition 3.7. *(a). Let I be a set and $\tilde{v} = \{(\tilde{F}, \mathcal{E})_i : i \in I\}$ be a family of subsets of $NSS(\mathbf{X}, \mathcal{E})$. If $(\tilde{F}, \mathcal{E})_i \subseteq U$ for $i \in I$ and $\bigcup_{i \in I}(\tilde{F}, \mathcal{E})_i = \tilde{1}_{\mathbf{X},\mathcal{E}}$, then $\tilde{v}$ is called a* cover *of the complex neutrosophic soft subset $\tilde{1}_{\mathbf{X},\mathcal{E}}$. If $(\tilde{F}, \mathcal{E})_i = \tilde{1}_{\mathbf{X},\mathcal{E}}$, then $\tilde{v}$ is called a* complex neutrosophic soft cover *of $\tilde{1}_{\mathbf{X},\mathcal{E}}$.*
(b). If the number of elements of $\tilde{v}$ is finite or countable, then $\tilde{v}$ is called a finite *or* countable *complex neutrosophic soft cover, respectively.*
(c). Let $\tilde{v} = \{(\tilde{F}, \mathcal{E})_i : i \in I\}$ be a complex neutrosophic soft cover of $\tilde{1}_{\mathbf{X},\mathcal{E}}$. If $\tilde{v}' = \{(\tilde{F}, \mathcal{E})_i : i \in I',\ I' \subset I\}$ is a complex neutrosophic soft subfamily of $\tilde{v}$ and it is also a cover of $\tilde{1}_{\mathbf{X},\mathcal{E}}$, then $\tilde{v}'$ is called a complex neutrosophic soft subcover *of $\tilde{v}$. (d). A family $\tilde{v}$ of complex neutrosophic soft sets is called a* centralized complex neutrosophic soft family *if every finite complex neutrosophic soft subfamily of $\tilde{v}$ has non-empty intersection.*

Definition 3.8. *(a). Let $(\mathbf{X}, \tau^{CNSS}, \mathcal{E})$ be a complex neutrosophic soft topological space over $\mathbf{X}$ and $\tilde{v}$ be a complex neutrosophic soft cover of $\tilde{1}_{\mathbf{X},\mathcal{E}}$. If every element of the cover $\tilde{v}$ is a complex neutrosophic soft open (closed) set in $(\mathbf{X}, \tau^{CNSS}, \mathcal{E})$, then $\tilde{v}$ is called a* complex neutrosophic soft open (closed) cover.
(b). If there is a complex neutrosophic soft neighborhood that intersects only finitely many elements of the cover $\tilde{v}$ of each $x^e_{(s_1', s_2', s_3')} \in CNSS(\mathbf{X}, \mathcal{E})$, then $\tilde{v}$ is called a complex neutrosophic soft locally finite cover.
(c). If each $(\tilde{F}, \mathcal{E})_i$ of the cover $\tilde{v}$ intersects only finitely many other elements, then $\tilde{v}$ is called a complex neutrosophic soft star finite cover.
(d). If each $x^e_{(s_1', s_2', s_3')} \in CNSS(\mathbf{X}, \mathcal{E})$ belongs to only finitely many elements of the cover $\tilde{v}$, then $\tilde{v}$ is called a complex neutrosophic soft point finite cover.

Remark 3.1. *If the complex neutrosophic soft coverings are open in Definition , each complex neutrosophic soft star with finite cover is complex neutrosophic soft locally finite, and every complex neutrosophic soft locally finite cover is complex neutrosophic soft point finite.*

Definition 3.9. *Let $(\mathbf{X}, \tau^{CNSS}, \mathcal{E})$ be a complex complex neutrosophic soft topological space over $\mathbf{X}$ and $(\tilde{F}, \mathcal{E}) \in CNSS(\mathbf{X}, \mathcal{E})$.*

(a) If every complex complex neutrosophic soft open cover of $(\mathbf{X}, \tau^{CNSS}, \mathcal{E})$ *has a finite complex complex neutrosophic soft subcover, then* $(\mathbf{X}, \tau^{CNSS}, \mathcal{E})$ *is called a* complex complex neutrosophic soft compact space.

(b) If $\left((\tilde{F}, \mathcal{E}), \tau^{CNSS}_{(\tilde{F},\mathcal{E})}\right)$ *is a complex complex neutrosophic soft compact space, then* $(\tilde{F}, \mathcal{E})$ *is called a* complex complex neutrosophic soft compact set *in* $(\mathbf{X}, \tau^{CNSS}, \mathcal{E})$.

Example 3.1. *Let* $X = \{x_1, x_2, x_3\}$ *be an initial universe and* $E = \{e_1, e_2\}$ *a set of parameters. Let*

$$\tau^{CNSS} = \{0_{(\mathbf{X},\mathcal{E})}, 1_{(\mathbf{X},\mathcal{E})}, (\tilde{F}_1, \mathcal{E}), (\tilde{F}_2, \mathcal{E}), (\tilde{F}_3, \mathcal{E})\}.$$

$$(\tilde{F}_1, \mathcal{E}) = \left\{ \begin{array}{l} e_1 = \{\langle x_1, (e^0, 0e^{\iota 1}, e^0)\rangle, \langle x_2, (0e^{\iota 1}, e^0, e^0)\rangle, \langle x_3, (0e^{\iota 1}, 0e^{\iota 1}, e^0)\rangle\}, \\ e_2 = \{\langle x_1, (0e^{\iota 1}, 0e^{\iota 1}, e^0)\rangle, \langle x_2, (e^0, 0e^{\iota 1}, e^0)\rangle, \langle x_3, (e^0, e^0, 0e^{\iota 1})\rangle\} \end{array} \right\}.$$

$$(\tilde{F}_2, \mathcal{E}) = \left\{ \begin{array}{l} e_1 = \{\langle x_1, (0e^{\iota 1}, e^0, 0e^{\iota 1})\rangle, \langle x_2, (e^0, e^0, 0e^{\iota 1})\rangle, \langle x_3, (e^0, e^0, 0e^{\iota 1})\rangle\}, \\ e_2 = \{\langle x_1, (e^0, e^0, 0e^{\iota 1})\rangle, \langle x_2, (e^0, e^0, 0e^{\iota 1})\rangle, \langle x_3, (0e^{\iota 1}, e^0, 0e^{\iota 1})\rangle\} \end{array} \right\}.$$

$$(\tilde{F}_3, \mathcal{E}) = \left\{ \begin{array}{l} e_1 = \{\langle x_1, (0e^{\iota 1}, 0e^{\iota 1}, e^0)\rangle, \langle x_2, (0e^{\iota 1}, e^0, e^0)\rangle, \langle x_3, (0e^{\iota 1}, 0e^{\iota 1}, e^0)\rangle\}, \\ e_2 = \{\langle x_1, (0e^{\iota 1}, 0e^{\iota 1}, e^0)\rangle, \langle x_2, (e^0, 0e^{\iota 1}, e^0)\rangle, \langle x_3, (0e^{\iota 1}, e^0, 0e^{\iota 1})\rangle\} \end{array} \right\}.$$

Since

$$1_{(\mathbf{X},\mathcal{E})} = \bigcup_{i=1}^{3} (\tilde{F}_i, \mathcal{E}),$$

the family

$$\{(\tilde{F}_1, \mathcal{E}), (\tilde{F}_2, \mathcal{E}), (\tilde{F}_3, \mathcal{E})\}$$

is a complex neutrosophic soft open cover of $(\mathbf{X}, \tau^{CNSS}, \mathcal{E})$.

Also,

$$1_{(\mathbf{X},\mathcal{E})} = (\tilde{F}_1, \mathcal{E}) \cup (\tilde{F}_2, \mathcal{E}),$$

which gives a finite subcover. Therefore, $(\mathbf{X}, \tau^{CNSS}, \mathcal{E})$ *is a complex neutrosophic soft compact space.*

Theorem 3.1. *Let* $(\mathbf{X}, \tau^{CNSS}, \mathcal{E})$ *be a complex neutrosophic soft topological space over* X *and* $(\tilde{F}, \mathcal{E}) \in CNSS(\mathbf{X}, \mathcal{E})$. $(\tilde{F}, \mathcal{E})$ *is a complex neutrosophic soft compact set if and only if every complex neutrosophic soft open cover of* $(\tilde{F}, \mathcal{E})$ *has a finite complex neutrosophic soft subcover in* $(\mathbf{X}, \tau^{CNSS}, \mathcal{E})$.

Proof. Let $(\tilde{F}, \mathcal{E}) \in CNSS(\mathbf{X}, \mathcal{E})$ be a complex neutrosophic soft compact set and the family $\tilde{v} = \{(\tilde{F}, \mathcal{E}) :\in I\}$ is a complex neutrosophic soft open cover $(\tilde{F}, \mathcal{E})$ in $(\mathbf{X}, \tau^{CNSS}, \mathcal{E})$. Then, $(\tilde{F}, \mathcal{E}) \subseteq \bigcup_{i\in I}(\tilde{F}, \mathcal{E})_i \to (\tilde{F}, \mathcal{E}) = \bigcup_{i\in I}((\tilde{F}, \mathcal{E}) \cap (\tilde{F}, \mathcal{E})_i)$ is obtained that is, family $\{(\tilde{F}, \mathcal{E})_{i_j}\}_{j=1,n}$ is a complex neutrosophic soft finite subcover of $(\tilde{F}, \mathcal{E})$.

Conversely, let family $\{(\tilde{G}, \mathcal{E})_i : i \in I\}$ be a complex neutrosophic soft open cover of $((\tilde{F}, \mathcal{E}), \tau^{NSS}_{(\tilde{F},\mathcal{E})})$. Since each $i \in I$ is $(\tilde{G}, \mathcal{E})_i \in \tau^{NSS}_{(\tilde{F},\mathcal{E})}$, there is $(\tilde{F}, \mathcal{E})_i \in \tau^{NSS}$ such that $(\tilde{G}, \mathcal{E})_i = (\tilde{F}, \mathcal{E}) \cap (\tilde{F}, \mathcal{E})_i$. Thus family $\{(\tilde{F}, \mathcal{E})_i : i \in I\}$ is a complex neutrosophic soft open covering of the $(\tilde{F}, \mathcal{E})$ in $(\mathbf{X}, \tau^{CNSS}, \mathcal{E})$ and $\exists (\tilde{F}, \mathcal{E})_{i1} \ldots (\tilde{F}, \mathcal{E})_{in} : (\tilde{F}, \mathcal{E}) \subseteq \bigcup_{j=1}^{n}(\tilde{F}, \mathcal{E})_{ij} \to (\tilde{F}, \mathcal{E}) = (\tilde{F}, \mathcal{E}) \cap (\bigcup_{j=1}^{n}(\tilde{F}, \mathcal{E})_{ij}) = \bigcup_{j=1}^{n}((\tilde{F}, \mathcal{E}) \cap (\tilde{F}, \mathcal{E})_{ij}) = \bigcup_{j=1}^{n}(\tilde{G}, \mathcal{E})_{ij}$ is obtained from the condition of theorem. □

It is sometimes quite difficult to prove that a given complex neutrosophic soft topological space is complex neutrosophic soft compact by appealing directly to the definition. The following theorems give several equivalent forms of complex neutrosophic soft compactness which are often easier to apply.

Theorem 3.2. *Let $(\mathbf{X}, \tau^{CNSS}, \mathcal{E})$ be a complex neutrosophic soft topological space over $\mathbf{X}$. $1_{(\mathbf{X},\mathcal{E})}$ is complex neutrosophic soft compact space if and only if every family of complex neutrosophic soft closed sets with empty intersection in $(\mathbf{X}, \tau^{CNSS}, \mathcal{E})$ has a finite subfamily with empty intersection.*

Proof. Let $(\mathbf{X}, \tau^{CNSS}, \mathcal{E})$ be a complex neutrosophic soft compact space, and the intersection of the family $\tilde{v} = \{(\tilde{F}, \mathcal{E})_i : i \in I\}$ is the complex neutrosophic soft closed sets family which is empty. Then, the family $\tilde{v} = \{(\tilde{G}, \mathcal{E})_i = 1_{(\mathbf{X},\mathcal{E})} \setminus (\tilde{F}, \mathcal{E})_i : i \in I\}$ is the complex neutrosophic soft open sets family and we obtain

$$\bigcup_{i\in I}(\tilde{G}, \mathcal{E})_i = \bigcup_{i\in I}(1_{(\mathbf{X},\mathcal{E})} \setminus (\tilde{F}, \mathcal{E})_i) = 1_{(\mathbf{X},\mathcal{E})} \setminus (\bigcap_{i\in I}(\tilde{F}, \mathcal{E})_i) = 1_{(\mathbf{X},\mathcal{E})} \setminus 0_{(\mathbf{X},\mathcal{E})} = 1_{(\mathbf{X},\mathcal{E})}.$$

Thus, the family $\tilde{v} = \{(\tilde{G}, \mathcal{E})_i\}$ is a complex neutrosophic soft open covering of $1_{(\mathbf{X},\mathcal{E})}$. Since $(\mathbf{X}, \tau^{CNSS}, \mathcal{E})$ is a complex neutrosophic soft compact space, $\exists (\tilde{G}, \mathcal{E})_{i1}, \ldots, (\tilde{G}, \mathcal{E})_{in} : 1_{(\mathbf{X},\mathcal{E})} = \bigcup_{j=1}^{n}(\tilde{G}, \mathcal{E})_{ij}$ is obtained.

Now the intersection of the finite subfamily $\{(\tilde{F}, \mathcal{E})_{ij}\}_{j=1,n}$ of the complex neutrosophic soft family $\tilde{v} = \{(\tilde{F}, \mathcal{E})_i\}_{i\in I}$ and we obtain

$$\bigcap_{j=1}^{n}(\tilde{F}, \mathcal{E})_{ij} = \bigcap_{j=1}^{n}(1_{(\mathbf{X},\mathcal{E})} \setminus (\tilde{G}, \mathcal{E})_{ij}) = 1_{(\mathbf{X},\mathcal{E})} \setminus \bigcup_{j=1}^{n}(\tilde{G}, \mathcal{E})_i = 1_{(\mathbf{X},\mathcal{E})} \setminus 1_{(\mathbf{X},\mathcal{E})} = 0_{(\mathbf{X},\mathcal{E})}.$$

Conversely, let family $\tilde{v} = \{(\tilde{G}, \mathcal{E})_i : i \in I\}$ be a complex neutrosophic soft open covering of $1_{(\mathbf{X},\mathcal{E})}$. The intersection of the complex neutrosophic soft closed sets family $\tilde{v} = \{(\tilde{F}, \mathcal{E})_i = 1_{(\mathbf{X},\mathcal{E})} \setminus (\tilde{G}, \mathcal{E})_i : i \in I\}$ is empty. Really,

$$\bigcap_{i\in I}(\tilde{F}, \mathcal{E})_i = \bigcap_{i\in I}(1_{(\mathbf{X},\mathcal{E})} \setminus (\tilde{G}, \mathcal{E})_i) = 1_{(\mathbf{X},\mathcal{E})} \setminus \bigcup_{i\in I}(\tilde{G}, \mathcal{E})_i = 1_{(\mathbf{X},\mathcal{E})} \setminus 1_{(\mathbf{X},\mathcal{E})} = 0_{(\mathbf{X},\mathcal{E})}.$$

Then, from the condition of theorem $\exists (\tilde{F}, \mathcal{E})_{i1}, \ldots, (\tilde{F}, \mathcal{E})_{in} : \bigcap_{j=1}^{n}(\tilde{F}, \mathcal{E})_{ij} = 0_{(\mathbf{X},\mathcal{E})}$ can be written. Hence,

$$\bigcup_{j=1}^{n}(\tilde{G}, \mathcal{E})_{ij} = \bigcup_{j=1}^{n}(1_{(\mathbf{X},\mathcal{E})} \setminus (\tilde{F}, \mathcal{E})_{ij}) = 1_{(\mathbf{X},\mathcal{E})} \setminus \bigcap_{j=1}^{n}(\tilde{F}, \mathcal{E})_i = 1_{(\mathbf{X},\mathcal{E})} \setminus 0_{(\mathbf{X},\mathcal{E})} = 1_{(\mathbf{X},\mathcal{E})}.$$

Thus, the complex neutrosophic soft finite sub-covering of complex neutrosophic soft $\tilde{v} = \{(\tilde{F}, \mathcal{E})_i\}_{i\in I}$ covering of $1_{(\mathbf{X},\mathcal{E})}$ was found. As a result, $(\mathbf{X}, \tau^{CNSS}, \mathcal{E})$ is complex neutrosophic soft compact space. □

Theorem 3.3. *Let $(\mathbf{X}, \tau^{CNSS}, \mathcal{E})$ be a complex neutrosophic soft topological space over $\mathbf{X}$. $(\mathbf{X}, \tau^{CNSS}, \mathcal{E})$ is a complex neutrosophic soft compact space if and only if the complex neutrosophic soft intersection of all sets of every complex neutrosophic soft centered closed sets family is different from empty in $1_{(\mathbf{X},\mathcal{E})}$.*

Proof. Let $(\mathbf{X}, \tau^{CNSS}, \mathcal{E})$ be a complex neutrosophic soft compact over $\mathbf{X}$, and $\tilde{v} = \{(\tilde{F}, \mathcal{E})_i\}_{i\in I}$ be complex neutrosophic soft centered closed sets family. Suppose it is $\bigcap_{i\in I}(\tilde{F}, \mathcal{E})_i = 0_{(\mathbf{X},\mathcal{E})}$. Then, family $\tilde{v} = \{(\tilde{G}, \mathcal{E})_i = 1_{(\mathbf{X},\mathcal{E})} \setminus (\tilde{F}, \mathcal{E})_i\}_{i\in I}$ is an open covering of $1_{(\mathbf{X},\mathcal{E})}$ since $(\mathbf{X}, \tau^{CNSS}, \mathcal{E})$ is a complex neutrosophic soft compact space. $\exists (\tilde{G}, \mathcal{E})_{i1}, \ldots, (\tilde{G}, \mathcal{E})_{in} : 1_{(\mathbf{X},\mathcal{E})} = \bigcup_{j=1}^{n}(\tilde{G}, \mathcal{E})_{ij}$ written. In this case $\bigcap_{j=1}^{n}(\tilde{F}, \mathcal{E})_{ij} = \bigcap_{j=1}^{n}(1_{(\mathbf{X},\mathcal{E})} \setminus (\tilde{G}, \mathcal{E})_{ij}) = 1_{(\mathbf{X},\mathcal{E})} \setminus (\bigcup_{j=1}^{n}(\tilde{G}, \mathcal{E})_i) = 1_{(\mathbf{X},\mathcal{E})} \setminus 1_{(\mathbf{X},\mathcal{E})} = 0_{(\mathbf{X},\mathcal{E})}$.

If it is, it contradicts with $\tilde{v}$ is a complex neutrosophic soft centered family. In that case, the assumption is wrong, so it is $\bigcap_{i\in I}(\tilde{F}, \mathcal{E})_i \neq 0_{(\mathbf{X},\mathcal{E})}$.

Conversely, the theorem is provided, but $(\mathbf{X}, \tau^{CNSS}, \mathcal{E})$ is not complex neutrosophic soft compact space. Then, there is no finite complex neutrosophic soft sub-covering of $\{(\tilde{G}, \mathcal{E})_i\}_{i\in I}$ complex neutrosophic soft open covering of $1_{(\mathbf{X},\mathcal{E})}$. Thus, $\bigcup_{j=1}^{n}(\tilde{G}, \mathcal{E})_i \neq 1_{(\mathbf{X},\mathcal{E})}$ is obtained for any $(\tilde{G}, \mathcal{E})_{i1}, \ldots, (\tilde{G}, \mathcal{E})_{in}$ finite complex neutrosophic soft subfamily of $\tilde{v}$ complex neutrosophic soft family. Consider the family of $\tilde{v} = \{(\tilde{F}, \mathcal{E})_i = 1_{(\mathbf{X},\mathcal{E})} \setminus (\tilde{G}, \mathcal{E})_i\}_{i\in I}$ complex neutrosophic soft closed sets. Here, because $\bigcap_{j=1}^{n}(\tilde{F}, \mathcal{E})_{ij} = \bigcap_{j=1}^{n}(1_{(\mathbf{X},\mathcal{E})} \setminus (\tilde{G}, \mathcal{E})_{ij}) = 1_{(\mathbf{X},\mathcal{E})} \setminus (\bigcup_{j=1}^{n}(\tilde{G}, \mathcal{E})_i) \neq 0_{(\mathbf{X},\mathcal{E})}$,

the $\tilde{v}$ family is a complex neutrosophic soft centered closed set family and the theorem of the condition $\bigcap_{i\in I}(\tilde{F}, \mathcal{E})_i \neq 1_{(\mathbf{X},\mathcal{E})}$. Then, $1_{(\mathbf{X},\mathcal{E})} = \bigcup_{i\in I}(\tilde{G}, \mathcal{E})_i = \bigcup_{i\in I}(1_{(\mathbf{X},\mathcal{E})} \setminus (\tilde{F}, \mathcal{E})_i) = 1_{(\mathbf{X},\mathcal{E})} \setminus (\bigcap_{i\in I}(\tilde{F}, \mathcal{E})_i) \neq 1_{(\mathbf{X},\mathcal{E})}$.

So, the assumption is wrong. Thus, the proof is completed. □

Theorem 3.4. *Every complex neutrosophic soft closed subset of a complex neutrosophic soft compact topological space is complex neutrosophic soft compact.*

Proof. Let $(\mathbf{X}, \tau^{CNSS}, \mathcal{E})$ be a complex neutrosophic soft compact space, complex neutrosophic soft sets family $\tilde{v} = \{(\tilde{F}, \mathcal{E})_i\}_{i\in I}$ be an open cover of $(\tilde{F}, \mathcal{E})$.

In this case, $(\tilde{F}, \mathcal{E}) \subseteq \bigcup_{i\in I}(\tilde{F}, \mathcal{E})_i$ and $(\tilde{F}, \mathcal{E})$ are complex neutrosophic soft closed, so the $1_{(\mathbf{X},\mathcal{E})} \setminus (\tilde{F}, \mathcal{E})$ set is open. On the other hand, it can also be written $\exists (\tilde{F}, \mathcal{E})_{i1}, \ldots, (\tilde{F}, \mathcal{E})_{in} : (\bigcup_{j=1}^{n}(\tilde{G}, \mathcal{E})_{ij}) \cup (1_{(\mathbf{X},\mathcal{E})} \setminus (\tilde{F}, \mathcal{E})_{ij}) = 1_{(\mathbf{X},\mathcal{E})}$.

Here, $(\tilde{F}, \mathcal{E}) \subseteq \bigcup_{j=1}^{n}(\tilde{F}, \mathcal{E})_{ij}$ is obtained. Then, it is obtained that $(\tilde{F}, \mathcal{E})$ is complex neutrosophic soft compact set from Theorem 3.1. □

Corollary 3.1. *$(\tilde{F}, \mathcal{E})_{i1}, \ldots, (\tilde{F}, \mathcal{E})_{in}$ complex neutrosophic soft sets, complex neutrosophic soft closed subsets be the family of $(\mathbf{X}, \tau^{CNSS}, \mathcal{E})$. $(\tilde{F}, \mathcal{E}) \subseteq \bigcup_{j=1}^{n}(\tilde{F}, \mathcal{E})_i$ is a complex neutrosophic soft compact set if and only if for each $i = 1, \ldots, n$, $(\tilde{F}, \mathcal{E})_i$ is a complex neutrosophic soft compact set.*

In Theorem we proved that every complex neutrosophic soft closed subset of a complex neutrosophic soft compact space is complex neutrosophic soft compact. We now use the preceding theorem to show that complex neutrosophic soft compact subset Hausdorff spaces are always complex neutrosophic soft closed.

Theorem 3.5. *Every complex neutrosophic soft compact subset in a complex neutrosophic soft Hausdorff topological space is a complex neutrosophic soft closed.*

Proof. Let $(\mathbf{X}, \tau^{CNSS}, \mathcal{E})$ be a complex neutrosophic soft Hausdorff space, $(\tilde{F}, \mathcal{E}) \subseteq NSS(\mathbf{X}, \mathcal{E})$ be a complex neutrosophic soft compact set. To show that $(\tilde{F}, \mathcal{E})$ is closed, it is enough to show that the

set $1_{(\mathbf{X},\mathcal{E})} \setminus (\tilde{F},\mathcal{E})$ is open. Let

$$x^{e}_{(s_1',s_2',s_3')} \in 1_{(\mathbf{X},\mathcal{E})} \setminus (\tilde{F},\mathcal{E})$$

be any point. Then, since $(\mathbf{X},\tau^{CNSS},\mathcal{E})$ is a complex neutrosophic soft Hausdorff space, for points

$$x^{e}_{(s_1',s_2',s_3')} \neq y^{e'}_{(s_1',s_2',s_3')} \in 1_{(\mathbf{X},\mathcal{E})},$$

there exist

$$(\mathbb{U},\mathcal{E})_{x^{e}_{(s_1',s_2',s_3')},y^{e'}_{(s_1',s_2',s_3')}}, \quad (\mathbb{U},\mathcal{E})_{y^{e'}_{(s_1',s_2',s_3')},x^{e}_{(s_1',s_2',s_3')}} \in \tau^{CNSS}$$

such that

$$x^{e}_{(s_1',s_2',s_3')} \in (\mathbb{U},\mathcal{E})_{x^{e}_{(s_1',s_2',s_3')},y^{e'}_{(s_1',s_2',s_3')}}, \quad y^{e'}_{(s_1',s_2',s_3')} \in (\mathbb{V},\mathcal{E})_{y^{e'}_{(s_1',s_2',s_3')},x^{e}_{(s_1',s_2',s_3')}}$$

and

$$(\mathbb{U},\mathcal{E})_{x^{e}_{(s_1',s_2',s_3')},y^{e'}_{(s_1',s_2',s_3')}} \cap (\mathbb{V},\mathcal{E})_{y^{e'}_{(s_1',s_2',s_3')},x^{e}_{(s_1',s_2',s_3')}} = 0_{(\mathbf{X},\mathcal{E})}.$$

If $y^{e'}_{(s_1',s_2',s_3')}$ runs over all points of the complex neutrosophic soft set $(\tilde{F},\mathcal{E})$, then the family

$$\{(\mathbb{V},\mathcal{E})_{y^{e'}_{(s_1',s_2',s_3')},x^{e}_{(s_1',s_2',s_3')}}\}_{y^{e'}_{(s_1',s_2',s_3')} \in (\tilde{F},\mathcal{E})}$$

is an open cover of $1_{(\mathbf{X},\mathcal{E})}$. Since $(\tilde{F},\mathcal{E})$ is complex neutrosophic soft compact, there exist finitely many

$$(\mathbb{U},\mathcal{E})_{1y^{e'}_{(s_1',s_2',s_3')},x^{e}_{(s_1',s_2',s_3')}}, \ldots, (\mathbb{V},\mathcal{E})_{ny^{e'}_{(s_1',s_2',s_3')},x^{e}_{(s_1',s_2',s_3')}}$$

such that

$$(\tilde{F},\mathcal{E}) \subseteq \bigcup_{i=1}^{n} (\mathbb{V},\mathcal{E})_{iy^{e'}_{(s_1',s_2',s_3')},x^{e}_{(s_1',s_2',s_3')}}.$$

Consider the neighborhoods

$$(\mathbb{U},\mathcal{E})_{x^{e}_{(s_1',s_2',s_3')},y^{e'}_{(s_1',s_2',s_3')}} \quad i = 1,\ldots,n$$

that provide

$$(\mathbb{U},\mathcal{E})_{x^{e}_{(s_1',s_2',s_3')},y^{e'}_{(s_1',s_2',s_3')}} \cap (\mathbb{V},\mathcal{E})_{y^{e'}_{(s_1',s_2',s_3')},x^{e}_{(s_1',s_2',s_3')}} = 0_{(\mathbf{X},\mathcal{E})}.$$

The set

$$(\mathbb{U},\mathcal{E})_{x^{e}_{(s_1',s_2',s_3')}} = \bigcap_{i=1}^{n} (\mathbb{U},\mathcal{E})_{x^{e}_{(s_1',s_2',s_3')},iy^{e'}_{(s_1',s_2',s_3')}}$$

is a complex neutrosophic soft open neighborhood of $x^{e}_{(s_1',s_2',s_3')}$ and satisfies

$$(\tilde{F},\mathcal{E}) \cap (\mathbb{U},\mathcal{E})_{x^{e}_{(s_1',s_2',s_3')}} = (\tilde{F},\mathcal{E}) \cap \bigcap_{j=1}^{n} (\mathbb{U},\mathcal{E})_{x^{e}_{(s_1',s_2',s_3')},iy^{e'}_{(s_1',s_2',s_3')}} \subseteq$$

$$\left(\bigcup_{j=1}^{n} (\mathbb{V},\mathcal{E})_{iy^{e'}_{(s_1',s_2',s_3')},x^{e}_{(s_1',s_2',s_3')}} \right) \cap \bigcap_{j=1}^{n} (\mathbb{U},\mathcal{E})_{x^{e}_{(s_1',s_2',s_3')},iy^{e'}_{(s_1',s_2',s_3')}} = 0_{(\mathbf{X},\mathcal{E})}.$$

Here,

$$x^{e}_{(s_1',s_2',s_3')} \in (\mathbb{U},\mathcal{E})_{x^{e}_{(s_1',s_2',s_3')}} \subseteq 1_{(\mathbf{X},\mathcal{E})} \setminus (\tilde{F},\mathcal{E}),$$

so $1_{(\mathbf{X},\mathcal{E})} \setminus (\tilde{F},\mathcal{E})$ is complex neutrosophic soft open. Therefore, $(\tilde{F},\mathcal{E})$ is a complex neutrosophic soft closed set. □

Theorem 3.6. *Every complex neutrosophic soft compact Hausdorff space is complex neutrosophic soft normal space.*

Proof. Let $(\mathbf{X},\tau^{CNSS},\mathcal{E})$ be a complex neutrosophic soft compact Hausdorff space and $(\tilde{F},\mathcal{E})_1$, $(\tilde{F},\mathcal{E})_2$ be two discrete complex neutrosophic soft closed sets. From Theorem 3, these sets are complex neutrosophic soft compact.

For each $x^{e}_{(s_1',s_2',s_3')} \in (\tilde{F},\mathcal{E})_1$ and $y^{e'}_{(s_1',s_2',s_3')} \in (\tilde{F},\mathcal{E})_2$ with $x^{e}_{(s_1',s_2',s_3')} \neq y^{e'}_{(s_1',s_2',s_3')}$, since $(\mathbf{X},\tau^{CNSS},\mathcal{E})$ is a complex neutrosophic soft Hausdorff space, there exist

$$(\mathbb{U},\mathcal{E})_{x^{e}_{(s_1',s_2',s_3')},y^{e'}_{(s_1',s_2',s_3')}},\ (\mathbb{U},\mathcal{E})_{y^{e'}_{(s_1',s_2',s_3')},x^{e}_{(s_1',s_2',s_3')}} \in \tau^{CNSS}$$

such that

$$x^{e}_{(s_1',s_2',s_3')} \in (\mathbb{U},\mathcal{E})_{x^{e}_{(s_1',s_2',s_3')},y^{e'}_{(s_1',s_2',s_3')}},\quad y^{e'}_{(s_1',s_2',s_3')} \in (\mathbb{V},\mathcal{E})_{y^{e'}_{(s_1',s_2',s_3')},x^{e}_{(s_1',s_2',s_3')}}$$

and

$$(\mathbb{U},\mathcal{E})_{x^{e}_{(s_1',s_2',s_3')},y^{e'}_{(s_1',s_2',s_3')}} \cap (\mathbb{V},\mathcal{E})_{y^{e'}_{(s_1',s_2',s_3')},x^{e}_{(s_1',s_2',s_3')}} = 0_{(\mathbf{X},\mathcal{E})}.$$

Can be written for $x^{e}_{(s_1',s_2',s_3')} \neq y^{e'}_{(s_1',s_2',s_3')} \in 1_{(\mathbf{X},\mathcal{E})}$. Let us keep ${}^{0}x^{e}_{(s_1',s_2',s_3')} \in (\tilde{F},\mathcal{E})_1$ constant. Then, for each $y^{e'}_{(s_1',s_2',s_3')} \in (\tilde{F},\mathcal{E})_2$ and fixed ${}^{0}x^{e}_{(s_1',s_2',s_3')} \in (\tilde{F},\mathcal{E})_1$, we have

$$(\mathbb{U},\mathcal{E})_{0x^{e}_{(s_1',s_2',s_3')},y^{e'}_{(s_1',s_2',s_3')}},\ (\mathbb{U},\mathcal{E})_{y^{e'}_{(s_1',s_2',s_3')},0x^{e}_{(s_1',s_2',s_3')}} \in \tau^{CNSS}$$

such that

$$0x^{e}_{(s_1',s_2',s_3')} \in (\mathbb{U},\mathcal{E})_{0x^{e}_{(s_1',s_2',s_3')},y^{e'}_{(s_1',s_2',s_3')}},\quad y^{e'}_{(s_1',s_2',s_3')} \in (\mathbb{V},\mathcal{E})_{y^{e'}_{(s_1',s_2',s_3')},0x^{e}_{(s_1',s_2',s_3')}}$$

and

$$(\mathbb{U},\mathcal{E})_{0x^{e}_{(s_1',s_2',s_3')},y^{e'}_{(s_1',s_2',s_3')}} \cap (\mathbb{V},\mathcal{E})_{y^{e'}_{(s_1',s_2',s_3')},0x^{e}_{(s_1',s_2',s_3')}} = 0_{(\mathbf{X},\mathcal{E})}.$$

It is clear that the family

$$\{(\mathbb{V},\mathcal{E})_{y^{e'}_{(s_1',s_2',s_3')},0x^{e}_{(s_1',s_2',s_3')}}\}_{y^{e'}_{(s_1',s_2',s_3')} \in (\tilde{F},\mathcal{E})_2}$$

of $(\tilde{F},\mathcal{E})_2$ is a complex neutrosophic soft open cover in $1_{(\mathbf{X},\mathcal{E})}$. Since $(\tilde{F},\mathcal{E})_2$ is complex neutrosophic soft compact, there exist finitely many sets

$$(\mathbb{V},\mathcal{E})_{1y^{e'}_{(s_1',s_2',s_3')},0x^{e}_{(s_1',s_2',s_3')}},\ldots,(\mathbb{V},\mathcal{E})_{ny^{e'}_{(s_1',s_2',s_3')},0x^{e}_{(s_1',s_2',s_3')}} \subseteq (\tilde{F},\mathcal{E})_2$$

such that

$$(\tilde{F},\mathcal{E})_2 \subseteq \bigcup_{i=1}^{n} (\mathbb{V},\mathcal{E})_{iy^{e'}_{(s_1',s_2',s_3')},0x^{e}_{(s_1',s_2',s_3')}}.$$

Consider the neighborhoods

$$(\mathbb{U},\mathcal{E})_{0x^{e}_{(s_1',s_2',s_3')},iy^{e'}_{(s_1',s_2',s_3')}} \qquad i = 1,\ldots,n$$

that provide the condition

$$(\mathbb{U},\mathcal{E})_{0x^e_{(s_1',s_2',s_3')},iy^{e'}_{(s_1',s_2',s_3')}} \cap (\mathbb{V},\mathcal{E})_{iy^{e'}_{(s_1',s_2',s_3')},0x^e_{(s_1',s_2',s_3')}} = 0_{(\mathbf{X},\mathcal{E})}.$$

Thus,

$$(\mathbb{U},\mathcal{E})_{0x^e_{(s_1',s_2',s_3')}} = \bigcap_{i=1}^{n}(\mathbb{U},\mathcal{E})_{0x^e_{(s_1',s_2',s_3')},iy^{e'}_{(s_1',s_2',s_3')}}, \quad (\mathbb{V},\mathcal{E})_{(\tilde{F},\mathcal{E})_2} = \bigcup_{i=1}^{n}(\mathbb{V},\mathcal{E})_{iy^{e'}_{(s_1',s_2',s_3')},0x^e_{(s_1',s_2',s_3')}}$$

are complex neutrosophic soft open neighborhoods of $x^e_{(s_1',s_2',s_3')}$ and $(\tilde{F},\mathcal{E})_2$ respectively, and

$$\begin{aligned}&(\mathbb{U},\mathcal{E})_{0x^e_{(s_1',s_2',s_3')},(\tilde{F},\mathcal{E})_2} \cap (\mathbb{V},\mathcal{E})_{(\tilde{F},\mathcal{E})_2,0x^e_{(s_1',s_2',s_3')}}\\ &= \bigcup_{i=1}^{n}\left((\mathbb{U},\mathcal{E})_{0x^e_{(s_1',s_2',s_3')},iy^{e'}_{(s_1',s_2',s_3')}} \cap (\mathbb{V},\mathcal{E})_{iy^{e'}_{(s_1',s_2',s_3')},0x^e_{(s_1',s_2',s_3')}}\right) = 0_{(\mathbf{X},\mathcal{E})}.\end{aligned}$$

Thus, each $x^e_{(s_1',s_2',s_3')}$ and $(\tilde{F},\mathcal{E})_2$ have neighborhoods so that for each $x^e_{(s_1',s_2',s_3')} \in (\tilde{F},\mathcal{E})_1$ and $(\tilde{F},\mathcal{E})_2$,

$$(\mathbb{U},\mathcal{E})_{x^e_{(s_1',s_2',s_3')},(\tilde{F},\mathcal{E})_2} \cap (\mathbb{V},\mathcal{E})_{(\tilde{F},\mathcal{E})_2,x^e_{(s_1',s_2',s_3')}} = 0_{(\mathbf{X},\mathcal{E})}.$$

Finally, by the compactness of $(\tilde{F},\mathcal{E})_1$, we can find finitely many neighborhoods

$$(\mathbb{U},\mathcal{E})_{1x^e_{(s_1',s_2',s_3')},(\tilde{F},\mathcal{E})_2}, \ldots, (\mathbb{U},\mathcal{E})_{kx^e_{(s_1',s_2',s_3')},(\tilde{F},\mathcal{E})_2}$$

such that

$$(\tilde{F},\mathcal{E})_1 \subseteq \bigcup_{i=1}^{k}(\mathbb{U},\mathcal{E})_{ix^e_{(s_1',s_2',s_3')},(\tilde{F},\mathcal{E})_2}, \quad (\tilde{F},\mathcal{E})_2 \subseteq \bigcap_{i=1}^{k}(\mathbb{V},\mathcal{E})_{(\tilde{F},\mathcal{E})_2,ix^e_{(s_1',s_2',s_3')}},$$

and

$$(\mathbb{U},\mathcal{E})_{(\tilde{F},\mathcal{E})_1} \cap (\mathbb{V},\mathcal{E})_{(\tilde{F},\mathcal{E})_2} = \bigcup_{i=1}^{k}(\mathbb{U},\mathcal{E})_{ix^e_{(s_1',s_2',s_3')},(\tilde{F},\mathcal{E})_2} \cap \bigcap_{i=1}^{k}(\mathbb{V},\mathcal{E})_{(\tilde{F},\mathcal{E})_2,ix^e_{(s_1',s_2',s_3')}} = 0_{(\mathbf{X},\mathcal{E})}.$$

Thus, the proof is completed. □

4. Complex Neutrosophic Soft Locally Compact Spaces

Now we can give a definition of complex neutrosophic soft locally compactness that is weaker than complex neutrosophic soft compactness.

Definition 4.1. *Let $(\mathbf{X},\tau^{CNSS},\mathcal{E})$ be a complex neutrosophic soft topological space over $\mathbf{X}$. $(\mathbf{X},\tau^{CNSS},\mathcal{E})$ is called a complex neutrosophic soft locally compact (locally countable compact) space if for each*

$$x^e_{(s_1',s_2',s_3')} \in CNSS(\mathbf{X},\mathcal{E}),$$

there exists a complex neutrosophic soft neighborhood $(\mathbb{U},\mathcal{E}) \in \tau^{CNSS}$ of $x^e_{(s_1',s_2',s_3')}$ with complex neutrosophic soft closure $\overline{(\mathbb{U},\mathcal{E})}$ complex neutrosophic soft compact.

When $(\mathbf{X},\tau^{CNSS},\mathcal{E})$ is also complex neutrosophic soft Hausdorff, the property of complex neutrosophic soft local compactness becomes much stronger. Let's state this as a theorem.

Theorem 4.1. *If $(\mathbf{X}, \tau^{CNSS}, \mathcal{E})$ is a complex neutrosophic soft locally compact and complex neutrosophic soft Hausdorff space, $(\tilde{F}, \mathcal{E}) \in CNSS(\mathbf{X}, \mathcal{E})$ is a complex neutrosophic soft compact set and $(\tilde{F}, \mathcal{E}) \subset (\mathbb{V}, \mathcal{E})$, $(\mathbb{V}, \mathcal{E}) \in \tau^{CNSS}$, then there exists $(\mathbb{U}, \mathcal{E}) \in \tau^{CNSS}$ such that the closure $\overline{(\mathbb{U}, \mathcal{E})}$ is complex neutrosophic soft compact and*

$$(\tilde{F}, \mathcal{E}) \subset (\mathbb{U}, \mathcal{E}) \subset \overline{(\mathbb{U}, \mathcal{E})} \subset (\mathbb{V}, \mathcal{E}).$$

Proof. Since $(\mathbf{X}, \tau^{CNSS}, \mathcal{E})$ is a complex neutrosophic soft Hausdorff space, there exists a $(\mathbb{V}, \mathcal{E})_{x^e_{(s'_1, s'_2, s'_3)}}$ neighborhood for each

$$x^e_{(s'_1, s'_2, s'_3)} \in (\tilde{F}, \mathcal{E}) \subset (\mathbb{V}, \mathcal{E})$$

such that

$$x^e_{(s'_1, s'_2, s'_3)} \in (\mathbb{V}, \mathcal{E})_{x^e_{(s'_1, s'_2, s'_3)}} \subset \overline{(\mathbb{V}, \mathcal{E})_{x^e_{(s'_1, s'_2, s'_3)}}} \subset (\mathbb{V}, \mathcal{E}).$$

Since $(\mathbf{X}, \tau^{CNSS}, \mathcal{E})$ is complex neutrosophic soft locally compact, each $x^e_{(s'_1, s'_2, s'_3)} \in (\tilde{F}, \mathcal{E})$ has a compact closure neighborhood

$$\overline{(\mathbb{W}, \mathcal{E})_{x^e_{(s'_1, s'_2, s'_3)}}}.$$

Therefore, for the neighborhood

$$(\mathbb{U}, \mathcal{E})_{x^e_{(s'_1, s'_2, s'_3)}} = (\mathbb{V}, \mathcal{E})_{x^e_{(s'_1, s'_2, s'_3)}} \cap (\mathbb{W}, \mathcal{E})_{x^e_{(s'_1, s'_2, s'_3)}}$$

of $x^e_{(s'_1, s'_2, s'_3)}$, the closure

$$\overline{(\mathbb{U}, \mathcal{E})_{x^e_{(s'_1, s'_2, s'_3)}}}$$

is compact, since

$$\overline{(\mathbb{U}, \mathcal{E})_{x^e_{(s'_1, s'_2, s'_3)}}} \subset \overline{(\mathbb{W}, \mathcal{E})_{x^e_{(s'_1, s'_2, s'_3)}}}.$$

Since the complex neutrosophic soft set $(\tilde{F}, \mathcal{E})$ is compact,

$$\{(\mathbb{U}, \mathcal{E})_{x^e_{(s'_1, s'_2, s'_3)}}\}_{x^e_{(s'_1, s'_2, s'_3)} \in (\tilde{F}, \mathcal{E})}$$

is a complex neutrosophic soft covering of $(\tilde{F}, \mathcal{E})$ and has a finite subcover

$$(\mathbb{U}, \mathcal{E})_{1x^e_{(s'_1, s'_2, s'_3)}}, \ldots, (\mathbb{U}, \mathcal{E})_{nx^e_{(s'_1, s'_2, s'_3)}}.$$

Here, for the open set

$$(\mathbb{U}, \mathcal{E}) = \bigcup_{i=1}^{n} (\mathbb{U}, \mathcal{E})_{ix^e_{(s'_1, s'_2, s'_3)}},$$

we have

$$(\tilde{F}, \mathcal{E}) \subset (\mathbb{U}, \mathcal{E}), \quad \overline{(\mathbb{U}, \mathcal{E})} = \bigcup_{i=1}^{n} \overline{(\mathbb{U}, \mathcal{E})_{ix^e_{(s'_1, s'_2, s'_3)}}} \subset \bigcup_{i=1}^{n} \overline{(\mathbb{V}, \mathcal{E})_{ix^e_{(s'_1, s'_2, s'_3)}}} \subset (\mathbb{V}, \mathcal{E}),$$

which provides the required conditions. □

Theorem 4.2. *If $(\mathbf{X}, \tau^{CNSS}, \mathcal{E})$ is a complex neutrosophic soft locally compact, complex neutrosophic soft Hausdorff space and $(\tilde{F}, \mathcal{E}) \in CNSS(\mathbf{X}, \mathcal{E})$ is a complex neutrosophic soft closed (open) set, then $((\tilde{F}, \mathcal{E}), \tau^{CNSS}_{(\tilde{F}, \mathcal{E})}\mathcal{E})$ is a complex neutrosophic soft locally compact space.*

Proof. Let $(\mathbf{X}, \tau^{CNSS}, \mathcal{E})$ be a complex neutrosophic soft locally compact Hausdorff space and $(\tilde{F}, \mathcal{E}) \in CNSS(\mathbf{X}, \mathcal{E})$ be a complex neutrosophic soft closed set. Consider the compact neighborhood $\overline{(\mathbb{U}, \mathcal{E})}$ of each

$$x^{e}_{(s_1', s_2', s_3')} \in (\tilde{F}, \mathcal{E})$$

in $(\mathbf{X}, \tau^{CNSS}, \mathcal{E})$. For the open neighborhood of $x^{e}_{(s_1', s_2', s_3')}$,

$$(\mathbb{U}, \mathcal{E}) \cap (\tilde{F}, \mathcal{E})$$

in $((\tilde{F}, \mathcal{E}), \tau^{CNSS}_{(\tilde{F}, \mathcal{E})}\mathcal{E})$, we have

$$\overline{(\mathbb{U}, \mathcal{E}) \cap (\tilde{F}, \mathcal{E})} \text{ is compact because } \overline{(\mathbb{U}, \mathcal{E}) \cap (\tilde{F}, \mathcal{E})} = \overline{(\mathbb{U}, \mathcal{E})} \cap (\tilde{F}, \mathcal{E}) \subset \overline{(\mathbb{U}, \mathcal{E})},$$

that is, $((\tilde{F}, \mathcal{E}), \tau^{CNSS}_{(\tilde{F}, \mathcal{E})}\mathcal{E})$ is a complex neutrosophic soft locally compact space.

When we make the proof for complex neutrosophic soft closed set, $(\mathbf{X}, \tau^{CNSS}, \mathcal{E})$ does not need to be a complex neutrosophic soft Hausdorff space.

Now, let $(\tilde{F}, \mathcal{E}) \in CNSS(\mathbf{X}, \mathcal{E})$ be a complex neutrosophic soft open set. Since the single-point set in a complex neutrosophic soft Hausdorff space is complex neutrosophic soft closed, $(\mathbb{U}, \mathcal{E}) \in \tau^{CNSS}$ is present so that

$$\{x^{e}_{(s_1', s_2', s_3')}\} \subset (\mathbb{U}, \mathcal{E}) \subset \overline{(\mathbb{U}, \mathcal{E})} \subset (\tilde{F}, \mathcal{E}),$$

with $(\mathbb{U}, \mathcal{E})$ compact provided for each $x^{e}_{(s_1', s_2', s_3')} \in (\tilde{F}, \mathcal{E})$ from Theorem 4.1. From there,

$$(\mathbb{U}, \mathcal{E}) \cap (\tilde{F}, \mathcal{E})$$

in $((\tilde{F}, \mathcal{E}), \tau^{CNSS}_{(\tilde{F}, \mathcal{E})}\mathcal{E})$ is a neighborhood of $x^{e}_{(s_1', s_2', s_3')}$ and

$$\overline{(\mathbb{U}, \mathcal{E}) \cap (\tilde{F}, \mathcal{E})} = \overline{(\mathbb{U}, \mathcal{E})} \cap (\tilde{F}, \mathcal{E}) \subset \overline{(\mathbb{U}, \mathcal{E})}$$

is compact, that is, $((\tilde{F}, \mathcal{E}), \tau^{CNSS}_{(\tilde{F}, \mathcal{E})}\mathcal{E})$ is a complex neutrosophic soft locally compact space. □

Theorem 4.3. *If $((\tilde{F}, \mathcal{E}), \tau^{CNSS}_{(\tilde{F}, \mathcal{E})}\mathcal{E})$ is a complex neutrosophic soft Hausdorff space and $(\mathbb{M}, \mathcal{E}) \in CNSS(\mathbf{X}, \mathcal{E})$ is a complex neutrosophic soft locally compact subspace, then $(\mathbb{M}, \mathcal{E})$ is a complex neutrosophic soft open set in $\overline{(\mathbb{M}, \mathcal{E})}$ and $(\mathbb{M}, \mathcal{E})$ can be written as*

$$(\mathbb{M}, \mathcal{E}) = (\tilde{F}, \mathcal{E}) \cap (\mathbb{V}, \mathcal{E}),$$

where $(\tilde{F}, \mathcal{E})$ and $(\mathbb{V}, \mathcal{E})$ are soft closed and complex neutrosophic soft open in $(\mathbf{X}, \tau^{CNSS}, \mathcal{E})$, respectively.

Proof. Since $((\mathbb{M}, \mathcal{E}), \tau^{CNSS}_{(\mathbb{M}, \mathcal{E})}\mathcal{E})$ is complex neutrosophic soft locally compact, a neighborhood $(\tilde{F}, \mathcal{E}) \in \tau^{CNSS}_{(\mathbb{M}, \mathcal{E})}$ of

$$x^{e}_{(s_1', s_2', s_3')} \in (\mathbb{M}, \mathcal{E})$$

can be found such that

$$\overline{(\mathbb{U}, \mathcal{E})} \cap (\mathbb{M}, \mathcal{E})$$

is complex neutrosophic soft compact in $(\mathbb{M},\mathcal{E})$. $(\mathbf{X},\tau^{CNSS},\mathcal{E})$ is a complex neutrosophic soft Hausdorff space. Therefore, the complex neutrosophic soft set

$$\overline{(\mathbb{U},\mathcal{E})}\cap(\mathbb{M},\mathcal{E})$$

is closed in $(\mathbf{X},\tau^{CNSS},\mathcal{E})$. For

$$(\mathbb{U},\mathcal{E})\subset\overline{(\mathbb{U},\mathcal{E})}\cap(\mathbb{M},\mathcal{E}),$$

we have

$$\overline{(\mathbb{U},\mathcal{E})}\subset\overline{(\mathbb{U},\mathcal{E})}\cap(\mathbb{M},\mathcal{E})\subset(\mathbb{M},\mathcal{E}).$$

We obtain

$$(\mathbb{U},\mathcal{E})=(\mathbb{M},\mathcal{E})\cap(\mathbb{W},\mathcal{E}),\quad(\mathbb{W},\mathcal{E})\in\tau^{CNSS}$$

for $(\mathbb{U},\mathcal{E})\in\tau^{CNSS}_{(\mathbb{M},\mathcal{E})}$. So, we consider that the complex neutrosophic soft set $(\mathbb{M},\mathcal{E})$ is a complex neutrosophic soft dense set in $\overline{(\mathbb{U},\mathcal{E})}$, then

$$x^{e}_{(s_1',s_2',s_3')}\in\overline{(\mathbb{W},\mathcal{E})}=\overline{((\mathbb{M},\mathcal{E})\cap(\mathbb{W},\mathcal{E}))}=\overline{(\mathbb{U},\mathcal{E})}\subset(\mathbb{M},\mathcal{E})$$

can be written. That is, $(\mathbb{M},\mathcal{E})$ is a complex neutrosophic soft open set. Hence,

$$\overline{(\mathbb{M},\mathcal{E})}=\overline{(\mathbb{M},\mathcal{E})}\cap(\mathbb{M},\mathcal{E})=(\tilde{F},\mathcal{E})\cap(\mathbb{V},\mathcal{E})$$

is obtained. □

5. Visual and Geometric Characterization of Cosine Similarity Patterns Between Signals and Templates (T_1-T_3)

The evaluation of directional match between different input (S_1-S_3) signals and reference (T_1-T_3) templates using cosine similarity is a broad analysis and visual model presented in this study. First, a cosine similarity matrix is constructed to gauge each signal-template pair's degree of geometric matching. A number of complementary visualization techniques, such as 2D heatmaps, 2D and 3D bar graphs, 3D surface plots, and trend analysis using splines, are used to further investigate raw and normalized similarity results in order to improve interpretability. Additional strong linkages between S_1-T_3 and S_3-T_3 are discovered, while moderate and weaker links reveal structured but less obvious correlations. Inter-signal dependencies with strong positive and strong negative linear connections can also be analyzed using Pearson correlation analysis. Latent structural patterns are found using dimensionality-reduction techniques like Principal Component Analysis (PCA) and t-distributed Stochastic neighbour Embedding (t-SNE), after which they are unsupervised clustered using KMeans. The results show that a strong and transparent framework for signal-template matching is provided by the idea of cosine similarity with the aid of graphical and statistical layer-based visualizations. Because it enables the identification of dominant alignments with the necessary degree of dependability, intermediate linkages, and structural diversity, the described approach can be used in classification, pattern recognition, and decision-support applications.

Methods:

Cosine Similarity Computation

Cosine similarity (Cos SM) was used to quantify the directional similarity of signals (S_1, S_2, S_3) and templates (T_1, T_2, T_3). Cosine similarity was computed for each signal and template as $Cosine_{SCNSS}(\mathfrak{T}_i, \mathfrak{C}_j) =$

$$\frac{1}{n}\sum_{i=1}^{n}\left|\frac{(T_{it})(\mathcal{T}_{jt})+(\mathcal{I}_{it})(\mathcal{I}_{jt})+(\mathcal{F}_{it})(\mathcal{F}_{jt})}{\sqrt{\mathcal{T}_{it^2}+\mathcal{I}_{it^2}+\mathcal{F}_{it^2}}\times\sqrt{\mathcal{T}_{jt^2}+\mathcal{I}_{jt^2}+\mathcal{F}_{jt^2}}}\right|$$

resulting in a 3×3 similarity matrix. Greater directional alignment is correlated with higher similarity values, all of which fall between 0 and 1.

Heat-map Visualisation

The raw and normalized cosine similarity matrices were visualized using heatmaps, which were two-dimensional displays created from a perceptually consistent Viridis color-map. Color intensity was used to describe the degree of resemblance, and it was simple to identify the dominant, moderate, and weak signal template alignments. Circular annotations were used to indicate the strongest correspondence.

Normalisation Procedure

The cosine similarity matrix was scaled linearly to the range [0,1] using minmax scaling to enable similarity across visualization techniques. This adjustment improves the visual contrast between the surface-based and color-mapped representations while preserving relative differences.

Bar Graph Representations

Cos SM values were categorically compared using both 2D and 3D bar graphs. The signals (S_1-S_3) were represented by bars, and the templates (T_1-T_3) were clustered in the 2D bar plots. This representation was elevated to a spatial level by the 3D bar graphs, which improved graph separation and significantly improved the sense of magnitude difference. To facilitate precise interpretation, the numerical values for each bar were displayed above.

Surface Plot Analysis

Cosine similarity was converted into 3D surface plots that represent the similarity between two vectors as the height of the surface. Peaks, ridges and valleys on raw and normalised surfaces represent strong, medium and weak matches respectively. These also provide a geometrical interpretation of the similarity matrix, in addition to its discrete representations.

Correlation Analysis

Pearson correlation coefficients between the signals (S_1-S_3) were computed in order to assess the linear interdependencies. To identify positive and negative correlations, the correlation matrix was shown using a diverging colormap. Regardless of template matching, this analysis supported the interpretation of comparable or contradictory signal behavior.

Clustering and Dimensionality Reduction

Principal Component Analysis (PCA) was applied to the cosine similarity data in order to visualize the structural segregation of the templates (T_1-T_3) in three dimensions and identify the prevalent

directions of variance. In parallel, t-SNE was employed to perform nonlinear manifold learning in order to preserve the local neighborhood relationships. The t-SNE embedding was then subjected to k-means clustering in order to detect latent grouping tendencies and assess cluster cohesiveness.

Spline-Based Trend Analysis

The changes in cosine similarity values between templates of all signals were represented using the similarity of evolving values of cubic spline interpolation. To find peaks, troughs, nonlinear behavior, and monotonic trends, raw and normalized splines were created. Visual tracking of similarity dynamics rather than discrete data points was made simple by this technology.

5.1. **Cotangent Similarity Measure.** Let $\mathfrak{T}_{\mathfrak{i}} = (\mathcal{T}_{\mathfrak{i}\mathfrak{k}}, \mathcal{I}_{\mathfrak{i}\mathfrak{k}}, \mathcal{F}_{\mathfrak{i}\mathfrak{k}})$, $\mathfrak{C}_{\mathfrak{j}} = (\mathcal{T}_{\mathfrak{j}\mathfrak{k}}, \mathcal{I}_{\mathfrak{j}\mathfrak{k}}, \mathcal{F}_{\mathfrak{j}\mathfrak{k}})$ are two CSVNSs. Each set is represented by three components for each feature k:

$\mathcal{T}_{\mathfrak{i}\mathfrak{k}}$: Truth-membership of feature $\mathfrak{k}\, for\, \mathfrak{T}_{\mathfrak{i}}$.

$\mathcal{I}_{\mathfrak{i}\mathfrak{k}}$: Indeterminacy-membership of feature $\mathfrak{k}\, for\, \mathfrak{T}_{\mathfrak{i}}$.

$\mathcal{F}_{\mathfrak{i}\mathfrak{k}}$: Falsity-membership degree of feature $\mathfrak{k}\, for\, \mathfrak{T}_{\mathfrak{i}}$.

The values typically satisfy: $\mathcal{T}_{\mathfrak{i}\mathfrak{k}}$, $\mathcal{I}_{\mathfrak{i}\mathfrak{k}}$, $F_{\mathfrak{i}\mathfrak{k}} \in [0,1]$

Similarly, for object $\mathfrak{C}_{\mathfrak{j}}$:

$\mathcal{T}_{\mathfrak{j}\mathfrak{k}}$: Truth-membership of feature $k for \mathfrak{C}_{\mathfrak{j}}$.

$\mathcal{I}_{\mathfrak{j}\mathfrak{k}}$: Indeterminacy-membership of feature $\mathfrak{k}\, for\, \mathfrak{C}_{\mathfrak{j}}$.

$\mathcal{F}_{\mathfrak{j}\mathfrak{k}}$: Falsity-membership degree of feature $\mathfrak{k}\, for\, \mathfrak{C}_{\mathfrak{j}}$.

The values typically satisfy: $\mathcal{T}_{\mathfrak{j}\mathfrak{k}}$, $\mathcal{I}_{\mathfrak{j}\mathfrak{k}}$, $\mathcal{F}_{\mathfrak{j}\mathfrak{k}} \in [0,1]$.

The cosine similarity measures between $\mathfrak{T}_{\mathfrak{i}}$ and $\mathfrak{C}_{\mathfrak{j}}$ is defined as:

$$Cosine_{SCNSS}(\mathfrak{T}_{\mathfrak{i}}, \mathfrak{C}_{\mathfrak{j}}) = \frac{1}{n}\sum_{i=1}^{n}\left|\frac{(T_{\mathfrak{i}\mathfrak{k}})(\mathcal{T}_{\mathfrak{j}\mathfrak{k}}) + (\mathcal{I}_{\mathfrak{i}\mathfrak{k}})(\mathcal{I}_{\mathfrak{j}\mathfrak{k}}) + (\mathcal{F}_{\mathfrak{i}\mathfrak{k}})(\mathcal{F}_{\mathfrak{j}\mathfrak{k}})}{\sqrt{\mathcal{T}_{\mathfrak{i}\mathfrak{k}^2} + \mathcal{I}_{\mathfrak{i}\mathfrak{k}^2} + \mathcal{F}_{\mathfrak{i}\mathfrak{k}^2}} \times \sqrt{\mathcal{T}_{\mathfrak{j}\mathfrak{k}^2} + \mathcal{I}_{\mathfrak{j}\mathfrak{k}^2} + \mathcal{F}_{\mathfrak{j}\mathfrak{k}^2}}}\right|$$

TABLE 1. Matrix of Target Intelligence Features Based on Cosine Similarity $(T \times S)$

	S_1	S_2	...	S_n
T_1	$\mathcal{T}_{11}, \mathcal{I}_{11}, \mathcal{F}_{11}$	$\mathcal{T}_{12}, \mathcal{I}_{12}, \mathcal{F}_{12}$	...	$\mathcal{T}_{1n}, \mathcal{I}_{1n}, \mathcal{F}_{1n}$
T_2	$\mathcal{T}_{21}, \mathcal{I}_{21}, \mathcal{F}_{21}$	$\mathcal{T}_{22}, \mathcal{I}_{22}, \mathcal{F}_{22}$	...	$\mathcal{T}_{2n}, \mathcal{I}_{2n}, \mathcal{F}_{2n}$
...	...	...	...	...
T_m	$\mathcal{T}_{m1}, \mathcal{I}_{m1}, \mathcal{F}_{m1}$	$\mathcal{T}_{m2}, \mathcal{I}_{m2}, \mathcal{F}_{m2}$	...	$\mathcal{T}_{mn}, \mathcal{I}_{mn}, \mathcal{F}_{mn}$

TABLE 2. Operational Classification Matrix for Target Surveillance Data $(T \times S \to C)$

Row-I	S_1	S_2	S_3	**Row-II**	C_1	C_2	C_3
T_1	$\begin{pmatrix}0.5e^{\iota\pi(0.6)}\\0.7e^{\iota\pi(0.5)}\\0.3e^{\iota\pi(0.3)}\end{pmatrix}$	$\begin{pmatrix}0.6e^{\iota\pi(0.7)}\\0.4e^{\iota\pi(0.4)}\\0.3e^{\iota\pi(0.4)}\end{pmatrix}$	$\begin{pmatrix}0.3e^{\iota\pi(0.2)}\\0.5e^{\iota\pi(0.5)}\\0.8e^{\iota\pi(0.3)}\end{pmatrix}$	S_1	$\begin{pmatrix}0.3e^{\iota\pi(0.4)}\\0.5e^{\iota\pi(0.7)}\\0.7e^{\iota\pi(0.7)}\end{pmatrix}$	$\begin{pmatrix}0.7e^{\iota\pi(0.6)}\\0.6e^{\iota\pi(0.5)}\\0.2e^{\iota\pi(0.3)}\end{pmatrix}$	$\begin{pmatrix}0.5e^{\iota\pi(0.8)}\\0.4e^{\iota\pi(0.7)}\\0.9e^{\iota\pi(0.3)}\end{pmatrix}$
T_2	$\begin{pmatrix}0.4e^{\iota\pi(0.6)}\\0.7e^{\iota\pi(0.9)}\\0.5e^{\iota\pi(0.7)}\end{pmatrix}$	$\begin{pmatrix}0.2e^{\iota\pi(0.4)}\\0.4e^{\iota\pi(0.9)}\\0.6e^{\iota\pi(0.3)}\end{pmatrix}$	$\begin{pmatrix}0.7e^{\iota\pi(0.7)}\\0.4e^{\iota\pi(0.3)}\\0.6e^{\iota\pi(0.6)}\end{pmatrix}$	S_2	$\begin{pmatrix}0.2e^{\iota\pi(0.5)}\\0.3e^{\iota\pi(0.2)}\\0.7e^{\iota\pi(0.3)}\end{pmatrix}$	$\begin{pmatrix}0.6e^{\iota\pi(0.6)}\\0.7e^{\iota\pi(0.8)}\\0.4e^{\iota\pi(0.3)}\end{pmatrix}$	$\begin{pmatrix}0.3e^{\iota\pi(0.6)}\\0.6e^{\iota\pi(0.7)}\\0.8e^{\iota\pi(0.9)}\end{pmatrix}$
T_3	$\begin{pmatrix}0.7e^{\iota\pi(0.9)}\\0.6e^{\iota\pi(0.5)}\\0.8e^{\iota\pi(0.8)}\end{pmatrix}$	$\begin{pmatrix}0.2e^{\iota\pi(0.4)}\\0.8e^{\iota\pi(0.5)}\\0.7e^{\iota\pi(0.6)}\end{pmatrix}$	$\begin{pmatrix}0.6e^{\iota\pi(0.9)}\\0.3e^{\iota\pi(0.6)}\\0.2e^{\iota\pi(0.3)}\end{pmatrix}$	S_3	$\begin{pmatrix}0.4e^{\iota\pi(0.4)}\\0.7e^{\iota\pi(0.5)}\\0.5e^{\iota\pi(0.9)}\end{pmatrix}$	$\begin{pmatrix}0.6e^{\iota\pi(0.2)}\\0.3e^{\iota\pi(0.5)}\\0.4e^{\iota\pi(0.4)}\end{pmatrix}$	$\begin{pmatrix}0.7e^{\iota\pi(0.2)}\\0.3e^{\iota\pi(0.8)}\\0.2e^{\iota\pi(0.3)}\end{pmatrix}$

$$Cosine_{SCNSS}(\mathfrak{T}_{\mathfrak{i}}, \mathfrak{C}_{\mathfrak{j}}) = \frac{1}{n}\sum_{i=1}^{n}\left|\frac{(T_{i\mathfrak{k}})(T_{j\mathfrak{k}}) + (I_{i\mathfrak{k}})(I_{j\mathfrak{k}}) + (F_{i\mathfrak{k}})(F_{j\mathfrak{k}})}{\sqrt{T_{i\mathfrak{k}2} + I_{i\mathfrak{k}2} + F_{i\mathfrak{k}2}} \times \sqrt{T_{j\mathfrak{k}^2} + I_{j\mathfrak{k}^2} + F_{j\mathfrak{k}^2}}}\right|$$

For $n = 3$ then $\mathfrak{R}_1 + \mathfrak{C}_1 \Rightarrow \cos_{SCNSS}(\mathfrak{T}_{\mathfrak{i}}, \mathfrak{C}_{\mathfrak{j}}) =$

$$\frac{1}{3}\Bigg[\left|\frac{(0.5e^{\iota\pi(0.6)})(0.3e^{\iota\pi(0.4)}) + (0.7e^{\iota\pi(0.5)})(0.5e^{\iota\pi(0.7)}) + (0.3e^{\iota\pi(0.3)})(0.7e^{\iota\pi(0.7)})}{\sqrt{(0.5e^{\iota\pi(0.6)})^2 + (0.7e^{\iota\pi(0.5)})^2 + (0.3e^{\iota\pi(0.3)})^2} \times \sqrt{(0.3e^{\iota\pi(0.4)})^2 + (0.5e^{\iota\pi(0.7)})^2 + (0.7e^{\iota\pi(0.7)})^2}}\right|$$
$$+\left|\frac{(0.6e^{\iota\pi(0.7)})(0.2e^{\iota\pi(0.5)}) + (0.4e^{\iota\pi(0.4)})(0.3e^{\iota\pi(0.2)}) + (0.3e^{\iota\pi(0.4)})(0.7e^{\iota\pi(0.3)})}{\sqrt{(0.6e^{\iota\pi(0.7)})^2 + (0.4e^{\iota\pi(0.4)})^2 + (0.3e^{\iota\pi(0.4)})^2} \times \sqrt{(0.2e^{\iota\pi(0.5)})^2 + (0.3e^{\iota\pi(0.2)})^2 + (0.7e^{\iota\pi(0.3)})^2}}\right|$$
$$+\left|\frac{(0.3e^{\iota\pi(0.2)})(0.4e^{\iota\pi(0.4)}) + (0.5e^{\iota\pi(0.5)})(0.7e^{\iota\pi(0.5)}) + (0.8e^{\iota\pi(0.3)})(0.5e^{\iota\pi(0.9)})}{\sqrt{(0.3e^{\iota\pi(0.2)})^2 + (0.5e^{\iota\pi(0.5)})^2 + (0.8e^{\iota\pi(0.3)})^2} \times \sqrt{(0.4e^{\iota\pi(0.4)})^2 + (0.7e^{\iota\pi(0.5)})^2 + (0.5e^{\iota\pi(0.9)})^2}}\right|\Bigg]$$
$$= \frac{1}{3}[0.8130 + 0.0394 + 0.9724] = 0.6083$$

For $n = 3$ then $\mathfrak{R}_1 + \mathfrak{C}_2 \Rightarrow \cos_{SCNSS}(\mathfrak{T}_{\mathfrak{i}}, \mathfrak{C}_{\mathfrak{j}}) =$

$$\frac{1}{3}\Bigg[\left|\frac{(0.5e^{\iota\pi(0.6)})(0.7e^{\iota\pi(0.6)}) + (0.7e^{\iota\pi(0.5)})(0.6e^{\iota\pi(0.5)}) + (0.3e^{\iota\pi(0.3)})(0.2e^{\iota\pi(0.3)})}{\sqrt{(0.5e^{\iota\pi(0.6)})^2 + (0.7e^{\iota\pi(0.5)})^2 + (0.3e^{\iota\pi(0.3)})^2} \times \sqrt{(0.7e^{\iota\pi(0.6)})^2 + (0.6e^{\iota\pi(0.5)})^2 + (0.2e^{\iota\pi(0.3)})^2}}\right|$$
$$+\left|\frac{(0.6e^{\iota\pi(0.7)})(0.6e^{\iota\pi(0.6)}) + (0.4e^{\iota\pi(0.4)})(0.7e^{\iota\pi(0.8)}) + (0.3e^{\iota\pi(0.4)})(0.4e^{\iota\pi(0.3)})}{\sqrt{(0.6e^{\iota\pi(0.7)})^2 + (0.4e^{\iota\pi(0.4)})^2 + (0.3e^{\iota\pi(0.4)})^2} \times \sqrt{(0.6e^{\iota\pi(0.6)})^2 + (0.7e^{\iota\pi(0.8)})^2 + (0.4e^{\iota\pi(0.3)})^2}}\right|$$
$$+\left|\frac{(0.3e^{\iota\pi(0.2)})(0.6e^{\iota\pi(0.2)}) + (0.5e^{\iota\pi(0.5)})(0.3e^{\iota\pi(0.5)}) + (0.8e^{\iota\pi(0.3)})(0.4e^{\iota\pi(0.4)})}{\sqrt{(0.3e^{\iota\pi(0.2)})^2 + (0.5e^{\iota\pi(0.5)})^2 + (0.8e^{\iota\pi(0.3)})^2} \times \sqrt{(0.6e^{\iota\pi(0.2)})^2 + (0.3e^{\iota\pi(0.5)})^2 + (0.4e^{\iota\pi(0.4)})^2}}\right|\Bigg]$$
$$= \frac{1}{3}[0.8571 + 0.8496 + 0.6642] = 0.8870$$

For $n=3$ then $\mathfrak{R}_1+\mathfrak{C}_3 \Rightarrow \cos_{SCNSS}(\mathfrak{T}_i,\mathfrak{C}_j)=$

$$\frac{1}{3}\Bigg[\left|\frac{(0.5e^{\iota\pi(0.6)})(0.5e^{\iota\pi(0.8)})+(0.7e^{\iota\pi(0.5)})(0.4e^{\iota\pi(0.7)})+(0.3e^{\iota\pi(0.3)})(0.9e^{\iota\pi(0.3)})}{\sqrt{(0.5e^{\iota\pi(0.6)})^2+(0.7e^{\iota\pi(0.5)})^2+(0.3e^{\iota\pi(0.3)})^2}\times\sqrt{(0.5e^{\iota\pi(0.8)})^2+(0.4e^{\iota\pi(0.7)})^2+(0.9e^{\iota\pi(0.3)})^2}}\right|$$
$$+\left|\frac{(0.6e^{\iota\pi(0.7)})(0.3e^{\iota\pi(0.6)})+(0.4e^{\iota\pi(0.4)})(0.6e^{\iota\pi(0.7)})+(0.3e^{\iota\pi(0.4)})(0.8e^{\iota\pi(0.9)})}{\sqrt{(0.6e^{\iota\pi(0.7)})^2+(0.4e^{\iota\pi(0.4)})^2+(0.3e^{\iota\pi(0.4)})^2}\times\sqrt{(0.3e^{\iota\pi(0.6)})^2+(0.6e^{\iota\pi(0.7)})^2+(0.8e^{\iota\pi(0.9)})^2}}\right|$$
$$+\left|\frac{(0.3e^{\iota\pi(0.2)})(0.7e^{\iota\pi(0.2)})+(0.5e^{\iota\pi(0.5)})(0.3e^{\iota\pi(0.8)})+(0.8e^{\iota\pi(0.3)})(0.2e^{\iota\pi(0.3)})}{\sqrt{(0.3e^{\iota\pi(0.2)})^2+(0.5e^{\iota\pi(0.5)})^2+(0.8e^{\iota\pi(0.3)})^2}\times\sqrt{(0.7e^{\iota\pi(0.2)})^2+(0.3e^{\iota\pi(0.8)})^2+(0.2e^{\iota\pi(0.3)})^2}}\right|\Bigg]$$
$$=\frac{1}{3}[0.5119+0.7855+0.4246]=0.5740$$

For $n=3$ then $\mathfrak{R}_2+\mathfrak{C}_1 \Rightarrow \cos_{SCNSS}(\mathfrak{T}_i,\mathfrak{C}_j)=$

$$\frac{1}{3}\Bigg[\left|\frac{(0.4e^{\iota\pi(0.6)})(0.3e^{\iota\pi(0.4)})+(0.7e^{\iota\pi(0.9)})(0.5e^{\iota\pi(0.7)})+(0.5e^{\iota\pi(0.7)})(0.7e^{\iota\pi(0.7)})}{\sqrt{(0.4e^{\iota\pi(0.6)})^2+(0.7e^{\iota\pi(0.9)})^2+(0.5e^{\iota\pi(0.7)})^2}\times\sqrt{(0.3e^{\iota\pi(0.4)})^2+(0.5e^{\iota\pi(0.7)})^2+(0.7e^{\iota\pi(0.7)})^2}}\right|$$
$$+\left|\frac{(0.2e^{\iota\pi(0.4)})(0.2e^{\iota\pi(0.5)})+(0.4e^{\iota\pi(0.9)})(0.3e^{\iota\pi(0.2)})+(0.6e^{\iota\pi(0.3)})(0.7e^{\iota\pi(0.3)})}{\sqrt{(0.2e^{\iota\pi(0.4)})^2+(0.4e^{\iota\pi(0.9)})^2+(0.6e^{\iota\pi(0.3)})^2}\times\sqrt{(0.2e^{\iota\pi(0.5)})^2+(0.3e^{\iota\pi(0.2)})^2+(0.7e^{\iota\pi(0.3)})^2}}\right|$$
$$+\left|\frac{(0.7e^{\iota\pi(0.7)})(0.4e^{\iota\pi(0.4)})+(0.4e^{\iota\pi(0.3)})(0.7e^{\iota\pi(0.5)})+(0.6e^{\iota\pi(0.6)})(0.5e^{\iota\pi(0.9)})}{\sqrt{(0.7e^{\iota\pi(0.7)})^2+(0.4e^{\iota\pi(0.3)})^2+(0.6e^{\iota\pi(0.6)})^2}\times\sqrt{(0.4e^{\iota\pi(0.4)})^2+(0.7e^{\iota\pi(0.5)})^2+(0.5e^{\iota\pi(0.9)})^2}}\right|\Bigg]$$
$$=\frac{1}{3}[0.7825+0.7965+0.5669]=0.7153$$

For $n=3$ then $\mathfrak{R}_2+\mathfrak{C}_2 \Rightarrow \cos_{SCNSS}(\mathfrak{T}_i,\mathfrak{C}_j)=$

$$\frac{1}{3}\Bigg[\left|\frac{(0.4e^{\iota\pi(0.6)})(0.7e^{\iota\pi(0.6)})+(0.7e^{\iota\pi(0.9)})(0.6e^{\iota\pi(0.5)})+(0.5e^{\iota\pi(0.7)})(0.2e^{\iota\pi(0.3)})}{\sqrt{(0.4e^{\iota\pi(0.6)})^2+(0.7e^{\iota\pi(0.9)})^2+(0.5e^{\iota\pi(0.7)})^2}\times\sqrt{(0.7e^{\iota\pi(0.6)})^2+(0.6e^{\iota\pi(0.5)})^2+(0.2e^{\iota\pi(0.3)})^2}}\right|$$
$$+\left|\frac{(0.2e^{\iota\pi(0.4)})(0.6e^{\iota\pi(0.6)})+(0.4e^{\iota\pi(0.9)})(0.7e^{\iota\pi(0.8)})+(0.6e^{\iota\pi(0.3)})(0.4e^{\iota\pi(0.3)})}{\sqrt{(0.2e^{\iota\pi(0.4)})^2+(0.4e^{\iota\pi(0.9)})^2+(0.6e^{\iota\pi(0.3)})^2}\times\sqrt{(0.6e^{\iota\pi(0.6)})^2+(0.7e^{\iota\pi(0.8)})^2+(0.4e^{\iota\pi(0.3)})^2}}\right|$$
$$+\left|\frac{(0.7e^{\iota\pi(0.7)})(0.6e^{\iota\pi(0.2)})+(0.4e^{\iota\pi(0.3)})(0.3e^{\iota\pi(0.5)})+(0.6e^{\iota\pi(0.6)})(0.4e^{\iota\pi(0.4)})}{\sqrt{(0.7e^{\iota\pi(0.7)})^2+(0.4e^{\iota\pi(0.3)})^2+(0.6e^{\iota\pi(0.6)})^2}\times\sqrt{(0.6e^{\iota\pi(0.2)})^2+(0.3e^{\iota\pi(0.5)})^2+(0.4e^{\iota\pi(0.4)})^2}}\right|\Bigg]$$
$$=\frac{1}{3}[0.8106+0.0395+0.9164]=0.5888$$

For $n=3$ then $\mathfrak{R}_2+\mathfrak{C}_3 \Rightarrow \cos_{SCNSS}(\mathfrak{T}_i,\mathfrak{C}_j)=$

$$\frac{1}{3}\Bigg[\left|\frac{(0.4e^{\iota\pi(0.6)})(0.5e^{\iota\pi(0.8)})+(0.7e^{\iota\pi(0.9)})(0.4e^{\iota\pi(0.7)})+(0.5e^{\iota\pi(0.7)})(0.9e^{\iota\pi(0.3)})}{\sqrt{(0.4e^{\iota\pi(0.6)})^2+(0.7e^{\iota\pi(0.9)})^2+(0.5e^{\iota\pi(0.7)})^2}\times\sqrt{(0.5e^{\iota\pi(0.8)})^2+(0.4e^{\iota\pi(0.7)})^2+(0.9e^{\iota\pi(0.3)})^2}}\right|$$
$$+\left|\frac{(0.2e^{\iota\pi(0.4)})(0.3e^{\iota\pi(0.6)})+(0.4e^{\iota\pi(0.9)})(0.6e^{\iota\pi(0.7)})+(0.6e^{\iota\pi(0.3)})(0.8e^{\iota\pi(0.9)})}{\sqrt{(0.2e^{\iota\pi(0.4)})^2+(0.4e^{\iota\pi(0.9)})^2+(0.6e^{\iota\pi(0.3)})^2}\times\sqrt{(0.3e^{\iota\pi(0.6)})^2+(0.6e^{\iota\pi(0.7)})^2+(0.8e^{\iota\pi(0.9)})^2}}\right|$$
$$+\left|\frac{(0.7e^{\iota\pi(0.7)})(0.7e^{\iota\pi(0.2)})+(0.4e^{\iota\pi(0.3)})(0.3e^{\iota\pi(0.8)})+(0.6e^{\iota\pi(0.6)})(0.2e^{\iota\pi(0.3)})}{\sqrt{(0.7e^{\iota\pi(0.7)})^2+(0.4e^{\iota\pi(0.3)})^2+(0.6e^{\iota\pi(0.6)})^2}\times\sqrt{(0.7e^{\iota\pi(0.2)})^2+(0.3e^{\iota\pi(0.8)})^2+(0.2e^{\iota\pi(0.3)})^2}}\right|\Bigg]$$
$$=\frac{1}{3}[0.5949+0.8100+0.8980]=0.7676$$

For $n=3$ then $\mathfrak{R}_3+\mathfrak{C}_1 \Rightarrow \cos_{SCNSS}(\mathfrak{T}_i,\mathfrak{C}_j)=$

$$\frac{1}{3}\Bigg[\left|\frac{(0.7e^{\iota\pi(0.9)})(0.3e^{\iota\pi(0.4)})+(0.6e^{\iota\pi(0.5)})(0.5e^{\iota\pi(0.7)})+(0.8e^{\iota\pi(0.8)})(0.7e^{\iota\pi(0.7)})}{\sqrt{(0.7e^{\iota\pi(0.9)})^2+(0.6e^{\iota\pi(0.5)})^2+(0.8e^{\iota\pi(0.8)})^2}\times\sqrt{(0.3e^{\iota\pi(0.4)})^2+(0.5e^{\iota\pi(0.7)})^2+(0.7e^{\iota\pi(0.7)})^2}}\right|$$
$$+\left|\frac{(0.2e^{\iota\pi(0.4)})(0.2e^{\iota\pi(0.5)})+(0.8e^{\iota\pi(0.5)})(0.3e^{\iota\pi(0.2)})+(0.7e^{\iota\pi(0.6)})(0.7e^{\iota\pi(0.3)})}{\sqrt{(0.2e^{\iota\pi(0.4)})^2+(0.8e^{\iota\pi(0.5)})^2+(0.7e^{\iota\pi(0.6)})^2}\times\sqrt{(0.2e^{\iota\pi(0.5)})^2+(0.3e^{\iota\pi(0.2)})^2+(0.7e^{\iota\pi(0.3)})^2}}\right|$$
$$+\left|\frac{(0.6e^{\iota\pi(0.9)})(0.4e^{\iota\pi(0.4)})+(0.3e^{\iota\pi(0.6)})(0.7e^{\iota\pi(0.5)})+(0.2e^{\iota\pi(0.3)})(0.5e^{\iota\pi(0.9)})}{\sqrt{(0.6e^{\iota\pi(0.9)})^2+(0.3e^{\iota\pi(0.6)})^2+(0.2e^{\iota\pi(0.3)})^2}\times\sqrt{(0.4e^{\iota\pi(0.4)})^2+(0.7e^{\iota\pi(0.5)})^2+(0.5e^{\iota\pi(0.9)})^2}}\right|\Bigg]$$
$$=\frac{1}{3}[0.8790+0.8662+0.7950]=0.8467$$

For $n=3$ then $\mathfrak{R}_3+\mathfrak{C}_2 \Rightarrow \cos_{SCNSS}(\mathfrak{T}_i,\mathfrak{C}_j)=$

$$\frac{1}{3}\Bigg[\left|\frac{(0.7e^{\iota\pi(0.9)})(0.7e^{\iota\pi(0.6)})+(0.6e^{\iota\pi(0.5)})(0.6e^{\iota\pi(0.5)})+(0.8e^{\iota\pi(0.8)})(0.2e^{\iota\pi(0.3)})}{\sqrt{(0.7e^{\iota\pi(0.9)})^2+(0.6e^{\iota\pi(0.5)})^2+(0.8e^{\iota\pi(0.8)})^2}\times\sqrt{(0.7e^{\iota\pi(0.6)})^2+(0.6e^{\iota\pi(0.5)})^2+(0.2e^{\iota\pi(0.3)})^2}}\right|$$
$$+\left|\frac{(0.2e^{\iota\pi(0.4)})(0.6e^{\iota\pi(0.6)})+(0.8e^{\iota\pi(0.5)})(0.7e^{\iota\pi(0.8)})+(0.7e^{\iota\pi(0.6)})(0.4e^{\iota\pi(0.3)})}{\sqrt{(0.2e^{\iota\pi(0.4)})^2+(0.8e^{\iota\pi(0.5)})^2+(0.7e^{\iota\pi(0.6)})^2}\times\sqrt{(0.6e^{\iota\pi(0.6)})^2+(0.7e^{\iota\pi(0.8)})^2+(0.4e^{\iota\pi(0.3)})^2}}\right|$$
$$+\left|\frac{(0.6e^{\iota\pi(0.9)})(0.6e^{\iota\pi(0.2)})+(0.3e^{\iota\pi(0.6)})(0.3e^{\iota\pi(0.5)})+(0.2e^{\iota\pi(0.3)})(0.4e^{\iota\pi(0.4)})}{\sqrt{(0.6e^{\iota\pi(0.9)})^2+(0.3e^{\iota\pi(0.6)})^2+(0.2e^{\iota\pi(0.3)})^2}\times\sqrt{(0.6e^{\iota\pi(0.2)})^2+(0.3e^{\iota\pi(0.5)})^2+(0.4e^{\iota\pi(0.4)})^2}}\right|\Bigg]$$
$$=\frac{1}{3}[0.6461+0.7394+0.8793]=0.7549$$

For $n = 3$ then $\Re_3 + \mathfrak{C}_3 \Rightarrow \cos_{SCNSS}(\mathfrak{T}_i, \mathfrak{C}_i) =$

$$\frac{1}{3}\Bigg[\left|\frac{(0.7e^{\iota\pi(0.9)})(0.5e^{\iota\pi(0.8)}) + (0.6e^{\iota\pi(0.5)})(0.4e^{\iota\pi(0.7)}) + (0.8e^{\iota\pi(0.8)})(0.9e^{\iota\pi(0.3)})}{\sqrt{(0.7e^{\iota\pi(0.9)})^2 + (0.6e^{\iota\pi(0.5)})^2 + (0.8e^{\iota\pi(0.8)})^2} \times \sqrt{(0.5e^{\iota\pi(0.8)})^2 + (0.4e^{\iota\pi(0.7)})^2 + (0.9e^{\iota\pi(0.3)})^2}}\right|$$

$$+\left|\frac{(0.2e^{\iota\pi(0.4)})(0.3e^{\iota\pi(0.6)}) + (0.8e^{\iota\pi(0.5)})(0.6e^{\iota\pi(0.7)}) + (0.7e^{\iota\pi(0.6)})(0.8e^{\iota\pi(0.9)})}{\sqrt{(0.2e^{\iota\pi(0.4)})^2 + (0.8e^{\iota\pi(0.5)})^2 + (0.7e^{\iota\pi(0.6)})^2} \times \sqrt{(0.3e^{\iota\pi(0.6)})^2 + (0.6e^{\iota\pi(0.7)})^2 + (0.8e^{\iota\pi(0.9)})^2}}\right|$$

$$+\left|\frac{(0.6e^{\iota\pi(0.9)})(0.7e^{\iota\pi(0.2)}) + (0.3e^{\iota\pi(0.6)})(0.3e^{\iota\pi(0.8)}) + (0.2e^{\iota\pi(0.3)})(0.2e^{\iota\pi(0.3)})}{\sqrt{(0.6e^{\iota\pi(0.9)})^2 + (0.3e^{\iota\pi(0.6)})^2 + (0.2e^{\iota\pi(0.3)})^2} \times \sqrt{(0.7e^{\iota\pi(0.2)})^2 + (0.3e^{\iota\pi(0.8)})^2 + (0.2e^{\iota\pi(0.3)})^2}}\right|\Bigg]$$

$$= \frac{1}{3}[0.6927 + 0.8448 + 0.8510] = 0.7960$$

All target-classification pairings are then averaged by adding the cosine values that were determined for each pair of targets and categorized profiles.

Values of the resulting cosine similarity:

$Cosine_{SCNSS}(T_1, \mathfrak{C}_1) = 0.6083$
$Cosine_{SCNSS}(T_1, \mathfrak{C}_2) = 0.8870$
$Cosine_{SCNSS}(T_1, \mathfrak{C}_3) = 0.5740$
$Cosine_{SCNSS}(T_2, \mathfrak{C}_1) = 0.7153$
$Cosine_{SCNSS}(T_2, \mathfrak{C}_2) = 0.5888$
$Cosine_{SCNSS}(T_2, \mathfrak{C}_3) = 0.7676$
$Cosine_{SCNSS}(T_3, \mathfrak{C}_1) = 0.8467$
$Cosine_{SCNSS}(T_3, \mathfrak{C}_2) = 0.7549$
$Cosine_{SCNSS}(T_3, \mathfrak{C}_3) = 0.7960.$

Table 3. Cosine Similarity scores between signal samples $(S_1 - S_3)$ and class templates $(T_1 - T_3)$

Cos SM	S_1	S_2	S_3
T_1	0.6083	0.8870	0.5740
T_2	0.7153	0.5888	0.7676
T_3	0.8467	0.7549	0.7960

6. Result and Discussion

A 2D Cosine Similarity Matrix Heatmap illustrating the degree of directional correlation between the input signals (S_1-S_3) and the templates (T_1-T_3) was created in Figure 1 using Virdis colormap, which provides a gradual transition of deep purple to bright yellow. The S_2-T_1 cell, located in the brightest yellow region of the matrix, has the highest similarity of 0.8870. Signal S_2 has the most

constant directional connection with Template T_1, as seen by the strong and conclusive relationship in this highlighted circular area of the entire matrix. S_1 T_3 (0.8467) and S_3 T_3 (0.7960) are two other regions with comparatively high similarity values. These are located in the yellow-orange region of the colormap and show strong and consistent correlations, suggesting that S_1 and S_3 are both geometrically significantly aligned with T_3. S_3-T_2 (0.7676), which is in the green-yellow spectrum yet shows a very apparent and practically significant degree of signal-template correspondence, also exhibits another commonality. The heatmap's greenish hues, such as T_2-S_1 (0.7153) and T_3-S_2 (0.7549), are full of moderate similarity values. These intermediate alignments are more suggestive of relatively constant directional affinity that is instructive and can be recognized as pattern recognition or classification than they are strong or weak. The bluish-green portion of the color map is where the lower similarity values (S_3 T_1 (0.5740) and S_2 T_2 (0.5888)) are located. These show a moderate relationship structure between the pertinent signal-template pairs, although being weaker than the primary matches. T_1 S_1 (0.6083) is the weakest point, however even in this case, the value is greater than the matrix's minimum, indicating that the dataset as a whole does not contain any significantly misaligned or contradicting relationships between signals. All things considered, the heatmap is a layered and easy-to-understand visual depiction of the degree of similarity, and the color's intensity indicates how confident one is in aligning with it. This makes it possible to show signal-to-template correlations in an understandable and straightforward manner, which is helpful in identifying those that are highly connected, somewhat aligned, or require more research.

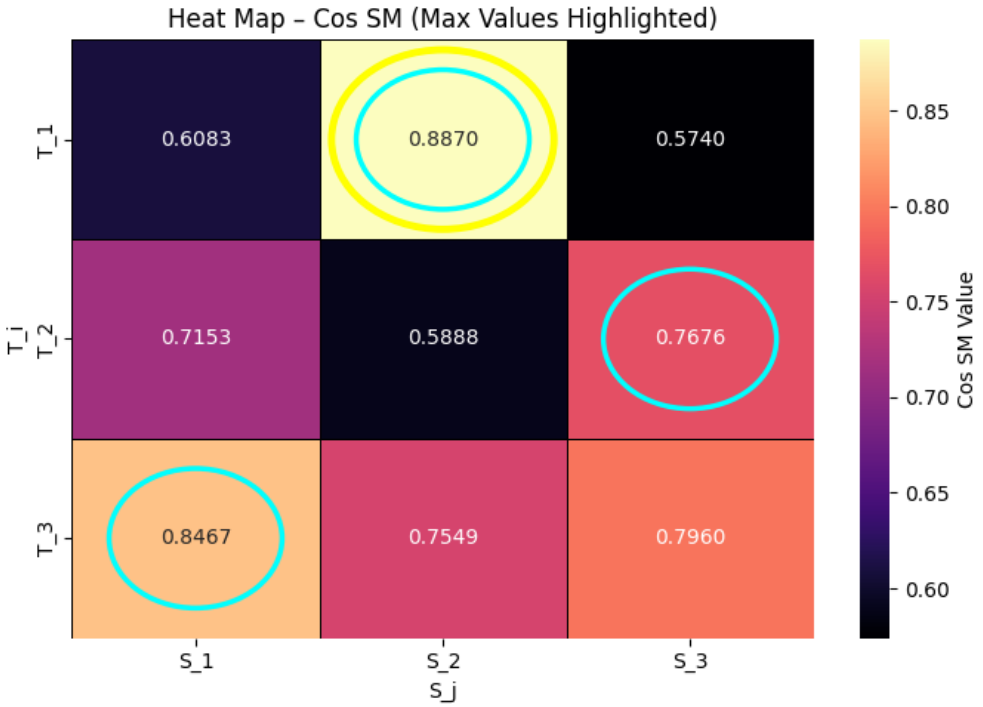

FIGURE 1. 2D Cosine Similarity Matrix Heatmap

TABLE 4

Numerical Value Range	Signal-Template Alignment	Strength Description	Interpretation Meaning	Color Representation (Heatmap)
0.55-0.60	Low	Weak Similarity	Minimal alignment; signals and templates do not share strong directional behaviour.	Dark Blue / Black
0.60-0.70	Medium	Moderate Similarity	Partial structural match; relationship is noticeable but not strong.	Purple
0.70-0.80	High	Strong Similarity	Signals and templates share clear similarity; reliable matching behaviour.	Red-Orange
0.80-0.90	Very High	Dominant Similarity	Strongest and most confident alignment; indicates the best correspondence.	

After normalizing the Cosine Similarity matrix to the range 0-1, Figure 2 was created using the Virdis colormap. This produced a smooth transition between dark purple (low similarity) and bright yellow (high similarity). The degree of directional relationship between the input signals (S_1 S_3) and the templates (T_1 T_3) is shown in this normalized 2D heatmap. The S_2-T_1 location (which corresponds to the initial similarity of 0.8870) has the maximum normalized value, 1.0. Signal S_2 has the best reliability and the strongest correlation with Template T_1, as evidenced by the most prominent and solid yellow region in the matrix. There are also significant parallels between S_1 T_3 (0.8467) and S_3 T_3 (0.7960). These values are seen in the colormap's darker yellow to orange region, indicating extremely dependable template alignment of the signals. These regions guarantee robust classification or matching tasks and imply uniform directionality in geometric terms. The other noteworthy similarity is displayed in S_3-T_2 (0.7676), which is represented by a warm orange color and indicates that there is a significant and well-organized association between the two vectors. The similarity ranges between T_2 and S_1 (0.7153) and T_3 and S_2 (0.7549) are reasonable and do not indicate strong or weak relationships. When matching on an interpretive or intermediate level is required, these pairs which have a respectable structural consistency are employed. The bluish-to-purple gradients have slightly lower similarity values, such as S_1-T_1 (0.6083) and S_2-T_2 (0.5888); these are not as conclusive as the high-intensity regions, but the associations are still present. S_3-T_1 (0.5740), the lowest cell in the matrix, is shown by a deeper purple blue region. Since the normalizing range will compress all values to 0-1, this is not a very low value; but, since this is the least aligned pair, it should be interpreted with extreme caution. Generally speaking, a normalized heatmap provides a user-friendly, stratified display of the degree of similarity, enabling the direct drawing of confidence levels based on color intensity. The strength of each signal-template relationship may be effectively seen with this enhanced 2D representation, which also offers a clear, descriptive picture of the underlying signal-template associations.

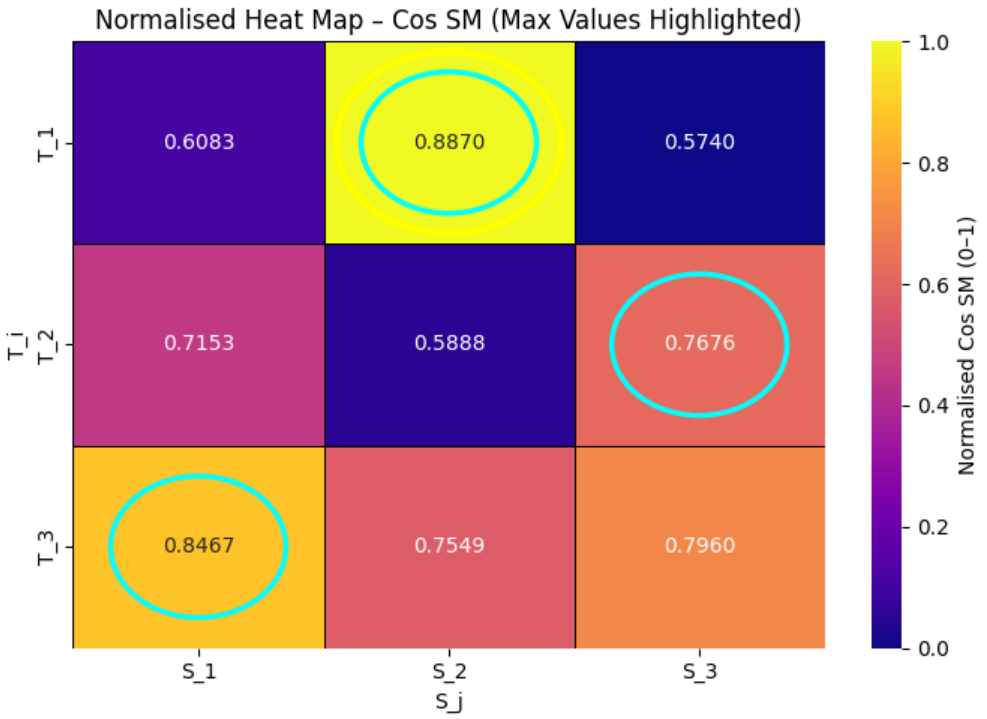

FIGURE 2. Normalized Heatmap

TABLE 5

Normalised Value Range	**Similarity Strength**	**Interpretation Meaning**	**Color Representation (Heatmap)**
0.00-0.20	Very Low	Weakest alignment; signals and templates share minimal similarity.	Dark Blue / Indigo
0.20-0.40	Low	Only mild alignment; structural matching is limited.	Purple
0.40-0.70	Medium	Moderate relational similarity; noticeable but not dominant.	Pink → Orange transition
0.70-0.90	High	Strong similarity; signal-template patterns align clearly.	Orange / Bright Red
0.90-1.00	Very High	Maximum similarity; most reliable match in the matrix.	Yellow

The Pearson Correlation Heatmap in Figure 3 is created using a diverging color map that alternates between deep blue (strong negative correlation), white (zero correlation), and dark red (high positive correlation). The linear correlation between the three signals (S_1, S_2, and S_3) is represented graphically in this 2D correlation table, where the correlation strength is directly

correlated with color intensity. As seen in a saturated red cell, S_1 and S_3 exhibit the largest positive correlation (0.894). There is a strong positive association between changes in S_1 and S_3 (r = 0.898), as this steep area shows. This association is very strong and consistent, which may indicate that these two signals have some underlying statistical or structural property. S_2 and S_3 (r = -0.760) and S_1 and S_2 (r=-0.388) have somewhat high negative associations. These blue areas represent negative associations: the probability of one signal being lower than another is higher. The value of -0.760, which is in an obviously strong negative domain, indicates significant opposition between S_2 and S_3. A weaker, but still significant negative relation between S_1 and S_2 is suggested by the less significant value of -0.388. The values in the diagonal (S_1-S_1, S_2-S_2 and S_3-S_3), are represented by the uniformly red squares; they are all 1.000 and are uncorrelated. They are used as a check to ensure that the desired matrix symmetry is obtained. There are no signal pairs that are uncorrelated (random) when the value is approximately zero. Instead, all relationships positive and negative have a structure that can be understood. All things considered, the heatmap offers a simple-to-understand layered representation of signal interdependence, where the intensity and color of the color instantly convey information about the degree of linear coupling. This makes it possible to clearly and descriptively assess how each signal interacts with the others in the system and determine which signals have the most mutual alignment or opposition.

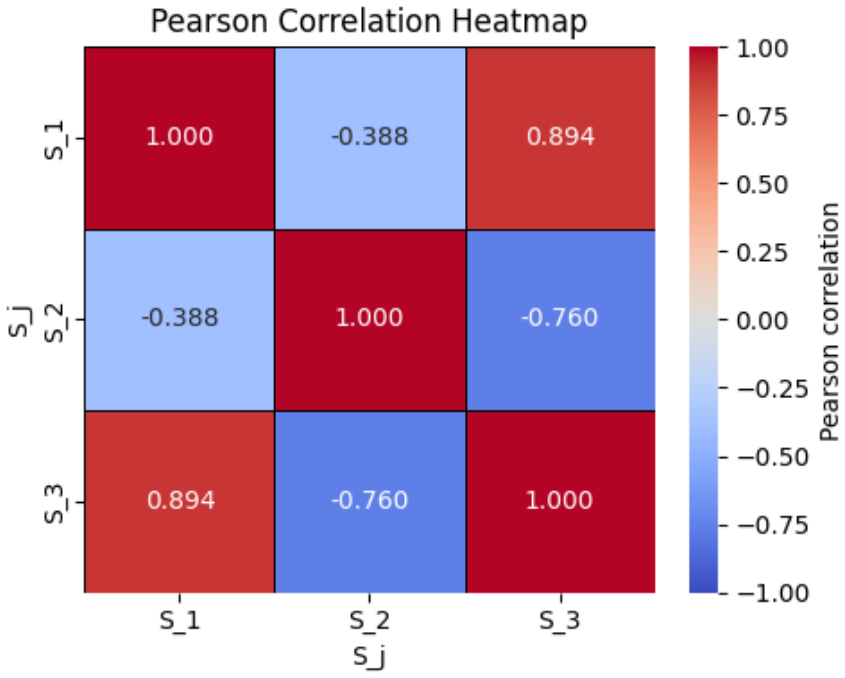

FIGURE 3. Pearson Correlation Heatmap

TABLE 6

Correlation Value Range	Relationship Strength	Interpretation Meaning	Color Representation
+0.70 to +1.00	Very Strong Positive	Signals increase together with high consistency; almost linear alignment.	Dark Red
+0.30 to +0.70	Moderate Positive	Signals tend to increase together, but with variability.	Light Red / Orange
-0.30 to +0.30	Weak / No Correlation	Little to no linear relationship.	White / Neutral
-0.30 to -0.70	Moderate Negative	As one signal increases, the other decreases consistently.	Light Blue
-0.70 to -1.00	Very Strong Negative	Opposite-direction behaviour; strong inverse alignment.	Dark Blue

Cosine Similarity (Cos SM) values between the three signals (S_1-S_3) and the three templates (T_1-T_3) are displayed in the 2D bar graph (Figure 4). Each bar color (black, green, and red) represents the degree of similarity between signals S_1, S_2, and S_3, respectively. The groups of bars are a collection of templates of T_i. This bar-based representation is useful in that it allows the comparison of signal-template pairs in specific categories, as opposed to the previous heatmap-based representations. The tallest green bar in the first group indicates that S_2 and T_1 have the highest similarity in the set, 0.8870. The fact that Signal S_2 shows the most definitive and reliable match with Template T_1 is reinforced by the fact that this peak is isolated from its group and highlighted by an elliptical highlight. This peak is consistent with the stability of the directional match of S_2 with T_1 in different viewpoints and is in agreement with the previous heatmap observations. There are also other close similarities between S_1-T_3 (0.8467) and S_3-T_3 (0.7960), which are marked by black and red tall bars in the T_3 group. These values, which are in the higher similarity range, suggest S_1 and S_3 have very good structural match with Template T_3. Another important peak is the similarity value of S_3T_2 (0.7676), which is visible in the T_2 group as a very tall red bar. The moderate similarity values of S_1T_2 (0.7153) and S_2 T_3 (0.7549) are indicated by the bar height. They represent a high but sub-optimal match between the respective signals and templates. They have quite similar geometric characteristics without being extremely matched, forming a moderate similarity match. Relatively short bars are used to illustrate smaller similarity values, such as S_3 T_1 (0.5740) and S_2T_2 (0.5888). The lighter shade in the heatmaps of the clusters represent these lower signal template relations. These data represent a lower confidence in the alignment of signals, despite their non-negligible similarity. Overall, the layered structure of the 2D bar graph which represents a hierarchy of similarity values, allows the perceivable classification of Cos SM values. The bar heights over this figure show a continuous trend of higher similarity values around T_1 and T_3 which is in accordance with the knowledge extracted from the heatmap analysis but S_2T_1 is the highest association.

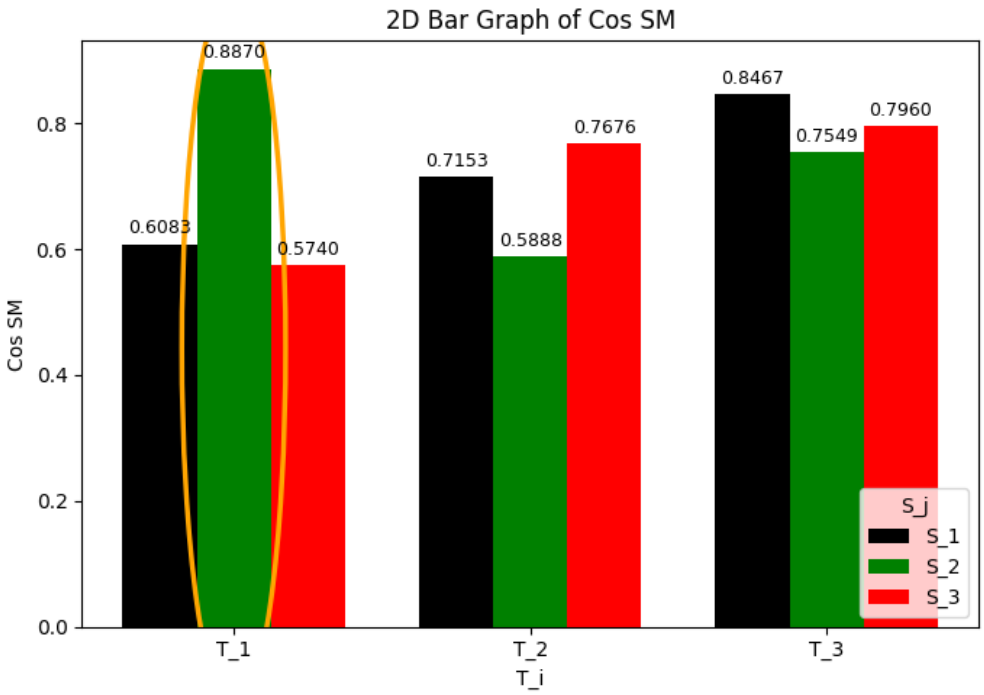

FIGURE 4. 2D Bar Graph

TABLE 7

Value Range (Cos SM)	Similarity Strength	Interpretation Meaning	Bar Colour Representation
0.55-0.60	Low	Weak alignment; signals show minimal similarity to the template.	Lower bar height, dull tones (e.g., red for S_3 at T_1).
0.60-0.70	Medium	Moderate alignment; noticeable but not strong similarity.	Mid-height bars (e.g., S_1 at T_1, S_1 at T_2).
0.70-0.80	High	Strong alignment; patterns match reliably.	Tall bars (e.g., S_3 at T_2, S_2 at T_3).
0.80-0.90	Very High	Dominant alignment; highest-quality similarity.	Tallest bars (e.g., S_2 at T_1, S_1 at T_3).

The Cosine Similarity (Cos SM) between the input signals (S_1-S_3) and templates (T_1-T_3) is shown in the 3D bar graph chart in Figure 5. This three-dimensional illustration adds extra dimensions and distances between each signal-template pairing to the comparison structure of the similarity matrix and allows for more visual differentiation of the relative magnitudes of each coupling. We also placed numerical values on top of each bar to assist with the interpretation and remove any magnitude uncertainty. This confirms that S_2 is the most strongly matched in the forward direction with Template T_1 similar to the dominant association in the 2D heat maps and bar graphs. This high value makes this match the most easily recognized in the dataset. The S_1-T_3 (0.8467) and S_3-T_3

(0.7960), both of which have high bars in the T_3 cluster, show additional noteworthy commonalities. The high values suggest a clear geometrical relationship between Template Transcript T_3 and S_1 and S_3. Further, there is a second very high bar, S_3 T_2 (0.7676), which suggests a steady and significant unidirectional connection in the second template cluster. Mid-level bars representing the average similarity values of S_1 T_2 (0.7153) and S_2 T_3 (0.7549) are displayed. These are persistent but not strong connections, and indicate that while the signals are acceptable in terms of the similarity to the particular templates, they are not as confident or convinced as the highest matches. Shorter bars, S_3-T_1 (0.5740) and S_2-T_2 (0.5888), show weaker alignments. These lower bars, which show weaker but still measurable connections, are at the lower level of the similarity hierarchy. Their bar lengths determine the order of the whole similarity space, and are graphically opposite to the strong matches. In most cases, the Cos SM values are presented as a stepped, dimensionally enhanced 3D bar graph. This three-dimensional categorisation of bars over strong, moderate, and weak associations can be readily distinguished, and is complemented by the bar colour contrast and value labelling. The findings from the heatmap analysis are reinforced by this three-dimensional representation, providing a rigorous and clear view of the similarities between the signal and template.

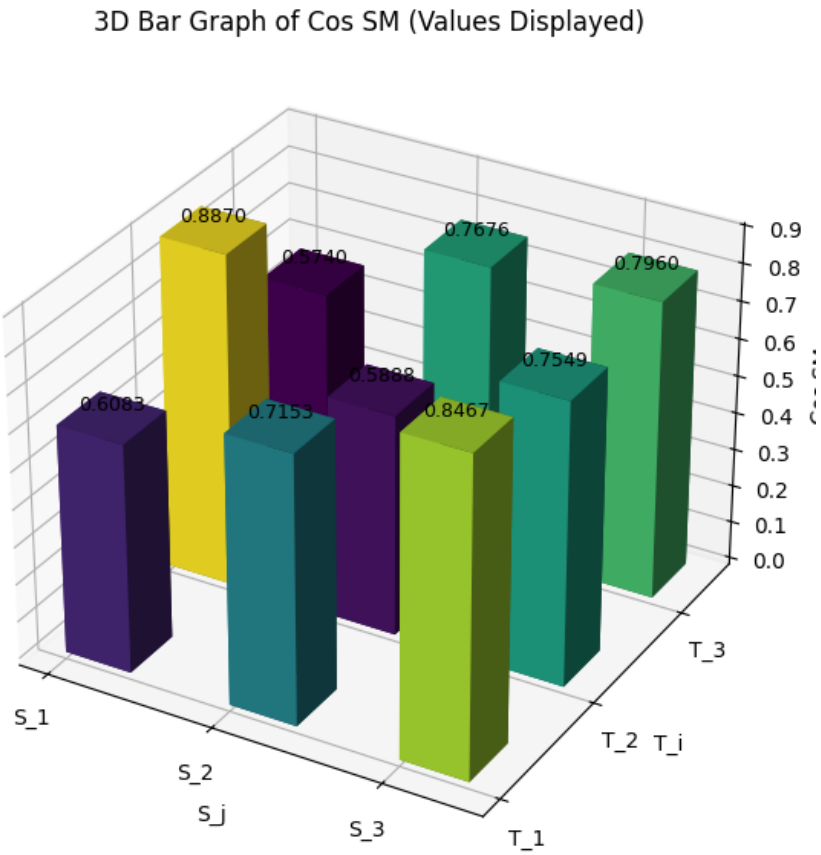

FIGURE 5. 3D Bar Graph

TABLE 8

Value Range (Cos SM)	Similarity Strength	Interpretation Meaning	3D Bar Appearance
0.55-0.60	Low	Weak alignment; weak match between signal and template.	Short bars (dark colors)
0.60-0.70	Medium	Moderate alignment; noticeable but not strong.	Mid-height bars
0.70-0.80	High	Strong alignment; reliable similarity.	Taller bars (green-teal)
0.80-0.90	Very High	Strongest match; dominant similarity.	Tallest bars (yellow-lime)

The Cosine Similarity (Cos SM) matrix can be further translated into a 3D surface map in Figure 6, which provides a smoothly continuous geometric view of the inter-relationships between the templates (T_1 T_3) and signals (S_1 S_3). This plot can be used to display a textured surface map with similarity values on the vertical axis and the textured surface is colour-coded with a viridis gradient. Thus, the hills and valleys of the landscape can be used to visually represent the relationships between the discrete matrix. The S_2-T_1 combination has the largest peak on the surface with Cos SM at 0.8870. The strong connection apparent from all the representations above is evident in the triangular peaked ridge, which is elevated above other areas of the surface. Evidence of the strength of this link is provided again as Signal S_2 is the most directionally similar to Template T_1. The surface has other areas of elevation. As plateaus emerge, the S_1T_3 (0.8467) and S_3T_3 (0.7960) regions exhibit high and effective levels of similarity. Elevations in the surface indicate that Template T_3 remains in contact with S_1 and S_3. Between the two vectors there is a closer structural relationship at S_3T_2 (0.7676), and a similar, although not as high peak is visible. Mid-elevation areas are used to display the intermediate similarity areas, such as S_1T_2 (0.7153) and S_2 T_3 (0.7549). These are sufficiently elevated to show a high degree of directionality, but not as high as the main peaks. The intermediateness in the similarity distribution is emphasised by the smooth connection of the levels in the surface. Lower similarity values, such as S_2T_2 (0.5888) and S_3T_1 (0.5740), appear as mild surface depressions. These saddles have weaker associations, but are still observable (relative to the central plateau). S_1T_1 (0.6083), located on the bottom edge of the range of surfaces, is the smallest trough. A 3D surface plot may be used to represent the topographical map of the layered Cos SM landscape. Good correlations are shown as peaks, moderate correlations as slopes and poor correlations as valleys. This 3D representation is a complement to the heatmap and bar plots in that it provides a continuous visual field that is easy for the viewer to comprehend, in terms of relative weight, balance and shape of signal-template correlations.

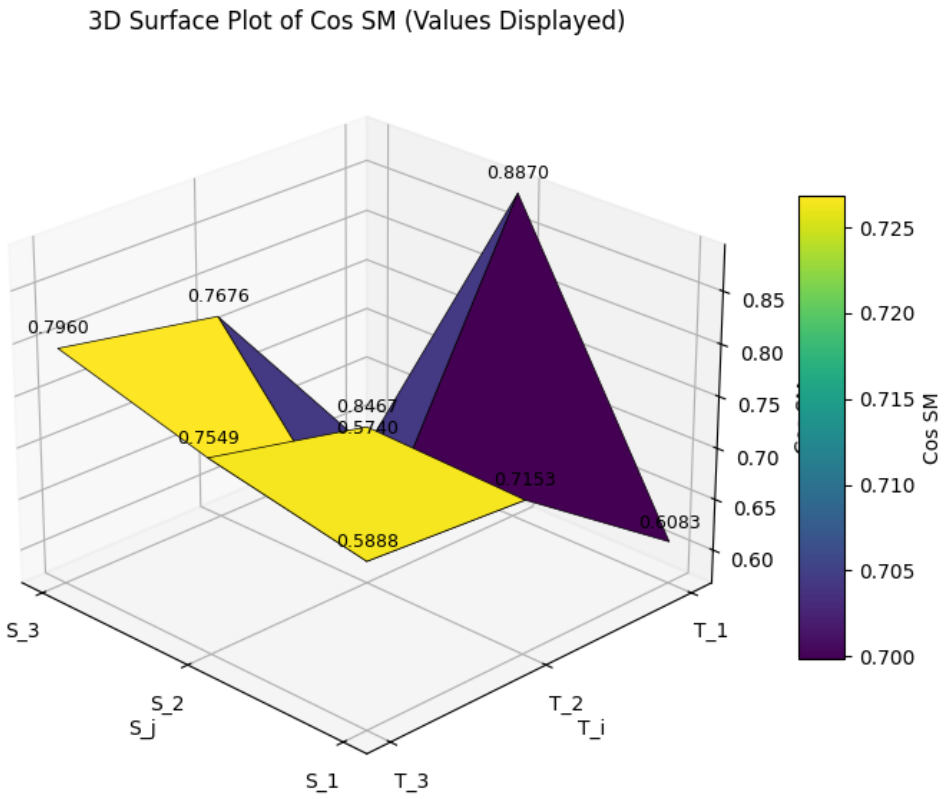

FIGURE 6. 3D Surface Plot

TABLE 9

(Cos SM) Range	Similarity Strength	Interpretation Meaning	3D Bar Appearance
0.55-0.60	Low	Weak similarity; surface dips or valleys.	Darker purple regions, low Z-height
0.60-0.70	Medium	Moderate similarity; transitional slopes.	Blue-green mid-level surfaces
0.70-0.80	High	Strong similarity; elevated surfaces forming ridges.	Yellow-green slopes

Figure 7 shows the 3D surface plot of the normalized Cosine similarity (Cos SM) matrix in [0-1] range which is a color-coded and/or height-coded representation of the similarity between the templates (T_1-T_3) and the signals (S_1-S_3). The original matrix can be converted to a geometrical structure of landscape by seamlessly blending between the relatively more similar parts in bright yellow and relatively less similar parts in dark purple on the surface using a perceptually uniform colormap. The S_2-T_1 combination which still remains the highest similarity after normalization (original=0.8870, normalized=1.0) is the highest peak. The surface is dominated by this very high triangle peak that shows that Signal S_2 is the most final and directionally sound conformance to

Template T_1 in yet another visual modality. S_1 T_3 (0.8467) and S_3 T_3 (0.7960), which are perceived as somewhat high plateaus on the surface, also show extensive areas of similarity. The results for these areas demonstrate that Template T_3 is the highly consistent match with S_1 and S_3 respectively. Another ridge that runs across S_3 4 T_2 (0.7676) further confirms the signal's similarity to the template. Normalized similarity values for intermediate values, like S_1-T_2 (0.7153) and S_2-T_3 (0.7549).

As a possible source of supportive but not conclusive information about structure, these intermediate areas gather significant but not the most dominant similarity connections that demonstrate moderate directional coherence. It's easy to spot the less similar regions using depressions in surface elevation. The weaker signal-template connections, S_2-T_2 (0.5888) and S_3-T_1 (0.5740), are linked to the most prominent depressions. The lowest depression of the data set (at S_1T_1 0.6083) has the lowest normalized similarity. These are located on the surface with reduced colour, resulting in a stronger emphasis on their lesser effects. Normalized 3D peaks and valley surfaces are often topographically hierarchical, and informative explanations of similarity magnitudes. Slopes indicate low matching, troughs indicate low matching and peaks indicate strong correlations. This spatial representation of the similarity matrix (continuously) provides a detailed and informative representation of the similarity between signals and templates, complementing previous patterns of analysis using heat maps and bar graphs.

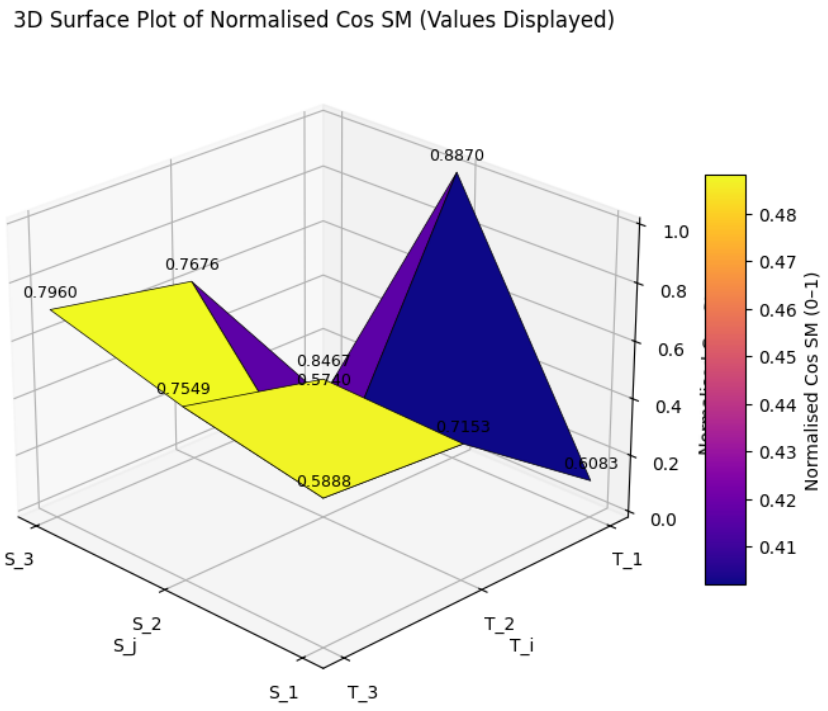

FIGURE 7. 3D Surface Plot of Normalized COS SM

TABLE 10

Normalised Value Range	Similarity Category	Interpretation Meaning	3D Surface Appearance
0.00-0.20	Very Low	Weakest relationship	Deep purple, lowest surface dips
0.20-0.40	Low	Below-average similarity	Dark blue troughs
0.40-0.60	Medium	Moderate similarity	Blue-orange mid-elevations
0.60-0.80	High	Strong similarity	Orange-yellow elevated ridges
0.80-1.00	Very High	Strongest similarity	Bright yellow peaks

Using the Cosine Similarity data, Figure 8 displays a 3D PCA clustering scatter plot data with dimension reduced to three orthogonal principal components (PC 0-PC 3). This adjustment enables a more precise spatial analysis of the relationship between the signals (T_1-T_3) and the original Cos SM to be made while preserving the greatest possible variance. The 3D scatter plot, which shows the exact triplets of each template, can be used for both numerical and geometric analysis. The clustering process divides the data into two clusters, which are displayed in two different colours. The triplet (0.6083, 0.8870, 0.5740) of the point corresponding to T_1 is located in a separate cluster. As a result of its very high similarity with signal S_2 that makes it unique in the PCA space, the clustering shows that Template T_1 has a very unique similarity profile among the templates. This distinctness is illustrated in terms of its position on the positive PC 1 and slightly higher PC 2 axes. The second cluster is made up of T_2 and T_3. Vector T_2 (0.7153, 0.5888, 0.7676) is placed in the fairly medium region of the PCA, suggesting that the pattern of the three signals is not very strong. T_3 (0.8467, 0.7549, 0.7960) holds a more advanced position on the positive PC1 axis since its similarity values are substantially greater than those of all the signals, which PCA naturally aggregates as high joint variance. A fundamental structural difference is shown by the gap between T_1 and the group of T_2, T_3. T_2 and T_3 have a more uniformly distributed similarity, with T_3 having an evenly high similarity in all signal dimensions, while T_1 has a single similarity (high alignment with S_2). Overall, the geometric representation of the similarity data provided by this 3D PCA projection is clear and expressive. The clustering pattern, which shows that T_1 and T_2 behave differently while T_3 is the most aligned template, supports earlier heatmap and surface-plot findings. As a result, PCA offers an appealing complementary viewpoint that uses variance-driven spatial segregation to reveal hidden structure in the similarity matrix.

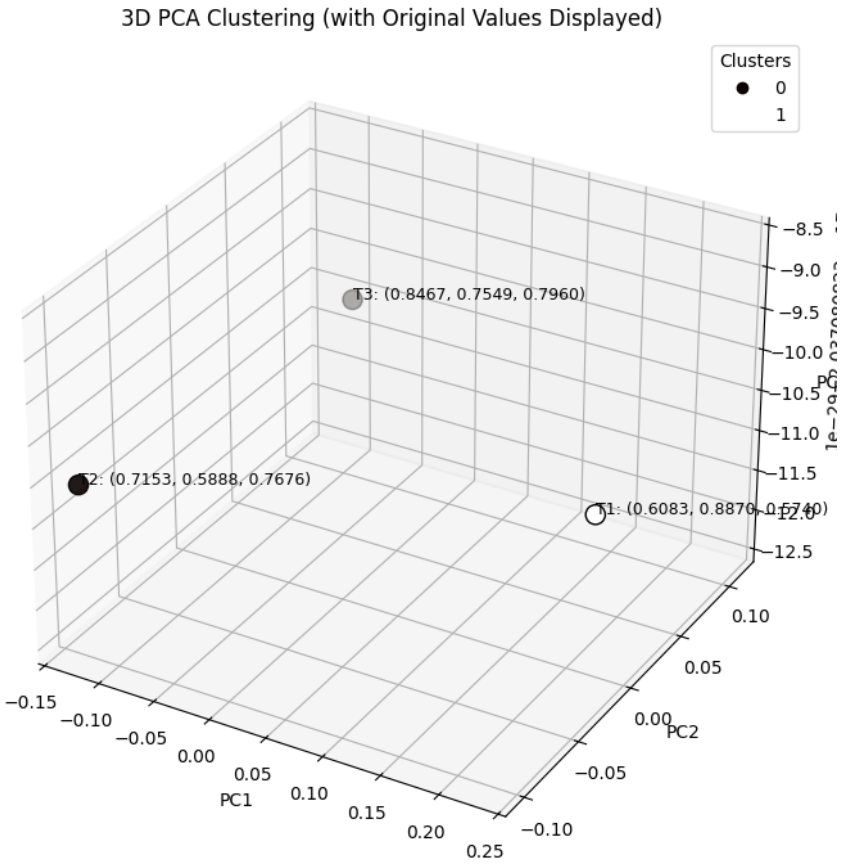

FIGURE 8. 3D PCA Clustering Visualization

TABLE 11

PCA Dimension Range	**Interpretation**	**Visual Effect in Plot**
PC1: -0.15 to +0.25	Shows the strongest separation between T_2 vs T_1, T_3	Horizontal spread
PC2: -0.10 to +0.10	Small variance → points remain close vertically	Slight vertical shift
PC3: -12.5×10^{-10} *to* -8.5×10^{-10}	Tiny variance → PCA compressed depth	Very shallow depth differences

Figure 9 displays a 3D t-SNE embedding of the Iris dataset. The four measurements of the flowers' original scale are projected into a nonlinear manifold of three dimensions using t-SNE, which maintains local neighborhood structure. The points are arranged so that flowers with similar feature patterns are close together and those with significant differences are farther apart. The distribution patterns of the three species Setosa, Versicolor, and Virginica can be directly compared thanks to the red, green, and blue markers used to symbolize them. Partially emergent

is the embedded clustering structure. According to the established morphological traits and minimal overlap with the other species, the setosa samples (red) are slightly concentrated in specific regions of the three-dimensional space. The second component of this classification verifies that setosa is the most prominent feature in the feature space and is a well-established tendency in dimensionality-reduction studies on the Iris dataset. On the other hand, the virginica points (blue) and versicolor (green) have a more intricate spatial structure. Additionally, they spread in similar local neighborhoods and largely overlap in their clusters, illustrating the more subtle differences between the two species. Versicolor and virginica sample the manifold in similar places by taking more measurements of their petals and sepals, which results in a mixed distribution that is typical of t-SNE visualization. These two species' nonlinear borders are likewise vulnerable to dispersal. Instead of clearly defined clusters, the entire embedding is in a layered, cloud-like spatial composition. The data's natural biological continuum is reflected in this finding: setosa may be divided into strong groups, and the division between versicolor and virginica is more gradient-like. As a result, the 3D projection provides an intuitive and understandable visual summary of the similarities and differences between species, and quantitative analysis can supplement the information with a geometric description of the underlying data that is perceptually relevant.

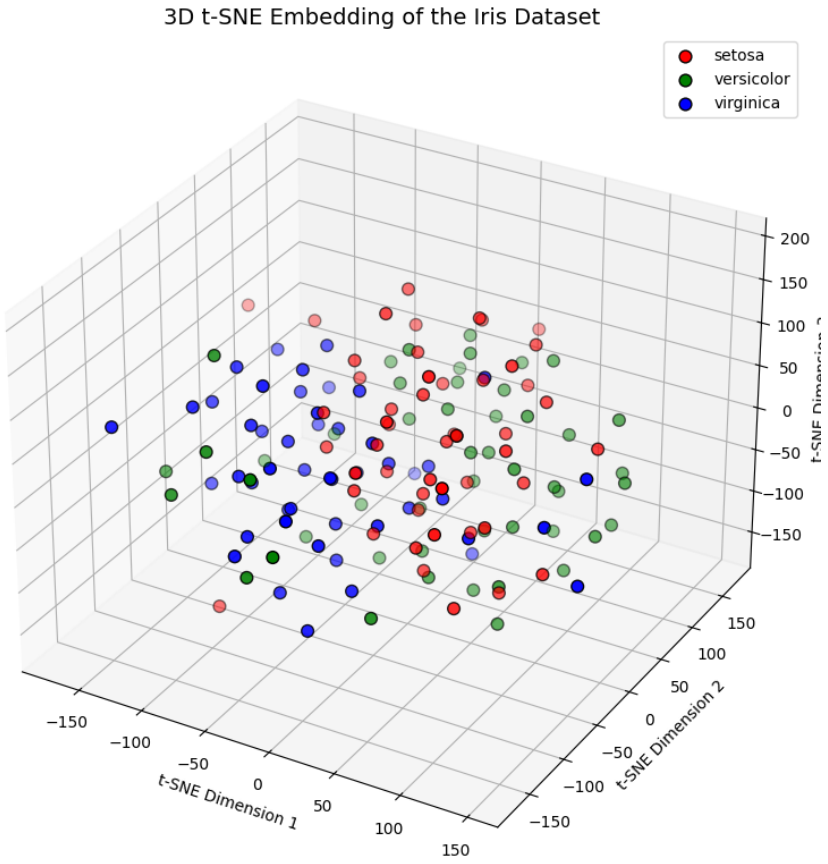

FIGURE 9. 3D t-SNE Embedding of the Iris dataset

TABLE 12

Numerical Value Range	**t-SNE Dimension 1**	**t-SNE Dimension 2**	**t-SNE Dimension 3**	**Color Representation (from plot)**
-200 to -100	Low	Low	Low to Medium	Blue / Dark-Blue cluster regions
-100 to 0	Medium-Low	Medium-Low	Medium-Low	Cool blue transitioning to greenish
0 to +100	Medium-High	Medium-High	Medium-High	Green / Light green
+100 to +200	High	High	High	Red / Orange clusters

The high dimensional feature vectors are mapped to a 3-dimensional nonlinear final dimension using an t-SNE 3D embedding of the dataset, as shown in Figure 10. Local neighborhood connections that is, points that are close to one another in this 3D space share comparable structural characteristics in the original feature space are preserved thanks to the t-SNE algorithm. The distribution of the categories can be visually distinguished by using red, green, and blue markers for each of the data classes, including Class 0, Class 1, and Class 2. A loosely clustered spatial structure is formed by the embedding. Class 0 (red) lacks a very compact group formation and is dispersed throughout several regions of the manifold. This means that the Class 0 samples are scattered across the t-SNE map and have a large variance. However, some substructures or sub patterns are shown in some regions of locally dense red spots. This is why some of the Class 1 (green) points overlap with Class 0 and Class 2 points. This is one of the transitional characteristics of Class 1 in the feature space; the members of the Class are not in the feature space completely isolated. This is generally the case when the class's characteristics are transitional or overlapping. The points in Class 2 (blue) are evenly distributed throughout the manifold's center and periphery. There are several Class2 samples jumbled up with the other two classes, despite the formation of a few blue clusters. Because of this broad dispersion, the data set exhibits smooth rather than rigorously defined class boundaries, which is characteristic of real-world data where categories may have statistical traits that overlap. The embedding in 3Dt-SNE generally shows a very heterogeneous yet largely disaggregated structure. The fact that not all classes form completely distinct clusters suggests that the data set is made up of nonlinear relationships between categories and overlapping feature distributions. An intuitive geometry-based picture of the relationships between the samples in terms of similarity, subtle subclusters, overlaps, and class transitions is provided by the visual layering produced by t-SNE.

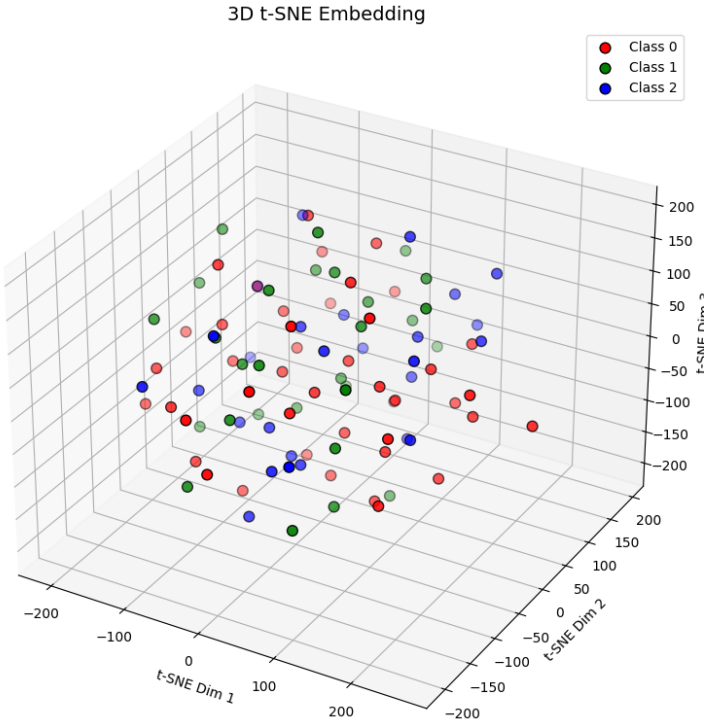

FIGURE 10. 3D t-SNE Embedding

TABLE 13

Value Range	t-SNE Dim 1	t-SNE Dim 2	t-SNE Dim 3	Interpretation
-200 to -100	Low	Low	Low	Points in this zone are strongly pulled toward one cluster boundary; often indicates compact or isolated class regions.
-100 to 0	Medium-Low	Medium-Low	Medium-Low	Transitional region where classes begin to mix without complete separation.
0 to +100	Medium-High	Medium-High	Medium-High	Stronger separation; indicates meaningful structural differences encoded by t-SNE.
+100 to +200	Very High	Very High	High	Points pushed far in embedding space, representing dense subclusters or high-contrast features.

A 3D t-SNE embedding with KMeans clustering is shown in Figure 11 to illustrate a dataset's nonlinear dimensionality reduction perspective and an unsupervised classification of the dataset's underlying structure. The KMeans algorithm splits the embedded space into three clusters, represented here by red, yellow, and black markers, while the t-SNE projection arranges the samples on a three-dimensional manifold that preserves local neighborhood relationships. The first cluster (red) was found in a dispersed but noticeable region of the t-SNE space's central and higher levels. The distribution it displays exhibits relatively high levels of cohesiveness, meaning that

the samples that belong to this cluster share a number of comparable feature patterns, but not enough to form a tight geometrical structure. Local commonalities that are mostly represented by t-SNE, which pushes points up along the third dimension, are consistent with this cluster. The second cluster (yellow) is more concentrated at the lower end of the 3D manifold and is more focused on the capacity to form a more compact structure. This population's spatial distribution refers to a fairly homogeneous set of samples, as seen by the tendency of SNE to find sites that are strikingly similar to one another. The dense sampling suggests that samples with the most distinctive and consistent underlying feature traits are likely linked to Cluster 2. Compared to the other groups, the third cluster (black) is dispersed throughout the embedding's left and middle regions, exhibiting a wider range of dispersion. This lengthy distribution suggests that the cluster of internal features is diverse. The points are arranged in a kind of gradient rather than being firmly clustered or entirely scattered, suggesting the presence of certain sub-internal patterns that KMeans classified into a single class. The 3D t-SNE + KMeans plot often presents a more or less comprehensible view of the data's grouping. Although the clusters show different spatial characteristics a tightness in yellow, a moderate aggregation in red, and a diffusion in black, there are still cross-boundaries in clusters which are common in real data sets with non-linear and smooth changing features. As a result, a hybrid of t-SNE and KMeans offers a layered perspective of global clustering tendency and local similarity relationships, giving a deep geometric understanding of the data set's structure.

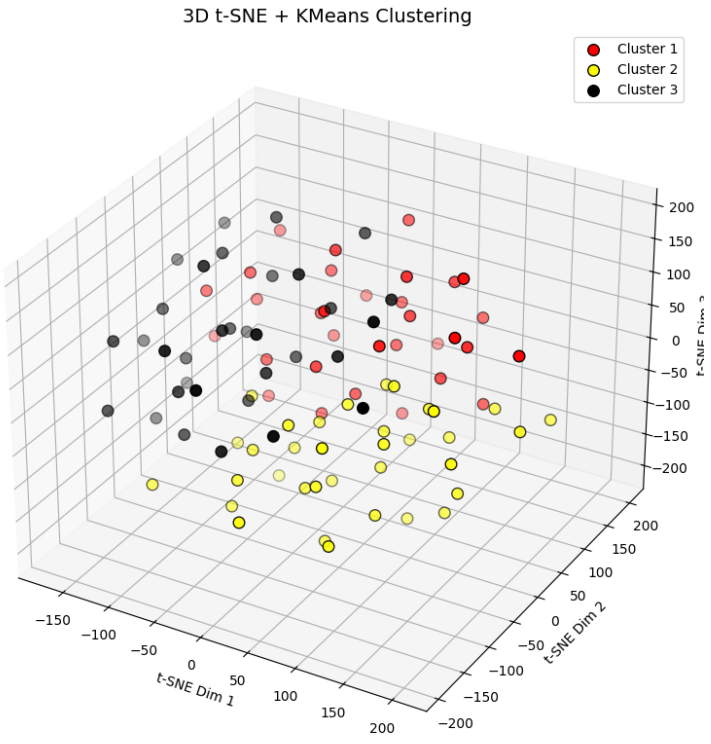

FIGURE 11. 3D t-SNE Embedding with KMeans Clustering

TABLE 14

Range	Interpretation of Position	Meaning in Cluster Space
-200 to -100	Low	Points lie in deep embedding basins → highly compact internal subclusters
-100 to 0	Medium-Low	Transitional region where clusters begin to overlap
0 to +100	Medium-High	Moderate separation; stable inter-cluster boundaries
+100 to +200	Very High	Strong nonlinearity; high local contrast; cluster peaks

Figure 12 shows the Cosine Similarity (Cos SM) value of three signals (S_1-S_3) on three templates (T_1-T_3) using cubic splines. The splines enable the representation of discrete similarity values in a continuous way, so that the trend, transition and curvature of the curve can be observed. To get both geometric as well as numerical information, the values from the table are used to label the curves. With a value of 0.6083 at T_1 and 0.8467 at T_3 the S_1 curve (blue) shows a relatively smooth growing trend. Due to the values that are monotonically increasing and have low curvature, the relationship between Signal S_1 and templates has a slow but continuous growth as T grows. This is easily seen in the spline, which shows that S I has been constantly getting closer and closer with the highest similarity at T-3 (0.8467). The S_2 curve (orange) has a different pattern. It starts with the peak similarity value of 0.8870 at T-1, then drops sharply to its lowest value of 0.5888 at T-2, to increase again at T-3 (0.7549). The U-shaped Signal S_2 is an excellent fit to Signal T_1 but it gets substantially weaker at T_2 and partially recovers at T_3. The spline highlights the sharp turn's noticeable curvature, showing S_2 is not monotonic. The green S_3 curve is an upward trend followed by a slight downward trend. It begins at the dataset's minimum (0.5740 at T_1), peaks at T_2 (0.7676), and then gradually descends into the dataset approaching 0.7960 at T_3. While the correlation is also high at T_3 and almost as high as the middle of the template sequence, the dome-shaped curve suggests that the best alignment of S_3 is in the middle of the template sequence. The spline's dome shape is the gradual shift from increasing to decreasing value. The different related aspects can be demonstrated by the three curves together:
Although the S_2 is very highly matched to templates, it is the most highly matched (0.8870).
S_1 is also high, steady and monotonic with an improvement at the end.
S_3 is high in T_2 and equal to following values.
In summary, the cubic spline shows the organized growth of the similarity for the individual signals with respect to the templates indices. The prominence of the peaks, troughs and transitions allows for a visual assessment of the alignment with more detail than is possible with just the table.

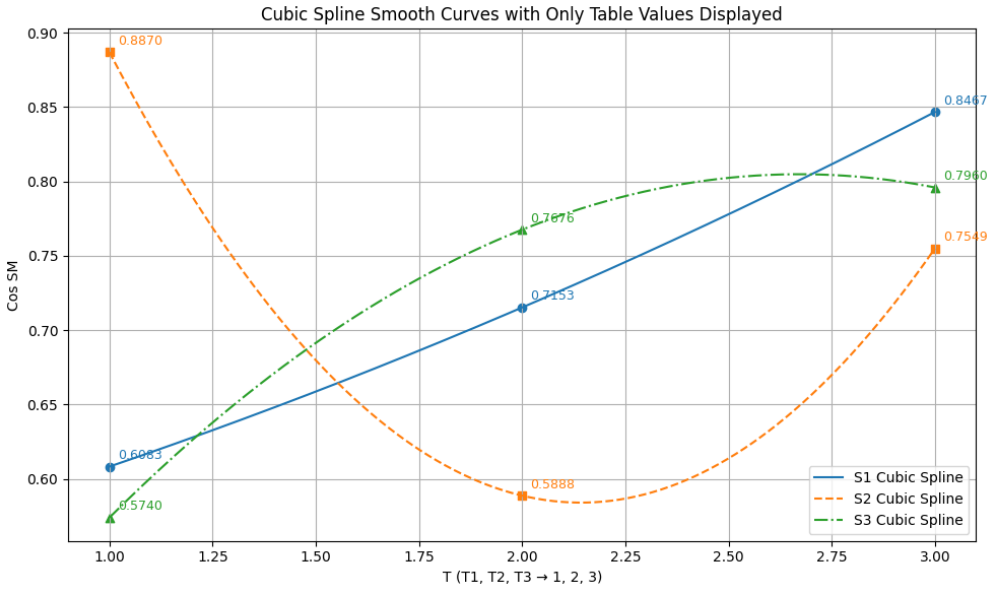

FIGURE 12. Cubic Spline Smooth Curves

The cubic spline interpolation of the Cos SM of the three signals (S_1 S_3) multiplied by 1/0 1 of the template is shown in Figure 13. To be able to compare the curves as equal, in terms of shape, direction, and structural change among templates T_1, T_2 and T_3, normalization is done with a relative approach to each other, by eliminating the influence of magnitude. As cubic splines are smooth, the dark red, yellow and black line colours help to increase contrast between the signals. The S_1 curve, which is dark red, shows a trend of a monotonically growing advancement from a low value of 0.110 to a high value of 0.871 at T_1 and T_3, respectively. The un-normalized trend of this curve is identical to this monotonic advancement trend, but has been scaled to be more visually noticeable. The slope displays a constant and increasingly intelligent similarity, showing that S_1 becomes increasingly similar to the template as the index of the template increases. The most dramatic change occurs in S_2 (in yellow). It begins at a normalized maximum of 1.000 at T_1, falls to a low of 0.047 at T_2, and then rises to 0.578 at T_3. The S_2 curve (yellow), which shows a strong U-shape, shows the normal function of S_2, which is very similar to T_1, substantially decreased at T_2 and slightly recovered at T_3. This curvature is enhanced by normalization and, as a result, is clearly visible and a measure of the relative difference between templates. The curve of S_3 (black) is slightly down and up. It starts at the normalized minimum (0.000 at T_1), increases to 0.679 at T_2, and concludes at 0.709 at T_3. This dome curve indicates that S_3 is quite strong at T_3 and most often close to T_2. The normalized spline is a better representation of the small curve than the raw data plot. In contrast:

S_1 is a simple growth pattern (progressively better).

S_2 has the greatest nonlinearity with a rise-fall-rise pattern.

S_3 has a slight curve between the linear growth pattern of S_1 and S_2 volatility.

The underlying relative structure of the similarity data (which is not scale-dependent) can be seen by summing the normalized splines. The visual signal enhancement of peaks, troughs and transitions on the relative scale of dynamism range of each signal makes it more intuitive to understand the similarity each signal has with the templates.

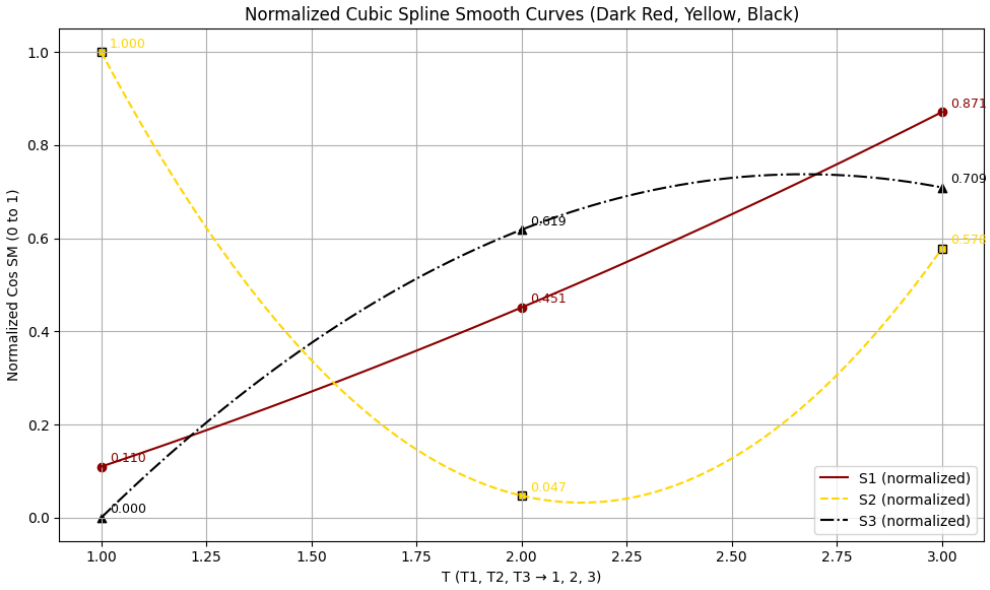

FIGURE 13. Normalized Cubic Spline Smooth Curves

7. Analytical Aspect-Based and Method-Based Evaluation of Cosine Similarity between Templates (T_1-T_3)

The Cosine Similarity of three signals (S_1 S_3) with templates (T_1 T_3) has been evaluated in this study using aspect-based and method-based evaluation methods. As the highest similarity is observed between S_2 and T_1 (0.8870), we found T_1 has the highest selective alignment. It has been found that T_3 shows high similarity, suggesting that it has a balanced alignment but T_2 has mixed signal behaviour. The combined approach of analysis has revealed the patterns in the similarity matrix and how Cosine Similarity can be effectively used to understand the direction correlations in multi-dimensional signal template systems.

7.1. **Aspect-based Analysis.** The Cosine Similarity correlations of the signals with the templates can be classified into three categories of similarity behaviour of T_1 to T_3 **Strong similarity (0.80-0.89):** S_2-T_1 (0.8870), the pivot point of the similarity and highest similarity in all the representations, is the strongest and most authoritative similarity. S_1-T_3 (0.8467) and S_3-T_3 (0.7960) are two more good correspondences that fall into the second level of good correspondences and provide good structural and categorization information.

Moderate alignments (0.70-0.79): Between S_1 T_2 (0.7153), S_3 T_2 (0.7676), and S_2 T_3 (0.7549), there exist intermediate similarity values. The non-dominant similarity (significant but moderate

reliability) is represented by these values. They are stable in their secondary reinforcement of signal-template matching tasks, despite not being definitive.

Weak alignments (0.57-0.60): The lower similarity zones are S_1 T_1 (0.6083), S_2 T_2 (0.5888), S_3 T_1 (0.5740), and are all found near to the lower end of the similarity strength interval. S_3-T_1 is the weakest of these, hence it is important to evaluate them carefully before using them to establish conclusive matching. With its strong connection with T_1, middling results with T_3 across all templates, and lowest results with T_2, Signal S_2 is the most common in the aspect-based analysis. Signal S_3 has mixed behavior (strongly on both T_2 and T_3, but considerably weaker on T_1), while Signal S_1 has mid-range behavior, particularly to T_2 and T_3.

7.2. **Method-based Analysis.** The methods-based analysis illustrates how the different computational and graphics methods can be used to investigate the similarities: Figures 1 and 2 clearly shows the existence of strong associations via colour intensity. In the absolute and normalized Cosine Similarity maps, S_2-T_1, being always in the bright yellow region, is easily spotted. Pearson correlation maps (Figure 3), which show both positive and negative correlations, make it possible to distinguish positive and negative trends that are more difficult to discern in the Cosine similarity maps, and a better understanding of linear associations. Grouped Bar Charts (Figures 4-5) explicitly compare the level of similarities between templates in explaining proportional contributions. For example, S_1 is less similar to T_1 than S_2 (0.6083 and 0.8870 respectively), confirming the hierarchical structure that is initially suggested by the heatmaps. To better illustrate the comparison, the 3D Bar Graphs (Figures 6-7) use altitude indicators and geographic distance to represent areas of the lower troughs for weaker correspondences and areas of the steeper peaks for stronger correspondences. The geometric similarity strength structure of the set of templates is illustrated by the steeple at T_1-S_2 and the larger plateau at T_3. Overall, these method-based visualizations offer a comprehensive and in-depth interpretation, validating the aspect-based results and a multi-tiered view of the distribution of Cosine Similarity within the matrix.

8. Interpreting Signal-Template Behaviour through a Hybrid Visual-Metric Analysis of Cosine Similarity

In this paper, we analyse the Cosine Similarity heat map in terms of the four interpretative aspects of visibility, associativity, dynamicity and scalability. Associations with a strong signal, such as S_2 T_1 are well visible, and the Viridis colormap offers a good contrast. The continuous gradients of the colormap show the dynamic variation between the templates, but the associative clusters are due to a continuous grouping. Despite the larger dataset, the visualization is still effective because of the matrix arrangement and the color value scaling. Generally speaking, the heatmap offers a straightforward, scalable, and behaviorally expressive depiction of signal-template similarity.

Visibility

Viridis was used to construct the heatmap in Figure 1, which has a high perceptual visibility due to

its brightness balanced color gradient of bright yellow (high values) to deep purple (low values). The dominant matches S_2 T_1 and S_2 T_4 become instantly apparent with the vivid yellow highlight as a result of the increased contrast in the similarity strengths. Strong, moderate, and weak alignments can be distinguished clearly without the requirement for numerical analysis thanks to intermediate regions (greens and oranges). Even the slightest modifications, such as the one that emerges between 0.7549 and 0.7960, are noticeable because there are no abrupt or misleading color shifts. The user can immediately and intuitively determine the similarity relationship because the figure is often visually apparent.

Associativity

The heatmap's ability to maintain and depict the relational structure between signals and templates is known as associativity. To encourage associative coherence between similar values arranged in similar color ranges, Figure 1 shows a colormap. This can be directly relational mapped. For example, the yellow-orange cluster surrounding T_3 shows that S_1 and S_3 are strongly associatively aligned, while the bluish-green area surrounding T_2 shows weaker associations. For example, S_2 is strongly aligned, but not to the same extent as S_1 and S_3 (0.5888). The identification of collective behavior is made easier by the spatial closeness of high-intensity cells (e.g., T_3 as a strongly associative template). As a result, the heatmap offers conceptual linkages between similarity patterns visual support.

Dynamicity

The feature of a visualization that can represent change, transition or gradient in the similarity landscape is called dynamicity. The Viridis colormap allows for the dynamic differences across the templates to be perceived and facilitates the perceptual smooth blending between low and high similarity. For example, the S_2 is dynamic in transition in that it is high at T_1, low at T_2 and intermediate at T_3. The transitions are smooth in uploading these changes. Likewise the dynamic positive transition of S_1-T_1 to S_1-T_2 and S_1-T_3 is dynamic in terms of the colors being warmer. This time-dependent mapping represents how the patterns of similarity progress between T_1 T_3.

Scalability

Being a matrix and using a colormap, the heatmap in Figure 1 is scalable. The set of possible signals (or templates) can be made larger and larger (i.e. the set can be scaled up) for a larger and larger heatmap. Since the Viridis colormap is uniformly distributed across the perceptual spectrum, there will be no confusion if more values are added. This makes scaling easier. Moreover, since the encoding of color is not dependent on the size of the matrix, the approach can be applied to larger matrices.

9. Sensitivity Analysis of Table 3: Cosine Similarity Scores between Signals (S_1-S_3) and Templates (T_1-T_3)

We examine the sensitivity of the similarity structure to the signal template pairs. It also identifies which relationships have the greatest impact on classification decisions and which matrix

elements are sensitive and resistant to perturbation. The consistency of these values can be used to show how consistently each signal maintains its geometric alignment with the templates because Cosine Similarity is a directional alignment measure. There are undoubtedly some extremely stable mountains and some unstable valleys in Table 6.3.3's gradient in the sensitivity of the similarity landscape. The dominant peak of the entire matrix, S_2 T_1 = 0.8870, has a very low sensitivity. The categorization it enforces (S_2 mapping consistently to T_1) would be robust even in the presence of a moderate quantity of noise because scores this high are structurally stable even to tiny perturbations of a few hundredths. S_1-T_3 at 0.8467 and S_3-T_3 at 0.7960 are two additional powerful zones that behave similarly. A high and geometrically meaningful fit is shown by their clustering at the upper band, close to the 0.80 mark. They do not change their relative rank in the T_3 template, the high contributors do not change their importance with perturbation. But they may switch their status as high or mid. These high-value regions can be thought of as mountains that retain their structure despite large deformations of the landscape. On the other hand, similar ratings that fall in the middle band (0.70-0.79) are more likely to be affected by small variations. S_1 T_2 at 0.7153, S_2 T_3 at 0.7549, and S_3 T_2 at 0.7676 are examples of values in a competitive regime, where small changes may shift their relative position to each other, alter the shape of PCA clusters, the curve of spline-based representations, or the concentration of heatmap colour. These mid-level similarity scores are short-lived regions. They are noisy, but not informative enough to have an effect on classification. They can be pushed to the low side of weak or the deep side of high, changing the relative interpretations of the signal-template relationship, by a small shift in order of magnitude, such as +0.05. This is the case with the lower band of the matrix. The most solid numbers in the landscape are S_3T_1 (0.5740), S_2 T_2 (0.5888), and S_1 T_1 (0.6083). These items are slightly above the weak-to-moderate threshold, and a slight change in any of these items would make them look very differently in heatmaps, and for them to decrease more quickly in surface plots, or may affect classification. In the graph models, the trough that formed earlier would get deeper with a slight decrease in S_1-T_1 but possibly force the exit from the weak zone with a slight increase in S_2-T_2 as in this example. Low-value regions could be considered as valleys whose width and depth vary drastically even for slight changes. This is confirmed by the template-wise gradient. The broadest distribution is for Template T_1 (its minimum is 0.57 and the maximum is 0.88). Because of this, S_2 is prominent, S_1 and S_3 exhibit unstable, noise-sensitive behavior, and T_1 is extremely sensitive to the signal with which it is linked. Additionally, Template T_2 is consistent and in equilibrium, with a mid-range that can alter categorization influence through disturbance. Due to its remarkable constancy of resemblance across signals, template T_3 is the most stable of all the templates. Because of its stability, the T_3 column in heatmaps, PCA maps, and spline-based presentations is both structurally and visually consistent. The greatest dynamic range is seen in Signal S_2 (0.5888-0.8870). One of the main sources of the system's nonlinearity is this wide divergence, which makes S_2 extremely sensitive to changes in the template. With sensitivity dominating the lower end around T_1, S_1 has a more monotone pattern. S_3's curvature

is delicate, having a central peak at T_2. Any change in the region surrounding this point will visually modify the PCA placement, heatmap gradients, and spline shapes. The entire world appears to be a tidy gradient of sensitivity on the matrix: the closer the details, the more stable and less sensitive the behavior; the intermediate values show the intermediate sensitivity; the crumbliest structural values are found at the ends. The geometry of peaks and troughs in 3D surfaces, the movement of PCA space segregations, the movements of smooth spline curves, and heatmap color changes all consistently exhibit this association. Overall, these patterns reveal that the high-value body segments, in particular the S_2-T_1 and high cluster around T_3 provide the best cues for classification. The moderate values give rise to ambiguity as a result of small changes in the order and understanding. As the most sensitive, the regions around T_1 and T_2 will be most prone to be misclassified if there are any changes. In general, the sensitivity map reveals the internal consistency of the system's similarity patterns: unstable regions (valleys) indicate the limits of reliability and the regions where extra caution should be taken in interpretation, while stable regions (peaks) provide the structure's backbone.

9.1. **3D Sensitivity Surface for Cosine Similarity Matrix. How the surface is computed?**

1. Calculate cubic splines for each signal curve (S_1, S_2, S_3).
2. Determine both splines' derivatives.
3. Create a matrix of sensitivity.

Table 15

Template Index	S_1 **Sensitivity**	S_2 **Sensitivity**	S_3 **Sensitivity**
$T_1 \to T_2$	dS_1/dT	dS_2/dT	dS_3/dT
$T_2 \to T_3$	dS_1/dT	dS_2/dT	dS_3/dT

4. Extrapolate these values to a 3D continuous surface.

This creates a 2D domain with Z = sensitivity magnitude (templates x signals).
3D Sensitivity Surface
Interpretation. Peak:
S_2 Near the T_1-T_2 Signal
At T_1 T_2, S_2 produces the biggest rise.
The magnitude of the massive fall is as follows:

$$0.8870 \to 0.5888(\Delta = -0.2982)0.8870 \to 0.5888 \quad (\Delta = -0.2982)0.8870 \to 0.5888(\Delta = -0.2982)$$

This region becomes a tall unstable area, confirming that S_2 is the most erratic signal.
Moderate Ridge: S_3 substantially increases around T_1-T_2

$$0.5740 \to 0.7676(\Delta = +0.1936)0.5740 \to 0.7676 \quad (\Delta = +0.1936)0.5740 \to 0.7676(\Delta = +0.1936)$$

This develops as a medium height ridge into moderately sensitive territory.
Smooth Plateau: S I Over all Templates.
S_1 changes smoothly:

$$0.6083 \rightarrow 0.7153 \rightarrow 0.8467 \rightarrow 0.6083 \rightarrow 0.7153 \rightarrow 0.84670.6083 \rightarrow 0.7153 \rightarrow 0.8467$$

The surface continues to exhibit minimal sensitivity, stability, and flatness.
One sharp peak (S_2), one medium ridge (S_3), and one soft hill (S_1) are the surface forms.
It creates an amazing three-dimensional terracape that graphically represents stability against volatility.
3D sensitivity surface (Figure 14). The Cosine Similarity value's first-derivative response across templates for signals S_1-S_3. The most sensitive and volatile in the data set is represented by the sharp slope to S_2 between T_1 and T_2. S_1 produces a low, smooth plateau, indicating consistent behavior, while S_3 exhibits moderate sensitivity over the same zone. The dynamics of instability and smoothness of all signal-template connections are displayed in this surface depiction.

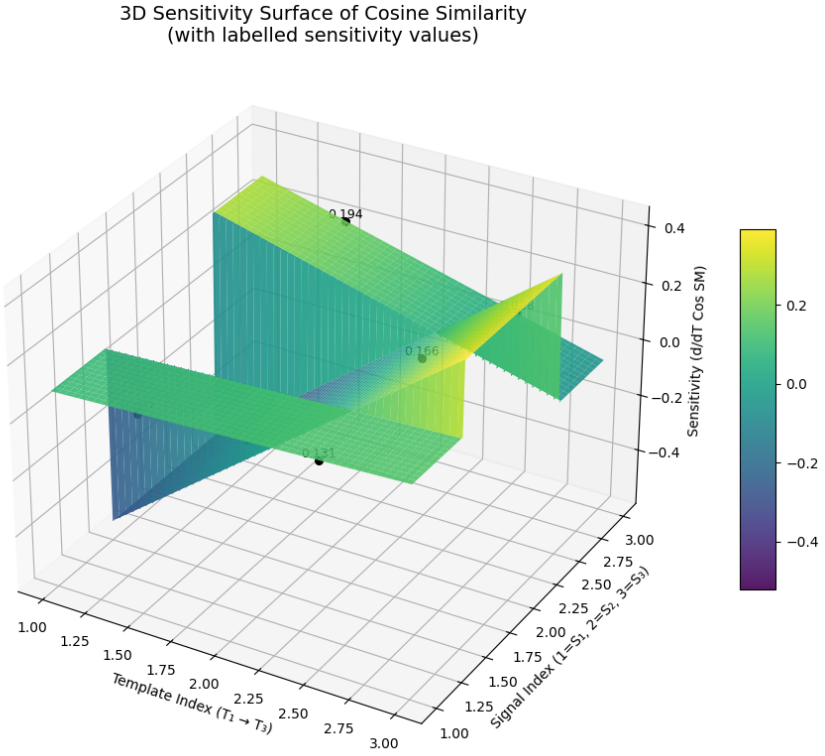

FIGURE 14. 3D Sensitivity Surface

Figure 15: Normalized sensitivity surface in three dimensions Cosine change values similarity to the S_1-S_3 signal templates. The interval 01 is used to normalize the sensitivity values, which are computed using absolute spline derivatives.
Tallest peak: The greatest variations of similarity behaviours are shown by Signal S_2 from T_1 to

T_2. The stability of the plateau of Signal S_1 and the middle-ridge of Signal S_3 are shown by their wide valley and mid-level ridge respectively. The specific values of normalised sensitivities at the template midpoints are indicated.

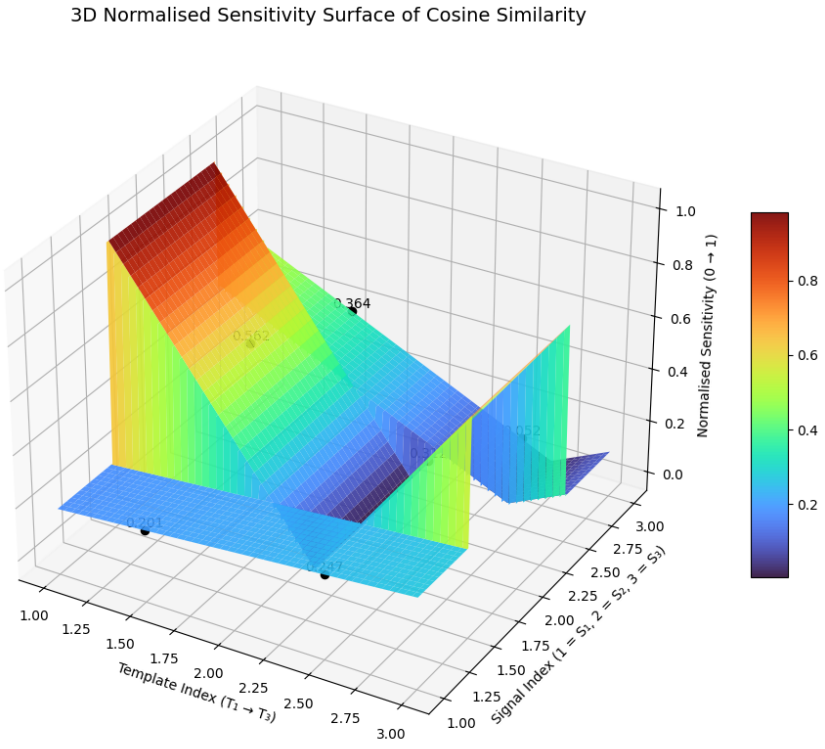

FIGURE 15. Normalized 3D Sensitivity Surface

10. Comparative Analysis

Cotangent similarity analysis [49] and cosine similarity analysis are two analyses of the same signal-template system that differ by an order of magnitude. Cosine similarity's more values and smooth distributions mean that overall patterns of alignment are readily visualized and easily explained. On the other hand, cotangent similarity does shrink the range of values and penalize uncertainty, thus giving low values and producing strong and weaker couplings. Although this may differ in scale, the two methods are in agreement about the main end state of the structure: $S_2 - T_1$ is the strongest and most stable pairing of the system. In the case of cosine similarity the dominance shows up as an exceptionally high peak (0.8870) whereas in the case of cotangent similarity, the same pairing is the global maximum (0.6653) albeit with less exaggeration. This consensus establishes the fact that the predominant alignment is not a factor of the similarity measure but rather of the data.

The point of divergence between the two approaches is in treating the secondary and ambiguous relationships. Cosine similarity describes templates like T_2 and T_3 as being moderately to strongly

consistent with several signals, and so more widely compatible and smoother in clustering behaviour. Cotangent similarity on the other hand, dilutes these same associations and especially in the case of T_2 when no signal in the signal bank matches decisively. This means that cosine similarity is likely to exaggerate borderline similarities whereas cotangent similarity is more violent. The difference between template T_3 and template T_1 can be well demonstrated by the similarity of cosine and cotangent: the former displays it as equally strong among signals, whereas the latter displays it as a weak or background profile that does not have any dominant association.

These differences are fairly stable across the different ways of representing the data. The consistency between heatmaps, bar charts, surface plots and spline curves and normalization of those point out the same story: similarity in form of cosine points out global structure and smoothness while similarity in form of cotangent points out selectivity, dominance and avoidance of weak couplings. Cosine similarity is more suited for exploration and initial grouping, while cotangent similarity is better suited for prioritisation and other things that are critical to decision making, where we cannot afford to be wrong. The two measures are complementary and not redundant. Cosine similarity identifies the matches and cotangent similarity identifies the matches that are good enough to be used.

Cosine and cotangent similarity also tell us that S_2T_1 is the most frequent match, which verify the robustness of the main result. Cosine similarity emphasizes the general patterns of alignment whereas cotangent similarity is more discriminating and selective of weak and ambiguous relations. Combined they offer an equal and trustworthy framework to signal-template classification. Cosine similarity is less specific and prone to exaggerate scores of alignment, but this is advantageous when one is interested in exploration and not classification. Cotangent similarity is more rigorous, more discriminating and more effective at the strong and weak/borderline matches, and is therefore more robust and of high dependability in final decision-making and prioritizing.

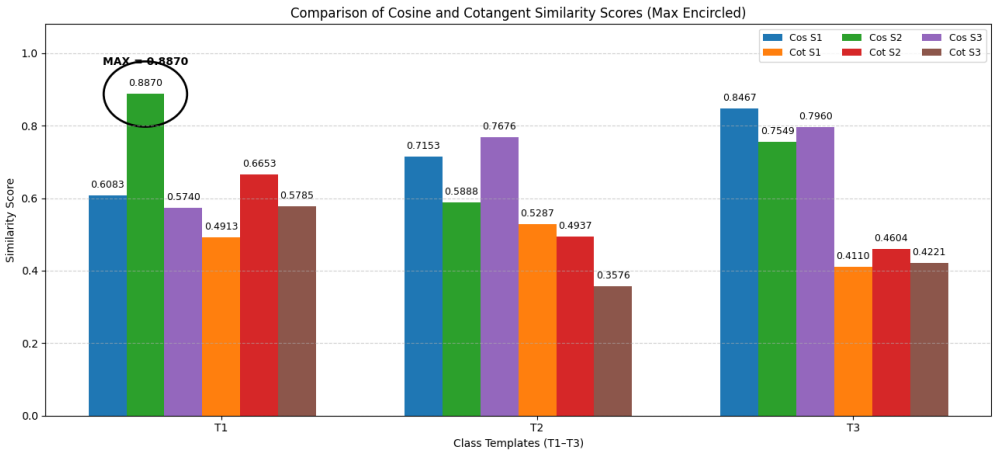

FIGURE 16. Comparison of Cosine and Cotangent Similarity Scores

11. Conclusion

This paper provides a comprehensive theoretical foundation for both locally compact space and complex neutrosophic soft compact space in complex neutrosophic soft topology. In order to apply traditional topological conclusions to the complex neutrosophic soft environment, a number of comparable definitions of compactness were developed based on open covers, finite sub-covers, intersections of closed sets, and centered families. After a thorough analysis of the fundamental relationships between compactness, closedness, Hausdorffness, normalcy, and stronger axioms of separation, it was discovered that a number of classical implications remain valid in the face of neutrosophic uncertainty. Strong inheritance features between open and closed subspaces were demonstrated, adding structural consistency to the theory, and the notion of complex neutrosophic soft local compactness was proposed as a helpful weakening of compactness. Concurrently, a hybrid visual-metric model for cosine similarity analysis of multidimensional signals and templates was proposed. The similarity structure was transformed into a readable and comprehensible geometric landscape that shows the predominant alignments, transitional, and sensitivity-prone areas by combining numerical similarity measurements with sophisticated visualization techniques. The effectiveness of the suggested method in strong pattern recognition and uncertainty-sensitive classification is demonstrated by the continuous observation of the pattern of strong signal-template correspondences and the sensitivity analysis using derivatives. In general, the paper provides a concrete and comprehensible foundation for handling localized uncertainty in complicated multidimensional systems by bridging the gap between abstract topological modeling and useful similarity analysis.

12. Limitations

Despite its depth in theory and analysis, the study has some shortcomings. Based on preset membership structures and axioms that may restrict the overlay to different neutrosophic or fuzzy generalizations, the suggested topological outcomes are built within a specific complicated neutrosophic soft framework. The test based on cosine similarity is mainly related to exploratory analysis and visualization, and the numerical studies are based on typical signal and template combinations, rather than on large real data. Also, the scalability and complexity of the hybrid visual-metric framework were not well explored, which affects its applicability to a streaming data scenario or very high dimensional data.

13. Future Work

This work can be carried out in a variety of ways in the future. Compactness and local compactness are mathematical concepts that can be studied in more generalized neutrosophic soft structures refined, bipolar, or higher-order complex neutrosophic models. They can also be studied in relation to other topological concepts like connectedness, paracompactness, and metrizability. On the applied side, the hybrid cosine similarity framework can be tested on substantial actual data

in the domains of signal processing, image analysis, medical diagnostics, and decision support systems. Other similarity metrics, uncertainty-sensitive distance functions, and learning-based dimensionality reduction techniques can all be used to achieve more. Finally, the development of automated and computationally effective visualization pipelines would make the suggested framework more practically applicable to large-scale.

Acknowledgments: We extend our sincere appreciation to Mindanao State University–Tawi-Tawi College of Technology and Oceanography (MSU-TCTO) for their generous financial support of this work.

Authors' Contributions: All the authors contributed significantly in writing this article. The authors read and approved the final manuscript.

Conflicts of Interest: The authors declare that there are no conflicts of interest regarding the publication of this paper.

References

[1] L.A. Zadeh, Fuzzy Sets, Inf. Control. 8 (1965), 338–353. https://doi.org/10.1016/S0019-9958(65)90241-X.

[2] K.T. Atanassov, Intuitionistic Fuzzy Sets, Fuzzy Sets Syst. 20 (1986), 87–96. https://doi.org/10.1016/S0165-0114(86)80034-3.

[3] J. Buckley, Fuzzy Complex Numbers, Fuzzy Sets Syst. 33 (1989), 333–345. https://doi.org/10.1016/0165-0114(89)90122-X.

[4] J.N. Mordeson, P.S. Nair, eds., Fuzzy Graphs and Fuzzy Hypergraphs, Physica-Verlag, Heidelberg, 2000. https://doi.org/10.1007/978-3-7908-1854-3.

[5] D. Ramot, R. Milo, M. Friedman, A. Kandel, Complex Fuzzy Sets, IEEE Trans. Fuzzy Syst. 10 (2002), 171–186. https://doi.org/10.1109/91.995119.

[6] E. Szmidt, J. Kacprzyk, An Application of Intuitionistic Fuzzy Set Similarity Measures to a Multi-Criteria Decision Making Problem, in: L. Rutkowski, R. Tadeusiewicz, L.A. Zadeh, J.M. Żurada (Eds.), Artificial Intelligence and Soft Computing - ICAISC 2006, Springer, Berlin, Heidelberg, 2006: pp. 314–323. https://doi.org/10.1007/11785231_34.

[7] I.K. Vlachos, G.D. Sergiadis, Intuitionistic Fuzzy Information – Applications to Pattern Recognition, Pattern Recognit. Lett. 28 (2007), 197–206. https://doi.org/10.1016/j.patrec.2006.07.004.

[8] G. Zhang, T.S. Dillon, K.Y. Cai, J. Ma, J. Lu, Operation Properties and δ-Equalities of Complex Fuzzy Sets, Int. J. Approx. Reason. 50 (2009), 1227–1249. https://doi.org/10.1016/j.ijar.2009.05.010.

[9] R. Parvathi, M.G. Karunambigai, K.T. Atanassov, Operations on Intuitionistic Fuzzy Graphs, in: 2009 IEEE International Conference on Fuzzy Systems, IEEE, Jeju Island, 2009: pp. 1396–1401. https://doi.org/10.1109/FUZZY.2009.5277067.

[10] A.S. Alkouri, A.R. Salleh, Complex Intuitionistic Fuzzy Sets, AIP Conf. Proc. 1482 (2012), 464–470. https://doi.org/10.1063/1.4757515.

[11] A.U.M. Alkouri, A.R. Salleh, Complex Atanassov's Intuitionistic Fuzzy Relation, Abstr. Appl. Anal. 2013 (2013), 287382. https://doi.org/10.1155/2013/287382.

[12] N. Alshehri, M. Akram, Intuitionistic Fuzzy Planar Graphs, Discret. Dyn. Nat. Soc. 2014 (2014), 397823. https://doi.org/10.1155/2014/397823.

[13] K.K. Myithili, R. Parvathi, M. Akram, Certain Types of Intuitionistic Fuzzy Directed Hypergraphs, Int. J. Mach. Learn. Cybern. 7 (2014), 287–295. https://doi.org/10.1007/s13042-014-0253-1.

[14] A. Nagoorgani, M. Akram, S. Anupriya, Double Domination on Intuitionistic Fuzzy Graphs, J. Appl. Math. Comput. 52 (2015), 515–528. https://doi.org/10.1007/s12190-015-0952-0.

[15] S. Broumi, F. Smarandache, Several Similarity Measures of Neutrosophic Sets, Neutrosophic Sets Syst. 1 (2013), 54–62.

[16] P. Majumdar, S.K. Samanta, On Similarity and Entropy of Neutrosophic Sets, J. Intell. Fuzzy Syst. 26 (2014), 1245–1252. https://doi.org/10.3233/IFS-130810.

[17] S. Broumi, F. Smarandache, New Distance and Similarity Measures of Interval Neutrosophic Sets, in: 17th International Conference on Information Fusion, Salamanca, Spain, pp. 249–255, 2014. https://digitalrepository.unm.edu/math_fsp/487.

[18] J. Ye, Similarity Measures Between Interval Neutrosophic Sets and Their Applications in Multicriteria Decision-Making, J. Intell. Fuzzy Syst. 26 (2014), 165–172. https://doi.org/10.3233/IFS-120724.

[19] R. Şahin, A. Küçük, On Similarity and Entropy of Neutrosophic Soft Sets, J. Intell. Fuzzy Syst. 27 (2014), 2417–2430. https://doi.org/10.3233/IFS-141211.

[20] K. Sinha, P. Majumdar, An Approach to Similarity Measure Between Neutrosophic Soft Sets, Neutrosophic Sets Syst. 30 (2019), 182–190.

[21] S. Broumi, F. Smarandache, Extended Hausdorff Distance and Similarity Measures for Neutrosophic Refined Sets and Their Application in Medical Diagnosis, J. New Theory 7 (2015), 64–78.

[22] D. Liu, G. Liu, Z. Liu, Some Similarity Measures of Neutrosophic Sets Based on the Euclidean Distance and Their Application in Medical Diagnosis, Comput. Math. Methods Med. 2018 (2018), 7325938. https://doi.org/10.1155/2018/7325938.

[23] V. Uluçay, I. Deli, M. Şahin, Similarity Measures of Bipolar Neutrosophic Sets and Their Application to Multiple Criteria Decision Making, Neural Comput. Appl. 29 (2016), 739–748. https://doi.org/10.1007/s00521-016-2479-1.

[24] T. Mahmood, U.U. Rehman, Z. Ali, Exponential and Non-Exponential Based Generalized Similarity Measures for Complex Hesitant Fuzzy Sets with Applications, Fuzzy Inf. Eng. 12 (2020), 38–70. https://doi.org/10.1080/16168658.2020.1779013.

[25] R. Chinram, T. Mahmood, U. Ur Rehman, Z. Ali, A. Iampan, Some Novel Cosine Similarity Measures Based on Complex Hesitant Fuzzy Sets and Their Applications, J. Math. 2021 (2021), 6690728. https://doi.org/10.1155/2021/6690728.

[26] O. DalKılıç, N. Demirtaş, Similarity Measures of Neutrosophic Fuzzy Soft Set and Its Application to Decision Making, J. Exp. Theor. Artif. Intell. 37 (2023), 513–529. https://doi.org/10.1080/0952813X.2023.2222720.

[27] A. Patel, S. Jana, J. Mahanta, Construction of Similarity Measure for Intuitionistic Fuzzy Sets and Its Application in Face Recognition and Software Quality Evaluation, Expert Syst. Appl. 237 (2024), 121491. https://doi.org/10.1016/j.eswa.2023.121491.

[28] H. Alolaiyan, A. Razaq, H. Ashfaq, D. Alghazzawi, U. Shuaib, et al., Improving Similarity Measures for Modeling Real-World Issues with Interval-Valued Intuitionistic Fuzzy Sets, IEEE Access 12 (2024), 10482–10496. https://doi.org/10.1109/ACCESS.2024.3351205.

[29] X. Wu, Z. Zhu, S.M. Chen, Strict Intuitionistic Fuzzy Distance/similarity Measures Based on Jensen-Shannon Divergence, Inf. Sci. 661 (2024), 120144. https://doi.org/10.1016/j.ins.2024.120144.

[30] N. Palaniappan, R. Srinivasan, Applications of Intuitionistic Fuzzy Sets of Root Type in Image Processing, in: NAFIPS 2009 - 2009 Annual Meeting of the North American Fuzzy Information Processing Society, IEEE, 2009, pp. 1–5. https://doi.org/10.1109/NAFIPS.2009.5156480.

[31] L. Dymova, P. Sevastjanov, A. Tikhonenko, A New Method for Comparing Interval-Valued Intuitionistic Fuzzy Values, in: L. Rutkowski, M. Korytkowski, R. Scherer, R. Tadeusiewicz, L.A. Zadeh, J.M. Zurada (Eds.), Artificial Intelligence and Soft Computing, Springer, Berlin, Heidelberg, 2012: pp. 221–228. https://doi.org/10.1007/978-3-642-29347-4_26.

[32] M. Akram, B. Davvaz, Strong Intuitionistic Fuzzy Graphs, Filomat 26 (2012), 177–196. https://doi.org/10.2298/FIL1201177A.

[33] A.U.M. Alkouri, A.R. Salleh, Some Operations on Complex Atanassov's Intuitionistic Fuzzy Sets, AIP Conf. Proc. 1571 (2013), 987–993. https://doi.org/10.1063/1.4858782.

[34] R.R. Yager, A.M. Abbasov, Pythagorean Membership Grades, Complex Numbers, and Decision Making, Int. J. Intell. Syst. 28 (2013), 436–452. https://doi.org/10.1002/int.21584.

[35] M. Karunambigai, M. Akram, R. Buvaneswari, Strong and Superstrong Vertices in Intuitionistic Fuzzy Graphs, J. Intell. Fuzzy Syst. 30 (2015), 671–678. https://doi.org/10.3233/IFS-151786.

[36] M. Akram, R. Akmal, Operations on Intuitionistic Fuzzy Graph Structures, Fuzzy Inf. Eng. 8 (2016), 389–410. https://doi.org/10.1016/j.fiae.2017.01.001.

[37] M. Ali, D.E. Tamir, N.D. Rishe, A. Kandel, Complex Intuitionistic Fuzzy Classes, in: 2016 IEEE International Conference on Fuzzy Systems (FUZZ-IEEE), IEEE, 2016, pp. 2027–2034. https://doi.org/10.1109/FUZZ-IEEE.2016.7737941.

[38] Q. Khan, T. Mahmood, J. Ye, Vector Similarity Measures for Simplified Neutrosophic Hesitant Fuzzy Set and Their Applications, J. Inequal. Spec. Funct. 7 (2016), 176–194.

[39] T. Wang, Distance of Single-Valued Neutrosophic Set and Its Application in Pattern Recognition, J. Phys.: Conf. Ser. 2025 (2021), 012019. https://doi.org/10.1088/1742-6596/2025/1/012019.

[40] T. Mahmood, U. Ur Rehman, Z. Ali, T. Mahmood, Hybrid Vector Similarity Measures Based on Complex Hesitant Fuzzy Sets and Their Applications to Pattern Recognition and Medical Diagnosis, J. Intell. Fuzzy Syst.: Appl. Eng. Technol. 40 (2020), 625–646. https://doi.org/10.3233/jifs-200418.

[41] F. Al-Sharqi, Y. Al-Qudah, N. Alotaibi, Decision-Making Techniques Based on Similarity Measures of Possibility Neutrosophic Soft Expert Sets, Neutrosophic Sets Syst. 55 (2023), 358–382.

[42] N.A. Alreshidi, Z. Shah, M.J. Khan, Similarity and Entropy Measures for Circular Intuitionistic Fuzzy Sets, Eng. Appl. Artif. Intell. 131 (2024), 107786. https://doi.org/10.1016/j.engappai.2023.107786.

[43] X. Ji, H. Geng, N. Akhtar, X. Yang, Floquet Engineering of Point-Gapped Topological Superconductors, Phys. Rev. B 111 (2025), 195419. https://doi.org/10.1103/physrevb.111.195419.

[44] F. Smarandache, Neutrosophic Set – A Generalisation of the Intuitionistic Fuzzy Sets, Int. J. Pure Appl. Math. 24 (2005), 287–297.

[45] D. Molodtsov, Soft Set Theory–First Results, Comput. Math. Appl. 37 (1999), 19–31. https://doi.org/10.1016/S0898-1221(99)00056-5.

[46] P.K. Maji, Neutrosophic Soft Set, Ann. Fuzzy Math. Inform. 5 (2013), 157–168.

[47] I. Deli and S. Broumi, Neutrosophic soft relations and some properties, Ann. Fuzzy Math. Inform. 9 (2015), 169–182.

[48] T. Bera, N.K. Mahapatra, Introduction to Neutrosophic Soft Topological Space, OPSEARCH 54 (2017), 841–867. https://doi.org/10.1007/s12597-017-0308-7.

[49] A.A zzam, A.M. Abd El-latif, B. Alreshidi, M. Aldawood, M.M. Awad, et al., Operations on Complex Neutrosophic Soft Sets and Their Topological Spaces: A New Approach with Applications to Decision-Making, Eur. J. Pure Appl. Math. 18 (2025), 7171. https://doi.org/10.29020/nybg.ejpam.v18i4.7171.

[50] A.A. Abubaker, R. Hatamleh, K. Matarneh, A. Al-Husban, On the Numerical Solutions for Some Neutrosophic Singular Boundary Value Problems by Using (LPM) Polynomials, Int. J. Neutrosophic Sci. 25 (2024), 197–205. https://doi.org/10.54216/IJNS.250217.

[51] A. Ahmad, R. Hatamleh, K. Matarneh, A. Al-Husban, On the Irreversible k-Threshold Conversion Number for Some Graph Products and Neutrosophic Graphs, Int. J. Neutrosophic Sci. 25 (2025), 183–196.

[52] Raed Hatamleh, Complex Tangent Trigonometric Approach Applied to (γ, τ)-Rung Fuzzy Set Using Weighted Averaging, Geometric Operators and Its Extension, Commun. Appl. Nonlinear Anal. 32 (2024), 133–144. https://doi.org/10.52783/cana.v32.2978.

[53] R. Hatamleh, A. Hazaymeh, On Some Topological Spaces Based on Symbolic n-Plithogenic Intervals, Int. J. Neutrosophic Sci. 25 (2025), 23–37. https://doi.org/10.54216/IJNS.250102.

[54] H. Qawaqneh, Fractional Analytic Solutions and Fixed Point Results with Some Applications, Adv. Fixed Point Theory 14 (2024), 1. https://doi.org/10.28919/afpt/8279.

[55] H. Qawaqneh, M.S.M. Noorani, H. Aydi, A. Zraiqat, A.H. Ansari, On Fixed Point Results in Partial b-Metric Spaces, J. Funct. Spaces 2021 (2021), 8769190. https://doi.org/10.1155/2021/8769190.

[56] H. Qawaqneh, M.S.M. Noorani, H. Aydi, Some New Characterizations and Results for Fuzzy Contractions in Fuzzy *B*-Metric Spaces and Applications, AIMS Math. 8 (2023), 6682–6696. https://doi.org/10.3934/math.2023338.

[57] H. Qawaqneh, J. Manafian, M. Alharthi, Y. Alrashedi, Stability Analysis, Modulation Instability, and Beta-Time Fractional Exact Soliton Solutions to the Van Der Waals Equation, Mathematics 12 (2024), 2257. https://doi.org/10.3390/math12142257.

[58] H. Qawaqneh, New Functions for Fixed Point Results in Metric Spaces with Some Applications, Indian J. Math. 66 (2024), 55–84.

[59] H. Qawaqneh, H.A. Hammad, H. Aydi, Exploring New Geometric Contraction Mappings and Their Applications in Fractional Metric Spaces, AIMS Math. 9 (2024), 521–541. https://doi.org/10.3934/math.2024028.

[60] M. Elbes, T. Kanan, M. Alia, M. Ziad, Covd-19 Detection Platform from X-Ray Images Using Deep Learning, Int. J. Adv. Soft Comput. Appl. 14 (2022), 197–211. https://doi.org/10.15849/ijasca.220328.13.

[61] T. Kanan, M. Elbes, K.A. Maria, M. Alia, Exploring the Potential of IoT-Based Learning Environments in Education, Int. J. Adv. Soft Comput. Appl. 15 (2023), 166–178.

[62] M. Abualhomos, A. Shihadeh, A.A. Abubaker, K. Al-Husban, T. Fujita, et al. Unified Framework for Type-n Extensions of Fuzzy, Neutrosophic, and Plithogenic Offsets: Definitions and Interconnections, J. Fuzzy Ext. Appl. 6 (2025), 689–726. https://doi.org/10.22105/jfea.2025.514314.1858

[63] A. Ahmad, M. Abualhomos, A. Atallah, A. Al-Husban, A Study of Some Neutrosophic Derivatives Problems Based on Newton's BDF and CDF Numerical Methods, Int. J. Neutrosophic Sci. 26 (2025), 1–8. https://doi.org/10.54216/IJNS.260401.

[64] H. Edduweh, A.S. Heilat, L. Razouk, S.A. Khalil, A.A. Alsaraireh, A. Al-Husban, On the Weak Fuzzy Complex Differential Equations and Some Types of the 1st Order 1st Degree WFC-ODEs, Int. J. Neutrosophic Sci. 25 (2025), 450–468. https://doi.org/10.54216/IJNS.250338.

[65] M. Abualhomos, W.M.M. Salameh, M. Bataineh, M.O. Al-Qadri, A. Alahmade, A. Al-Husban, An Effective Algorithm for Solving Weak Fuzzy Complex Diophantine Equations in Two Variables, Int. J. Neutrosophic Sci. 23 (2024), 386–394. https://doi.org/10.54216/IJNS.230431.

[66] H. Zureigat, A.U. Alkouri, A. Al-khateeb, E. Abuteen, A.G. Sana, Numerical Solution of Fuzzy Heat Equation with Complex Dirichlet Conditions, Int. J. Fuzzy Log. Intell. Syst. 23 (2023), 11–19. https://doi.org/10.5391/IJFIS.2023.23.1.11.

[67] X. Yang, Y. Feng, A. Wahab, H. Geng, Non-Hermitian Second-Order Topological Phases and Bipolar Skin Effect in Photonic Kagome Crystals, Phys. Rev. 113 (2026), 023506. https://doi.org/10.1103/s26b-8bdl.